NASA Technical Paper 1355

A Study of Canard-Wing Interference Using Experimental Pressure Data at Transonic Speeds

Blair B. Gloss and Karen E. Washburn

JANUARY 1979

NASA

NASA Technical Paper 1355

A Study of Canard-Wing Interference Using Experimental Pressure Data at Transonic Speeds

Blair B. Gloss and Karen E. Washburn
Langley Research Center
Hampton, Virginia

NASA
National Aeronautics
and Space Administration

**Scientific and Technical
Information Office**

1979

SUMMARY

A close-coupled canard-wing model was tested in the Langley 8-foot transonic pressure tunnel at Mach numbers from 0.70 to 1.20 to determine the canard-wing interference effects on canard and wing loadings. The canard had an exposed area of 28.0 percent of the wing reference area and was located in the chord plane of the wing or in a position 18.5 percent of the wing mean geometric chord above or below the wing chord plane. The canard leading-edge sweep was 51.7°, and the wing leading-edge sweep was 60°.

The results indicated that the direct canard downwash effects on the wing loading are limited to the forward half of the wing directly behind the canard. The wing leading-edge vortex is located farther forward for the wing in the presence of the canard than for the wing-alone configuration.

The wake, from the canard located below the wing chord plane, physically interacts with the wing inboard surface and produces a substantial loss of wing lift. For the Mach number 0.70 case, the presence of the wing increased the loading on the canard for the higher angles of attack. However, at Mach numbers of 0.95 and 1.20, the presence of the wing had the unexpected result of unloading the canard.

INTRODUCTION

Past investigations (refs. 1 to 13) have indicated that the proper use of canard surfaces on maneuvering aircraft can offer several attractive features such as potentially higher trimmed-lift capability, improved pitching-moment characteristics, and reduced trimmed drag; these attractive features are manifested to a higher degree when used in conjunction with an unstable aircraft. In addition, the geometric characteristics of close-coupled canard configurations offer a potential for improved longitudinal progression of cross-sectional area which could result in reduced wave drag at low supersonic speeds, and would allow placement of the horizontal control surfaces out of the wing downwash and jet exhaust. Flow-visualization studies (ref. 14) and analytical studies (refs. 15 and 16) have indicated that the favorable interference of the canard on the wing flow field can produce a complex flow field on the wing surface. Although there have been several papers published that discuss the total forces and moments produced by close-coupled canard-wing configurations, very little data are available on the load distribution on the canard and wing surfaces for close-coupled canard-wing configurations; references 17 and 18 discuss some of the available load distribution data.

This paper reports on a continuation of the work presented in reference 4. This wind-tunnel investigation obtained aerodynamic load distributions, at transonic speeds, on both the canard and wing surfaces of a model that is geometrically identical to that used in reference 4. The primary purpose of this paper is to improve the understanding of the cause and effects of the

canard-wing interference. The present investigation was conducted in the Langley 8-foot transonic pressure tunnel; the Mach numbers ranged from 0.70 to 1.20 and data were taken for angles of attack from 0° to approximately 16° at 0° sideslip. Tabulated results from this study are presented in reference 19.

SYMBOLS

The physical quantities used in this paper are given in the International System of Units (SI). Measurements and calculations were made in U.S. Customary Units.

A	aspect ratio, b_w^2/S
b'	distance from wing-fuselage juncture to wing tip
b_w	wing span, cm
b_c	canard span, cm
C_p	pressure coefficient, $\frac{\text{Static pressure - Reference static pressure}}{q_\infty}$
ΔC_p	pressure coefficient on lower surface minus pressure coefficient on upper surface
c	local chord length, cm
$\bar{c}$	wing mean geometric chord, cm
c_{av}	average chord length, cm
c_n	section normal-force coefficient, $\frac{\text{Section normal force}}{q_\infty c}$
M_∞	free-stream Mach number
q_∞	free-stream dynamic pressure, Pa
S	reference area of wing with leading and trailing edges extended to plane of symmetry, cm^2
S_c	exposed canard area, cm^2
V_∞	free-stream velocity, cm/sec
w	downwash velocity induced by canard, cm/sec
x	chordwise coordinate measured from wing leading edge, cm
y	spanwise coordinate measured from wing-fuselage juncture, cm
z	vertical coordinate measured from mid plane of fuselage, cm

α angle of attack, deg

η nondimensional spanwise coordinate, y/b'

Λ leading-edge sweep, deg

Subscripts:

c canard

w wing

MODEL DESCRIPTION

A sketch of the model used in this wind-tunnel investigation is presented in figure 1. This model was designed so that various wing and canard planforms could be attached to the common fuselage and the positional relationship of the lifting surfaces (canards and wings) could also be varied. The wings and canards were instrumented with pressure orifices located as shown in figure 1. Tables I and II give the orifice locations for the wing and canard, respectively. Both the instrumented canards and instrumented wings could not be tested simultaneously because of space restriction in the model caused by the pressure tube installation; thus, when both the canards and wings were on the model at the same time, either the wings or canards are uninstrumented. Figure 2 is a photograph of the model with instrumented and uninstrumented canards and wings shown. Table III presents the pertinent geometric parameters associated with this model.

The 60° swept, untwisted wing had uncambered circular-arc airfoil sections and a maximum thickness distribution which varied linearly from 6 percent of the chord at the root (the root in this paper is the wing-fuselage intersection) to 4 percent of the chord at the tip.

The canard had a leading-edge sweep angle of 51.7° and an exposed area of 28.0 percent of the wing reference area S. The canard was tested in the wing chord plane ($z/\bar{c} = 0.0$) and in positions 18.5 percent of the wing mean geometric chord above and below the wing chord plane ($z/\bar{c} = 0.185$ and -0.185). To obtain the configuration with the canard located below the wing chord plane, the model with the canard in the high position was rolled 180° on the sting; thus, the resulting configurations had canard-fuselage fairings on the bottom of the fuselage and had a different fuselage shape in the vicinity of the canard. The canard was untwisted and had uncambered circular-arc airfoil sections. The maximum thickness varied linearly from 6 percent of the chord at the root (canard-fuselage intersection) to 4 percent at the tip.

APPARATUS, TESTS, AND CORRECTIONS

This investigation was conducted in the Langley 8-foot transonic pressure tunnel which is a continuous-flow facility. Tests were made at Mach numbers of 0.70, 0.90, 0.95, 1.03, and 1.20 corresponding to Reynolds numbers, based on

the wing mean geometric chord, of 1.35×10^6, 1.52×10^6, 1.54×10^6, 1.58×10^6, and 1.61×10^6, respectively. Because of flow separation at the sharp leading edges of the canard and wing, the Reynolds number effect should be small. (See ref. 20.) Tests were made at angles of attack from approximately 0° to 16° at 0° sideslip. Angles of attack were corrected for effects of sting deflection due to aerodynamic load. All tests were made with boundary-layer transition fixed on the model by means of narrow strips of carborundum grit placed on the body, wings, and canards by using the methods outlined in reference 21.

PRESENTATION OF RESULTS

Reference 19 presents all the data obtained in this wind-tunnel test in tabulated form; selected portions of these data are presented in this paper in plotted form. An outline of the contents of these data plots follows:

RESULTS AND DISCUSSION

When comparisons are made between configurations with the wing-on and the wing-off or between canard-on and canard-off configurations, it should be noted that the two configurations are not exactly at the same angle of attack because of sting bending. Based on the data shown in this report, these differences in angle of attack do not appear to affect the discussions made herein.

Reference 19 contains the tabulated results presented in this paper plus other data not included herein. In this paper, the phrase high canard refers to the canard being located above the wing chord plane ($z/\bar{c} = 0.185$); mid canard refers to the canard being located in the chord plane ($z/\bar{c} = 0.0$); and low canard refers to the canard being located below the wing chord plane ($z/\bar{c} = -0.185$).

Effect of Canard on Wing Flow Field

The data in figures 3 to 11 show the effect of the canard flow field on the wing pressure distributions for all three canard configurations.

Mid canard.- For the mid canard the direct effects of the canard flow field on the wing are limited to a region directly behind the canard. (See figs. 3 to 5.) The spanwise location of the canard tip is between wing stations 5 and 6. At span stations 1 and 2, in particular, rather drastic reduction in leading-edge vortex strength (the leading-edge vortex strength and position are qualitatively determined by the pressure peaks shown in the figures) is noted for the wing in the presence of the canard.

The wing lower-surface pressure distribution may be a more reliable indicator of the canard downwash effects on the wing, since there is no leading-edge vortex there to complicate the flow field. The canard downwash is seen to affect the wing lower surface out to span station 4. The effects of the canard downwash tend to be concentrated in the forward 50 percent of the wing at span stations 1 to 4; this observation can be noted a little easier in the data shown in figure 12, where a plot of ΔC_p against x/c is presented. Also, the direct downwash effects decay rather quickly in going from span stations 1 to 4. (See figs. 3 to 5.) This decay, both chordwise and spanwise, of the canard downwash effects is not surprising since the downwash from the canard will decay inversely with distance from the canard and the canard wake. When at angle of attack it should be noted that traversing either downstream chordwise or outboard spanwise along constant percent chord lines has the net effect of moving away from the canard wake in the vertical direction. Lower surface pressure distributions show no evidence of canard upwash at wing stations 6 to 8.

By use of an attached-flow vortex-lattice computer program, the canard downwash was calculated at the wing leading edge and wing 40-percent-chord locations. (See fig. 13.) This particular computer program does not account for wake rollup. Since the canard has no camber and has a sharp leading edge, there will be a leading-edge vortex and the shed vorticity is more diffuse than

for a wing with attached flow. Thus, the results in figure 13 are not meant to be quantitative but rather qualitative; these results, however, do indicate a chordwise and spanwise decay of canard-induced downwash, and substantiate the earlier discussion.

The upper-surface pressure distributions from span station 3 and outboard (figs. 3 to 5) illustrate a secondary effect of the canard downwash on the wing. The location of the leading-edge vortex is farther aft on the wing for the wing-alone configuration than for the canard-wing configuration. The altering of the leading-edge vortex strength and growth rates inboard by the canard downwash delays the leading-edge vortex aft movement.

The effects of canard downwash on the wing pressure distribution discussed hold in general with angle-of-attack change and Mach number change. However, the data for Mach number 1.20 show that the downwash effects on the lower surface extend to larger η values than those for the other Mach numbers.

At span stations 5, 6, and 7 depending on the configuration (canard on or off), angle of attack, and Mach number, the Kutta condition may appear to be unsatisfied; as a result, there is a pressure discontinuity at the trailing edge. For many of these cases, the leading-edge vortex passes over the wing in the vicinity of the trailing edge and causes the reattachment line to fall aft of the wing trailing edge; this then does not allow the Kutta condition at the wing trailing edge to be satisfied.

For Mach numbers 0.70 and 0.95 (figs. 3 and 4) at span stations 1 and 2, and $\alpha \approx 4^{\circ}$, there appears to be evidence from the upper surface pressure distribution that the wake from the canard is interfering with the wing. Note in the leading-edge region of the wing that the pressure coefficients are positive. From the flow-visualization photographs in reference 14, it is not surprising to find the canard wake interfering with the wing for low angles of attack.

High canard.- Downwash effects induced by the high canard on the wing are similar in nature but substantially less than those induced by the mid canard. (See figs. 6 to 8.) This result should be expected since the canard wake is located farther above the wing. In addition, there is no evidence of canard wake interference with the wing surface; this condition is substantiated by the flow photographs shown in reference 14.

Low canard.- Figures 9 to 11 present the effect of the low canard on the wing pressure distribution. The primary distinguishing difference between the low- and mid-canard configurations is that there appears to be substantial canard wake interference with the wing. The data indicate wake interference for all Mach numbers and angles of attack presented at the wing inboard stations. The wake interference appears more severe at an angle of attack of 12° than for any other angle of attack. The flow-visualization photographs of reference 14 show the canard wake interference with the wing at low speeds. In general, with the exception of the wake interference problem, the discussion made for the mid-canard configuration holds for the low-canard configuration.

The previous discussion on the effect of canard location on the wing pressure distribution is for the particular configuration described in this report. Configurational changes such as rounding the canard leading edge so there is attached flow or cambering the canard could substantially change the canard downwash at a given angle of attack. The data indicate that the downwash from the canard and the canard shed vorticity are the mechanisms that cause the canard wing interference; thus, altering the canard downwash or spatial distribution of shed vorticity will affect the pressure distribution on the wing.

The effect of canard location on wing span load distribution is shown in figure 14 for two angles of attack; nominal values of α are 4° and 12°. These data show that the effect of the canard is primarily limited to the region directly behind the canard, and that the low-canard wake interference with the wing at $\alpha \approx 12^\circ$ has caused substantial loss of inboard wing lift beyond even that caused by the downwash from the mid canard. The effects of the location of the canard on the wing sectional center of pressure are shown in figure 15. The changes in wing sectional center-of-pressure location due to canard location is restricted to that region of the wing inboard of the canard tip. The data in figure 16 show the effect of canard location on wing center-of-pressure location and, as would be expected, the center of pressure moves outboard because of the previously discussed induced effects.

The data in reference 6 show that for low Mach numbers up to an angle of attack of approximately 32°, there is no favorable canard interference with the wing and this result is substantiated for angles of attack of 4° and 12° by the data in figure 15. (The model discussed in ref. 6 is geometrically identical with the present model.) However, reference 6 shows that a 44° swept wing in the presence of a canard has large lift gains when compared with the wing-alone configuration for higher angles of attack. It is felt that the data presented in this paper and in reference 6 indicate that the favorable interference of the canard with moderately swept wings ($\Lambda = 44^\circ$) must be the result of the canard downwash reducing the effective angle of attack of the wing at inboard sections where the leading-edge vortex originates, and this then delays the wing leading-edge vortex bursting. Further wind-tunnel testing is needed for this effect to be definitive.

Effect of Wing on Canard Flow Field

The effect of wing flow field on the canard pressure distribution is presented in figures 17 to 19; all the data presented are for the mid-canard configuration. The subsonic data (fig. 17) show that for the nominal angles of attack of 8° and 12°, there is very little effect of the wing on the canard flow field. However, at a nominal angle of attack of 16°, the upwash from the wing produces a measurable increase in canard loading.

At Mach numbers of 0.95 and 1.20 (figs. 18 and 19), the inboard pressure distributions show no effect of the presence of the wing for the lower angles of attack. However, the presence of the wing produced a loss in canard load on

the outboard sections. In fact, for the data at an angle of attack of 16°, this wing interference effect is observed inboard as well as outboard. Careful examination of the data presented in reference 4 shows that the total lift on the canard in the presence of the wing is less than that for the canard-alone configuration for the Mach numbers and angle-of-attack range discussed herein. (The model tested in ref. 4 is geometrically identical with the model discussed herein.) No explanation for this unexpected phenomena is given here; further tests are needed for a better understanding of this flow phenomena.

SUMMARY OF RESULTS

A close-coupled canard-wing model was tested in the Langley 8-foot transonic pressure tunnel at Mach numbers from 0.70 to 1.20 to determine the canard-wing interference effects on canard and wing loadings. The primary results of this investigation may be summarized as follows:

1. The direct canard downwash effects on the wing loading are in general primarily limited to the forward half of the wing directly behind the canard.

2. The wing leading-edge vortex is located farther forward for the wing in the presence of the canard than for the wing-alone configuration.

3. The wake from the canard located below the wing chord plane physically interacts with the wing surface and causes substantial loss of wing lift.

4. For the Mach number 0.70 case, the presence of the wing increased the loading on the canard for the higher angles of attack. However, at Mach numbers of 0.95 and 1.20, the presence of the wing had the unexpected result of unloading the canard.

Langley Research Center
National Aeronautics and Space Administration
Hampton, VA 23665
October 25, 1978

REFERENCES

1. McKinney, Linwood W.; and Dollyhigh, Samuel M.: Some Trim Drag Considerations for Maneuvering Aircraft. J. Aircr., vol. 8, no. 8, Aug. 1971, pp. 623-629.

2. Dollyhigh, Samuel M.: Static Longitudinal Aerodynamic Characteristics of Close-Coupled Wing-Canard Configurations at Mach Numbers From 1.60 to 2.86. NASA TN D-6597, 1971.

3. Gloss, Blair B.; and McKinney, Linwood W.: Canard-Wing Lift Interference Related to Maneuvering Aircraft at Subsonic Speeds. NASA TM X-2897, 1973.

4. Gloss, Blair B.: Effect of Canard Location and Size on Canard-Wing Interference and Aerodynamic-Center Shift Related to Maneuvering Aircraft at Transonic Speeds. NASA TN D-7505, 1974.

5. Gloss, Blair B.: The Effect of Canard Leading-Edge Sweep and Dihedral Angle on the Longitudinal and Lateral Aerodynamic Characteristics of a Close-Coupled Canard-Wing Configuration. NASA TN D-7814, 1974.

6. Gloss, Blair B.: Effect of Wing Planform and Canard Location and Geometry on the Longitudinal Aerodynamic Characteristics of a Close-Coupled Canard Wing Model at Subsonic Speeds. NASA TN D-7910, 1975.

7. Behrbohm, Hermann: Basic Low Speed Aerodynamics of the Short-Coupled Canard Configuration of Small Aspect Ratio. SAAB TN 60, Saab Aircraft Co. (Linköping, Sweden), July 1965.

8. Lacey, David W.; and Chorney, Stephen J.: Subsonic Aerodynamic Characteristics of Close-Coupled Canards With Varying Area and Position Relative to a 50° Swept Wing. Tech. Note AL-199, Naval Ship Res. & Develop. Center, Mar. 1971. (Available from DDC as AD 882 702L.)

9. Ottensoser, Jonah: Wind Tunnel Data on the Transonic Aerodynamic Characteristics of Close-Coupled Canards With Varying Planform, Position and Deflection Relative to a 50° Swept Wing. Test Rep. AL-88, Naval Ship Res. & Develop. Center, May 1972.

10. Krouse, John R.: Effects of Canard Planform on the Subsonic Aerodynamic Characteristics of a 25° and a 50° Swept-Wing Research Aircraft Model. Evaluation Rep. AL-91, Naval Ship Res. & Develop. Center, May 1972.

11. Lacey, David W.: Transonic Characteristics of Close-Coupled Canard and Horizontal Tail Installed on a 50 Degree Sweep Research Aircraft Model. Evaluation Rep. AL-81, Naval Ship Res. & Develop. Center, Aug. 1972.

12. Gloss, Blair B.; Henderson, William P.; and Huffman, Jarrett K.: Effect of Canard Position and Wing Leading-Edge Flap Deflection on Wing Buffet at Transonic Speeds. NASA TM X-72681, 1975.

13. Re, Richard J.; and Capone, Francis J.: An Investigation of a Close-Coupled Canard as a Direct Side-Force Generator on a Fighter Model at Mach Numbers From 0.40 to 0.90. NASA TN D-8510, 1977.

14. Miner, Dennis D.; and Gloss, Blair B.: Flow Visualization Study of Close-Coupled Canard-Wing and Strake-Wing Configuration. NASA TM X-72668, 1975.

15. Lamar, John E.; and Gloss, Blair B.: Subsonic Aerodynamic Characteristics of Interacting Lifting Surfaces With Separated Flow Around Sharp Edges Predicted by a Vortex-Lattice Method. NASA TN D-7921, 1975.

16. Lamar, John E.: Some Recent Applications of the Suction Analogy to Vortex-Lift Estimates. NASA TM X-72785, 1976.

17. Gingrich, P. B.; Child, R. D.; and Panageas, G. N.: Aerodynamic Configuration Development of the Highly Maneuverable Aircraft Technology Remotely Piloted Research Vehicle. NASA CR-143841, 1977.

18. Gloss, Blair B.; and Washburn, Karen E.: Load Distribution on a Close-Coupled Wing Canard at Transonic Speeds. J. Aircr., vol. 15, no. 4, Apr. 1978, pp. 234-239.

19. Washburn, Karen E.; and Gloss, Blair B.: Aerodynamic Load Distributions at Transonic Speeds for a Close-Coupled Wing-Canard Configuration: Tabulated Pressure Data. NASA TM-78780, 1978.

20. Henderson, William P.: Studies of Various Factors Affecting Drag Due to Lift at Subsonic Speeds. NASA TN D-3584, 1966.

21. Braslow, Albert L.; Hicks, Raymond M.; and Harris, Roy V., Jr.: Use of Grit-Type Boundary-Layer-Transition Trips on Wind-Tunnel Models. NASA TN D-3579, 1966.

TABLE I.- WING PRESSURE ORIFICE LOCATIONS

	Wing pressure orifice locations							
Span station . . .	1	2	3	4	5	6	7	8
y (upper and lower surfaces), cm . . .	2.54	5.08	7.62	10.16	12.70	15.24	17.78	20.32
x/c_w (upper and lower surfaces) . .	0.0125	0.0125	0.0125	0.0125				
	.0250	.0250	.0250	.0250	0.0250	0.0250	0.0250	
	.0500	.0500	.0500	.0500	.0500	.0500	.0500	0.0500
	.1000	.1000	.1000	.1000	.1000	.1000	.1000	.1000
	.1500	.1500	.1500	.1500	.1500	.1500	.1500	.1500
	.2250	.2250	.2250	.2250	.2250	.2250	.2250	.2250
	.3000	.3000	.3000	.3000	.3000	.3000	.3000	.3000
	.4500	.4500	.4500	.4500	.4500	.4500	.4500	.4500
	.6000	.6000	.6000	.6000	.6000	.6000	.6000	.6000
	.7500	.7500	.7500	.7500	.7500	.7500	.7500	.7500
	.9000	.9000	.9000	.9000	.9000	.9000	.9000	.9000
	.9500	.9500	.9500	.9500	.9500	.9500		
c_w, cm	27.09	24.38	21.67	18.97	16.26	13.56	10.84	8.13

TABLE II.- CANARD PRESSURE ORIFICE LOCATIONS

	Canard pressure orifice locations								
Span station	1	2	3	4	5	6	7	8	9
y (upper and lower surfaces), cm . .	2.54	3.81	5.08	6.35	7.62	8.89	10.16	11.43	12.90
x/c_c (upper and lower surfaces . .	0.0250 .0500 .1000 .1500 .2250 .3000 .4500 .6000 .7500 .9000 .9500 .9750	0.0250 .0500 .1000 .1500 .2250 .3000 .4500 .6000 .7500 .9000 .9500 .9750	0.0250 .0500 .1000 .1500 .2250 .3000 .4500 .6000 .7500 .9000 .9500 .9750	0.0250 .0500 .1000 .1500 .2250 .3000 .4500 .6000 .7500 .9000 .9500	0.0250 .0500 .1000 .1500 .2250 .3000 .4500 .6000 .7500 .9000 .9500	0.0500 .1000 .1500 .2250 .3000 .4500 .6000 .7500 .9000 .9500	0.0500 .1000 .1500 .2250 .3000 .4500 .6000 .7500 .9000	0.0500 .1000 .1500 .2250 .3000 .4500 .6000 .7500 .9000	0.1000 .1500 .2250 .3000 .4500 .6000 .7500 .9000
c_c, cm	15.21	13.85	12.50	11.15	9.79	8.44	7.08	5.73	4.38

TABLE III.- GEOMETRIC CHARACTERISTICS

Body length, cm	96.52
Wing (wings I and II except when specified):	
A (b_w^2/S)	2.5
$b_w/2$, cm	25.4
Λ_w, deg	60
$\bar{c}$, cm	23.31
Airfoil section	Circular arc
S (area extended to plane of symmetry), cm^2	1032.2
Root chord, cm	29.80
Tip chord, cm	6.77
Maximum thickness at —	
Root, percent chord	6
Tip, percent chord	4
Canard:	
A (b_c^2/S_c)	4.12
Λ_c, deg	51.7
$\bar{c}$, cm	14.83
Airfoil section	Circular arc
S_c (exposed area), cm^2	288.73
$b_c/2$, cm	17.25
Root chord, cm	17.92
Tip chord, cm	3.59
Maximum thickness at —	
Root, percent chord	6
Tip, percent chord	4

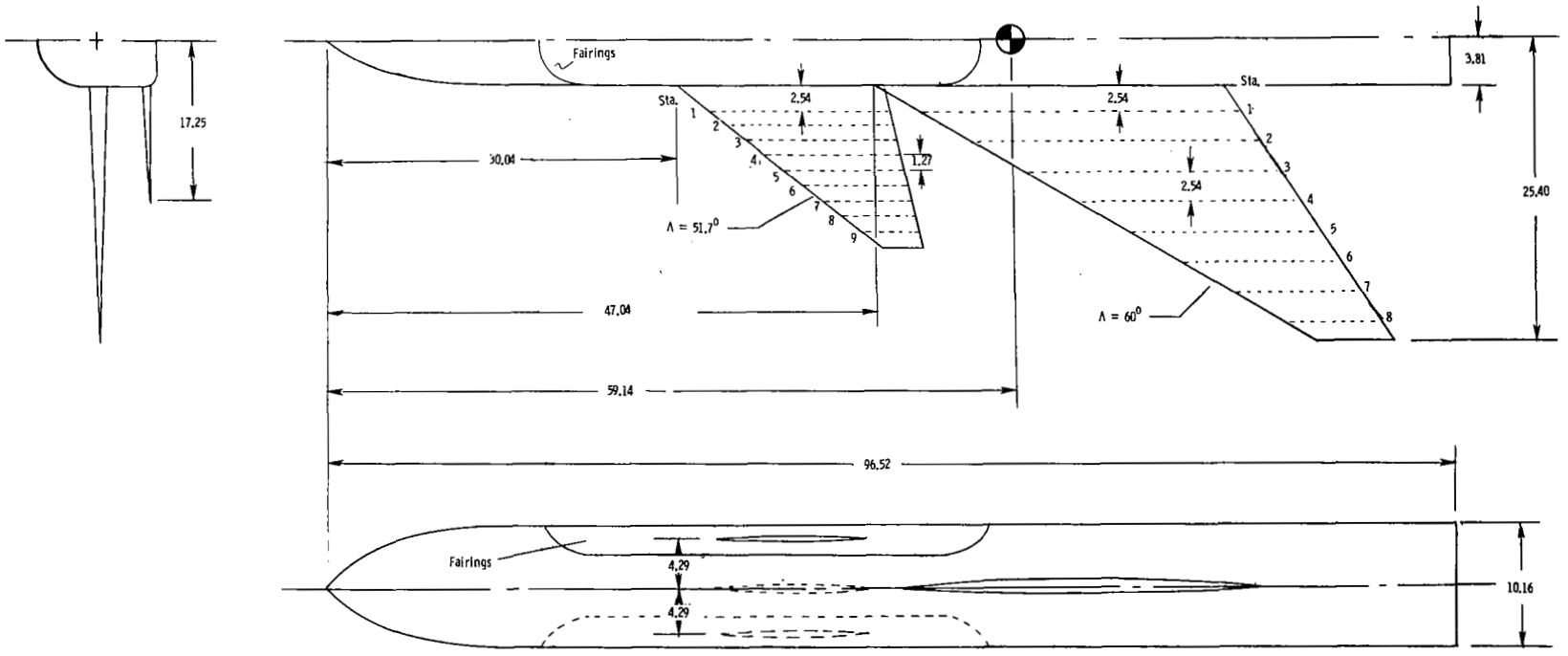

Figure 1.- Sketch of model. All linear dimensions are in centimeters. (Upper and lower surface pressure orifices are not located in same lifting panel.)

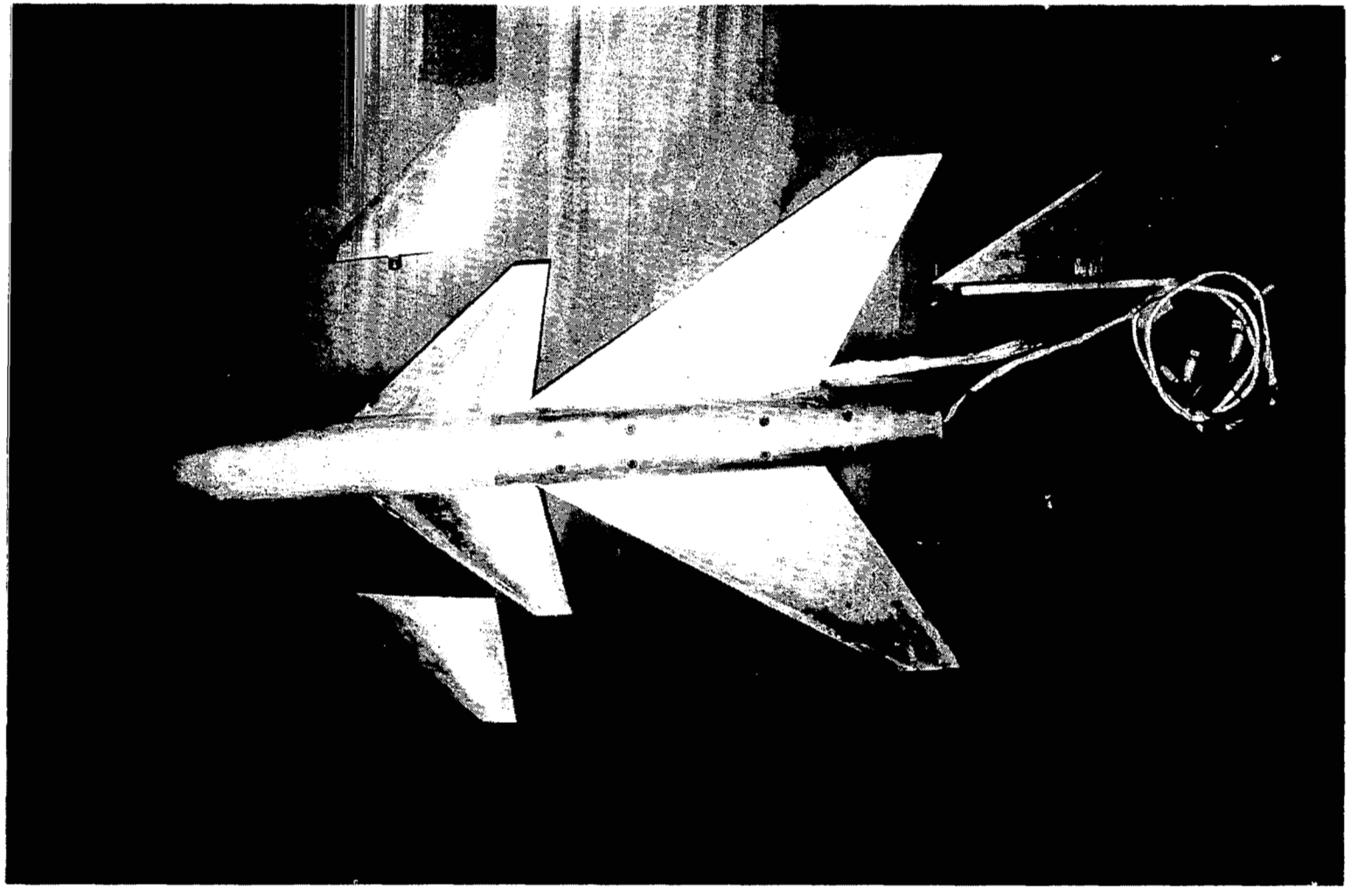

L-77-3463

Figure 2.- Photograph of close-coupled canard-wing model.

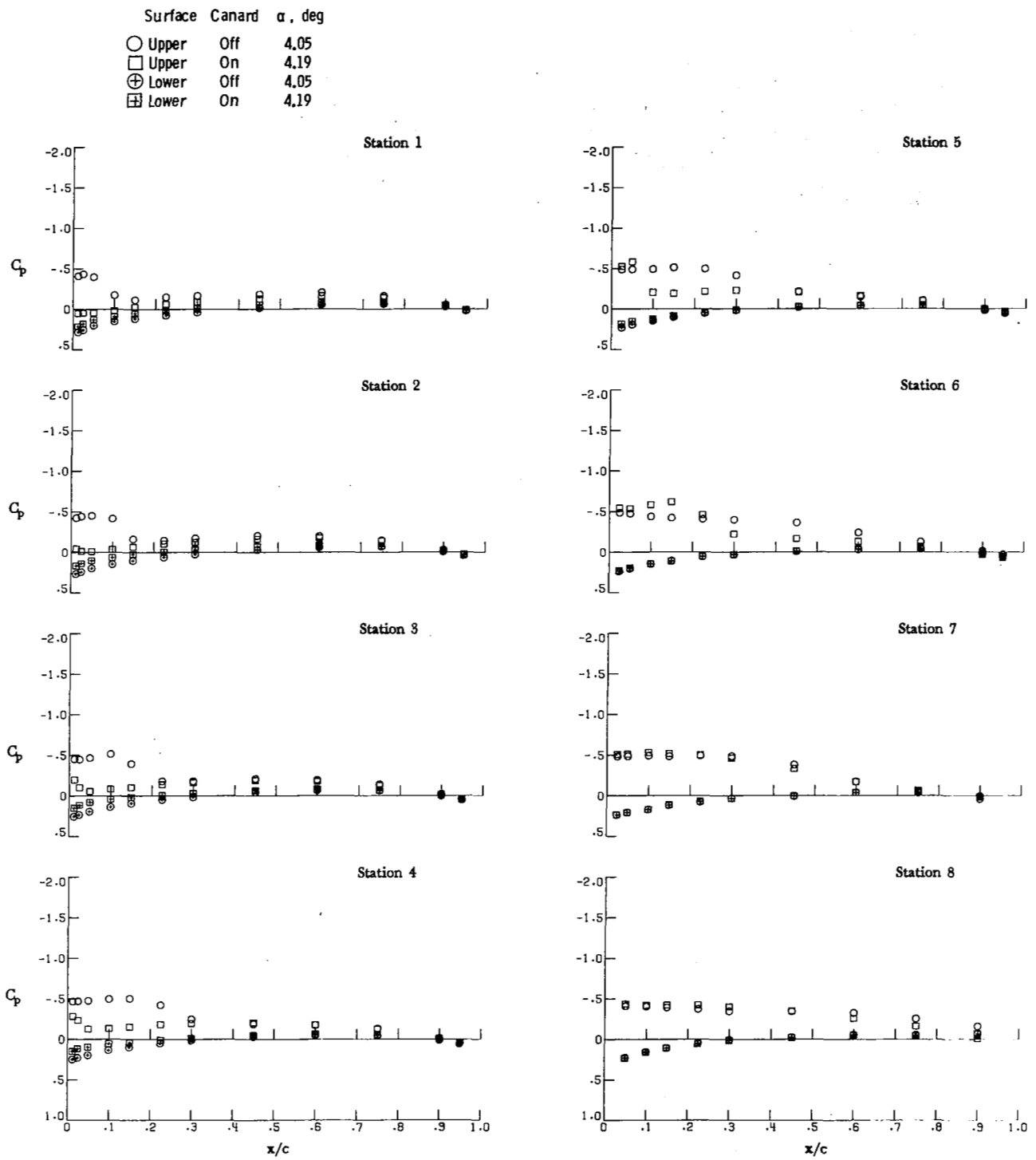

(a) $\alpha \approx 4^{\circ}$.

Figure 3.- Effect of canard flow field on wing pressures for $z/\bar{c} = 0.0$; $M_\infty = 0.70$.

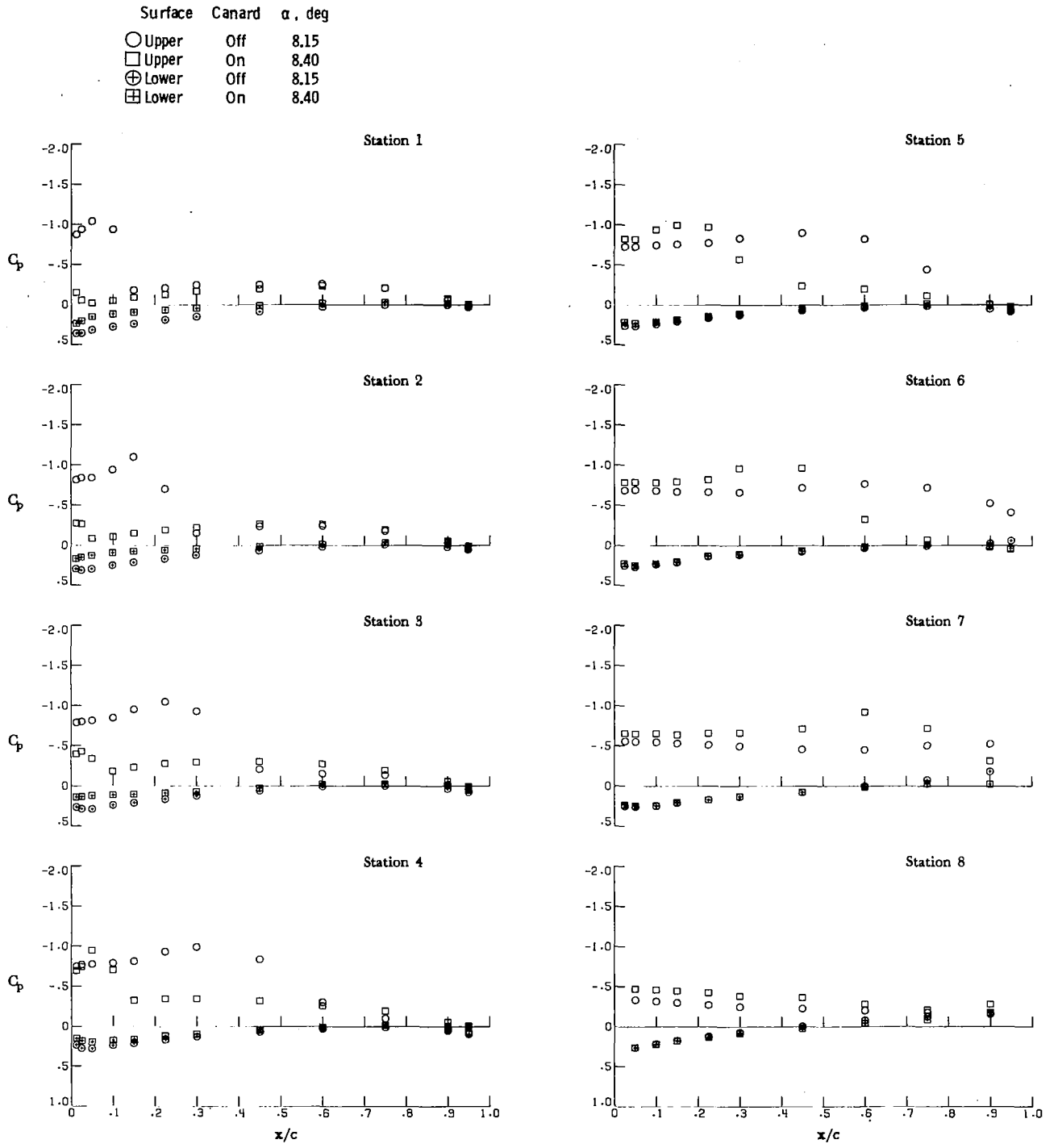

(b) $\alpha \approx 8^{\circ}$.

Figure 3.- Continued.

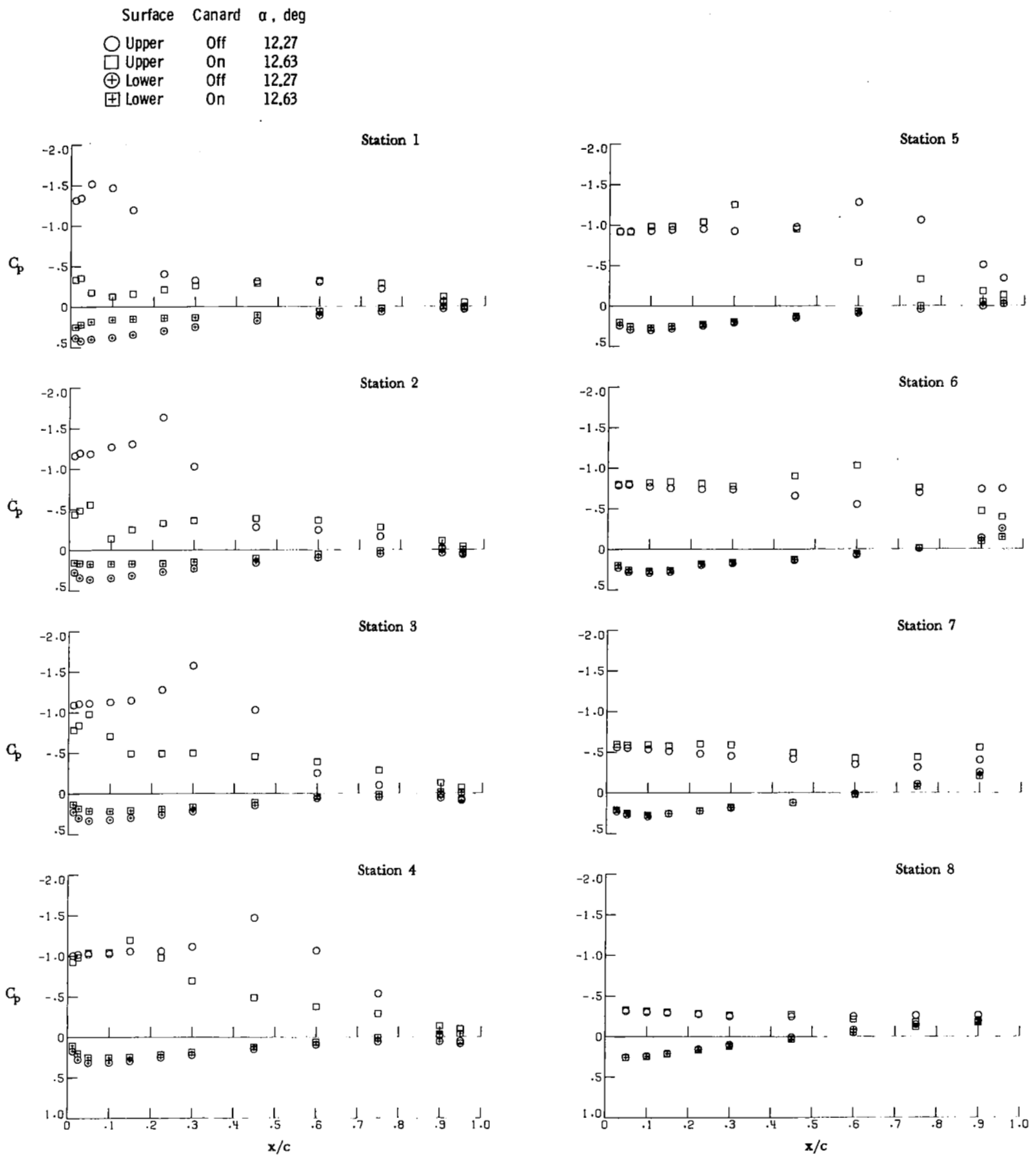

(c) $\alpha \approx 12^{\circ}$.

Figure 3.- Continued.

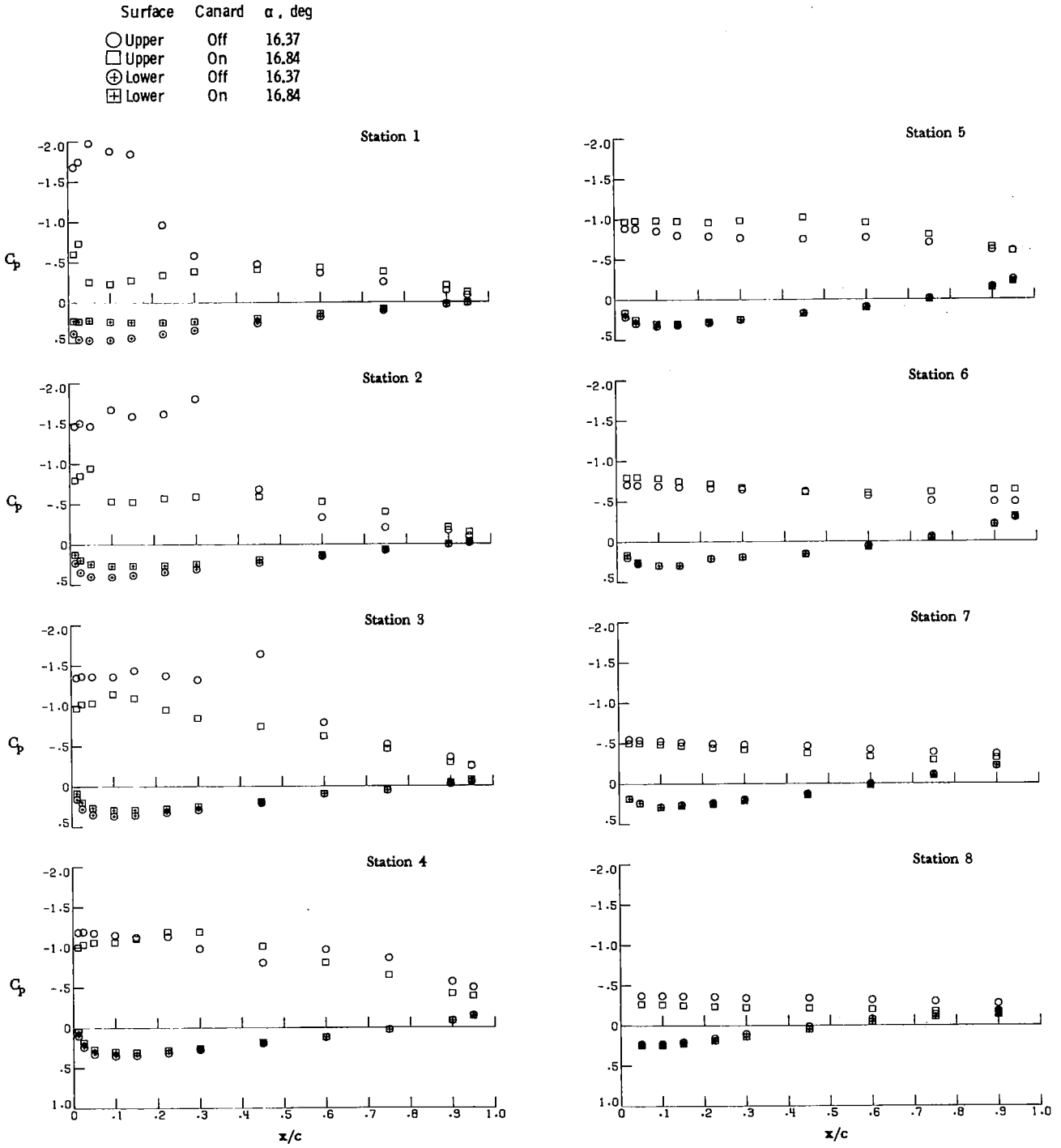

(d) $\alpha \approx 16°$.

Figure 3.- Concluded.

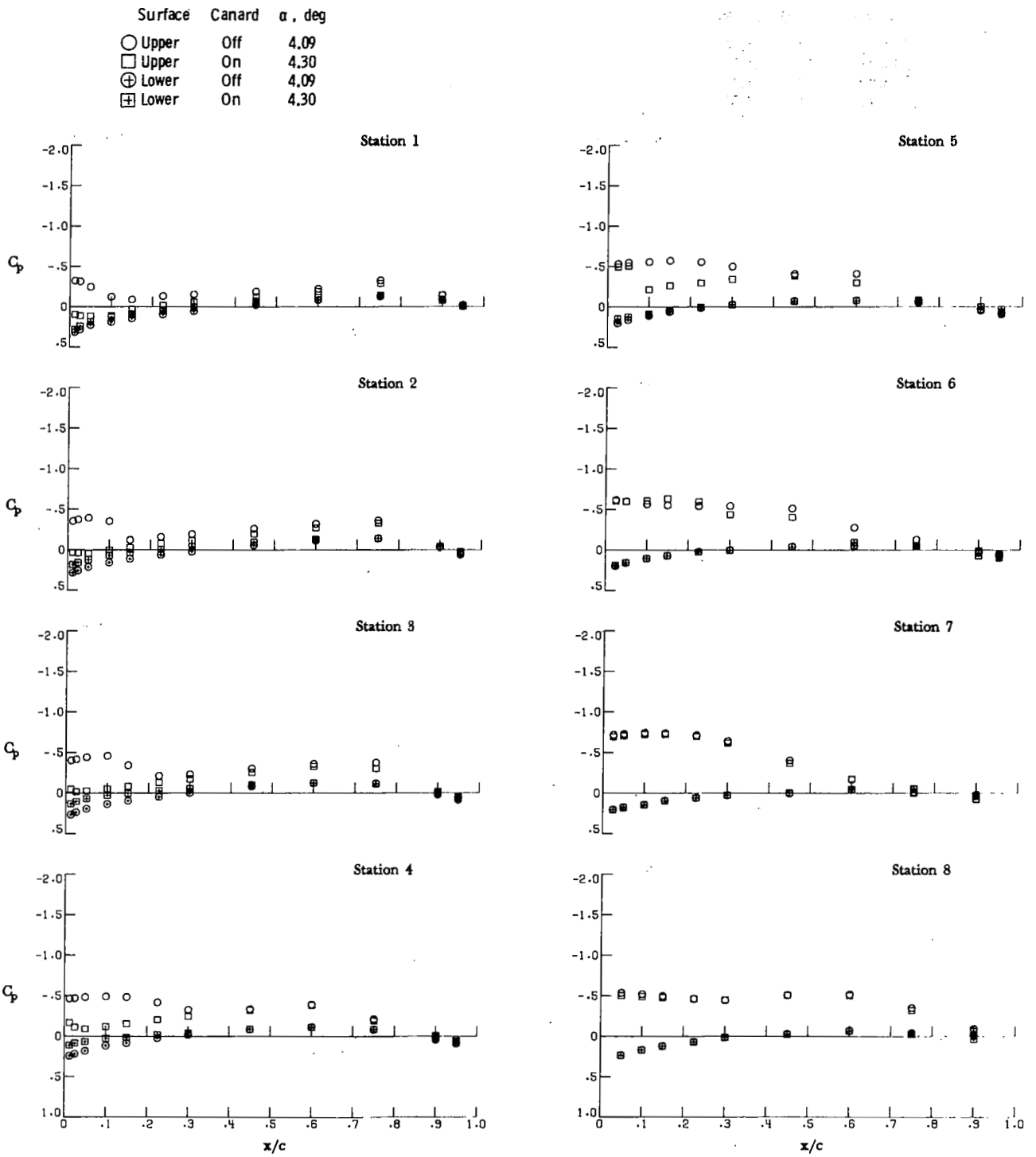

(a) $\alpha \approx 4^{\circ}$.

Figure 4.- Effect of canard flow field on wing pressures for $z/\bar{c} = 0.0$; $M_\infty = 0.95$.

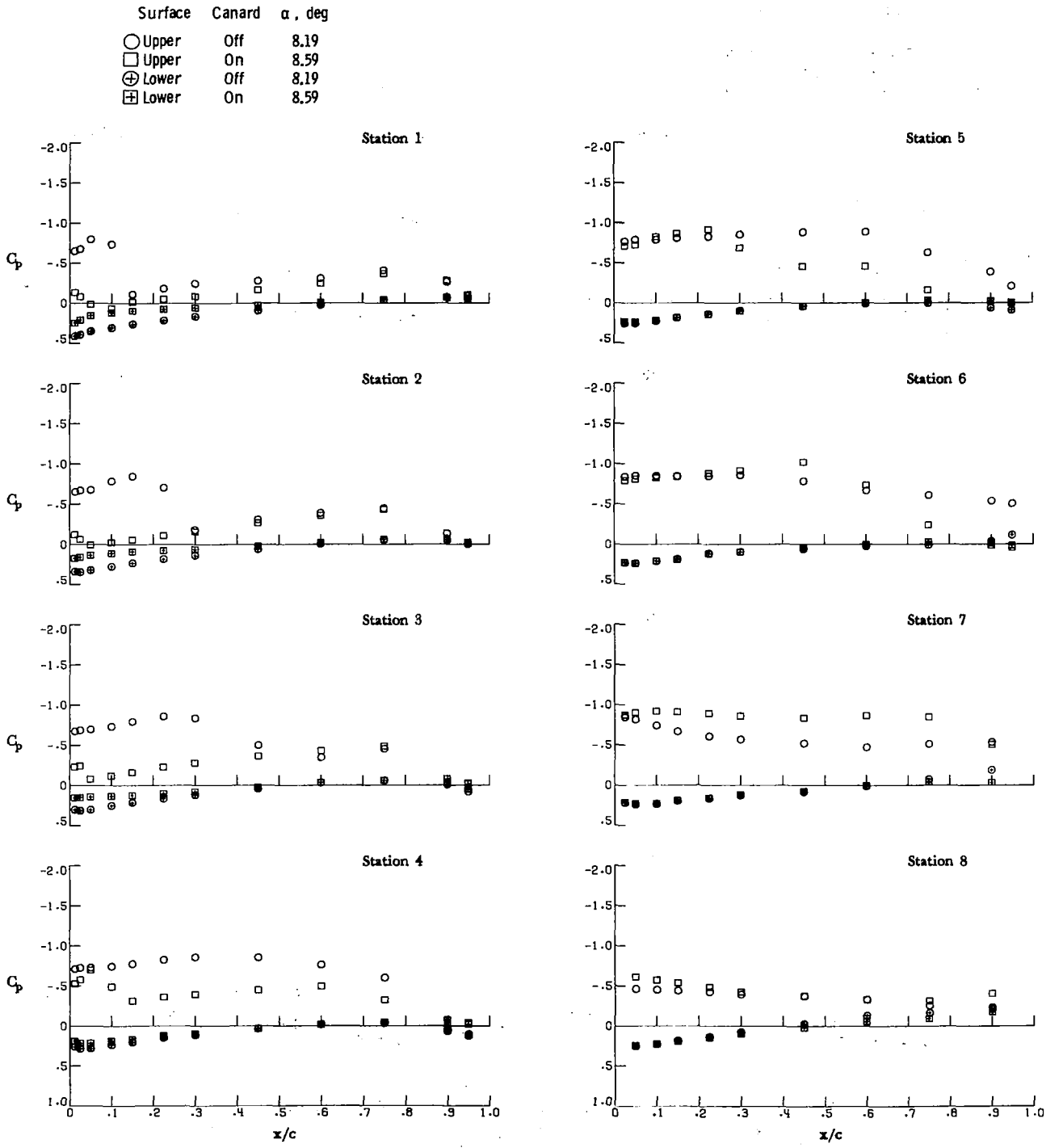

(b) $\alpha \approx 8^{\circ}$.

Figure 4.- Continued.

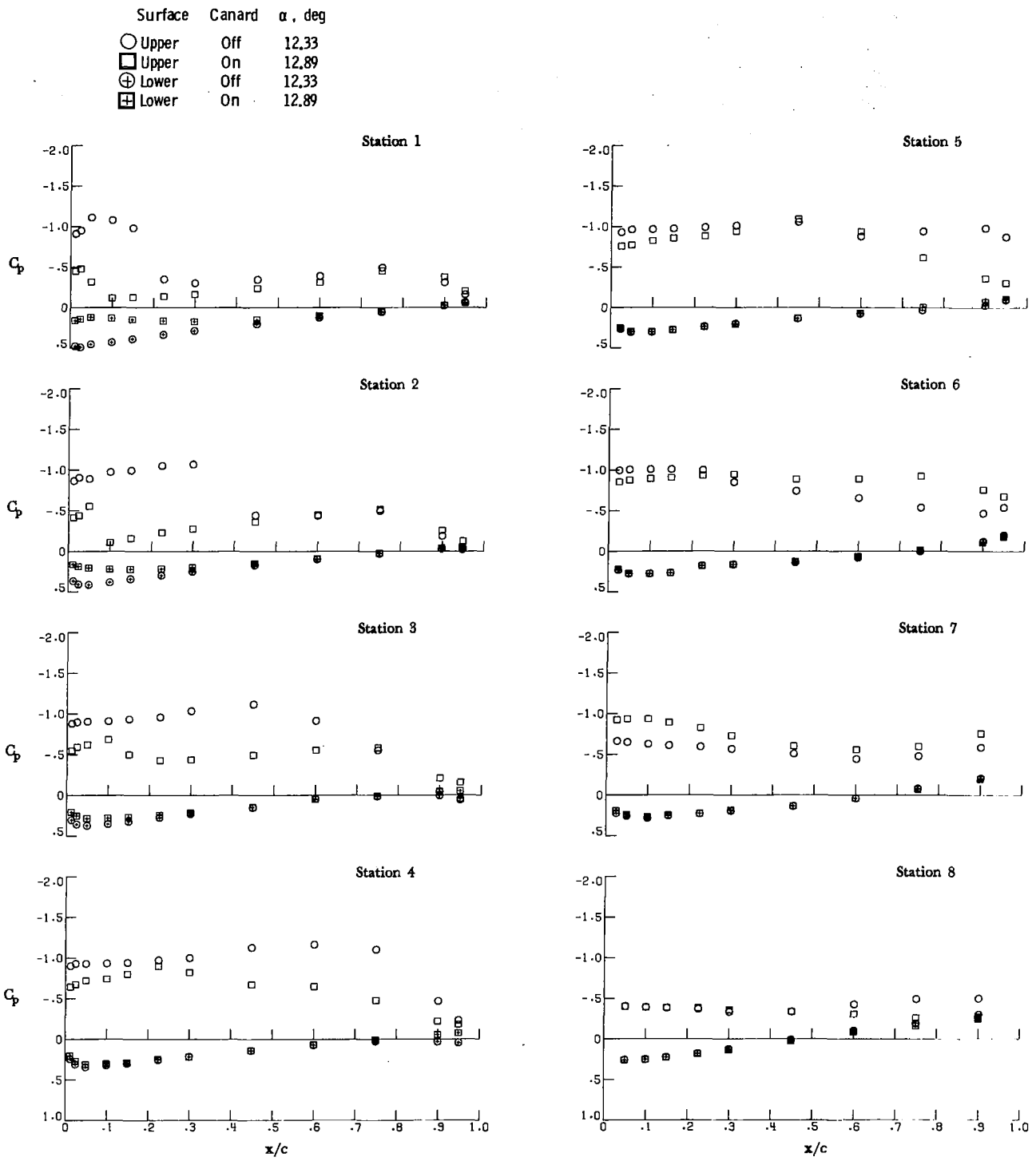

(c) $\alpha \approx 12^{\circ}$.

Figure 4.- Continued.

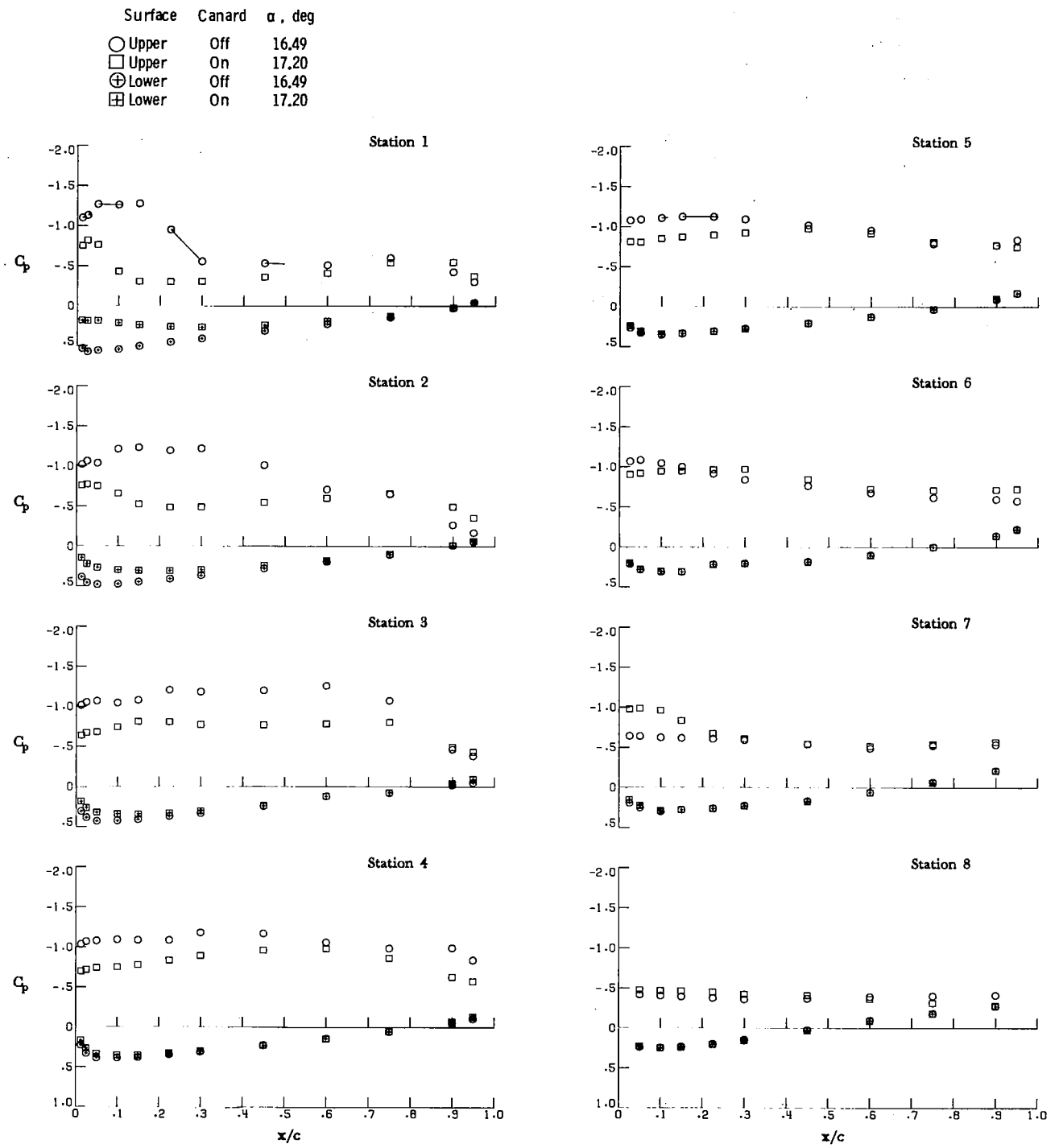

(d) $\alpha \approx 16°$.

Figure 4.- Concluded.

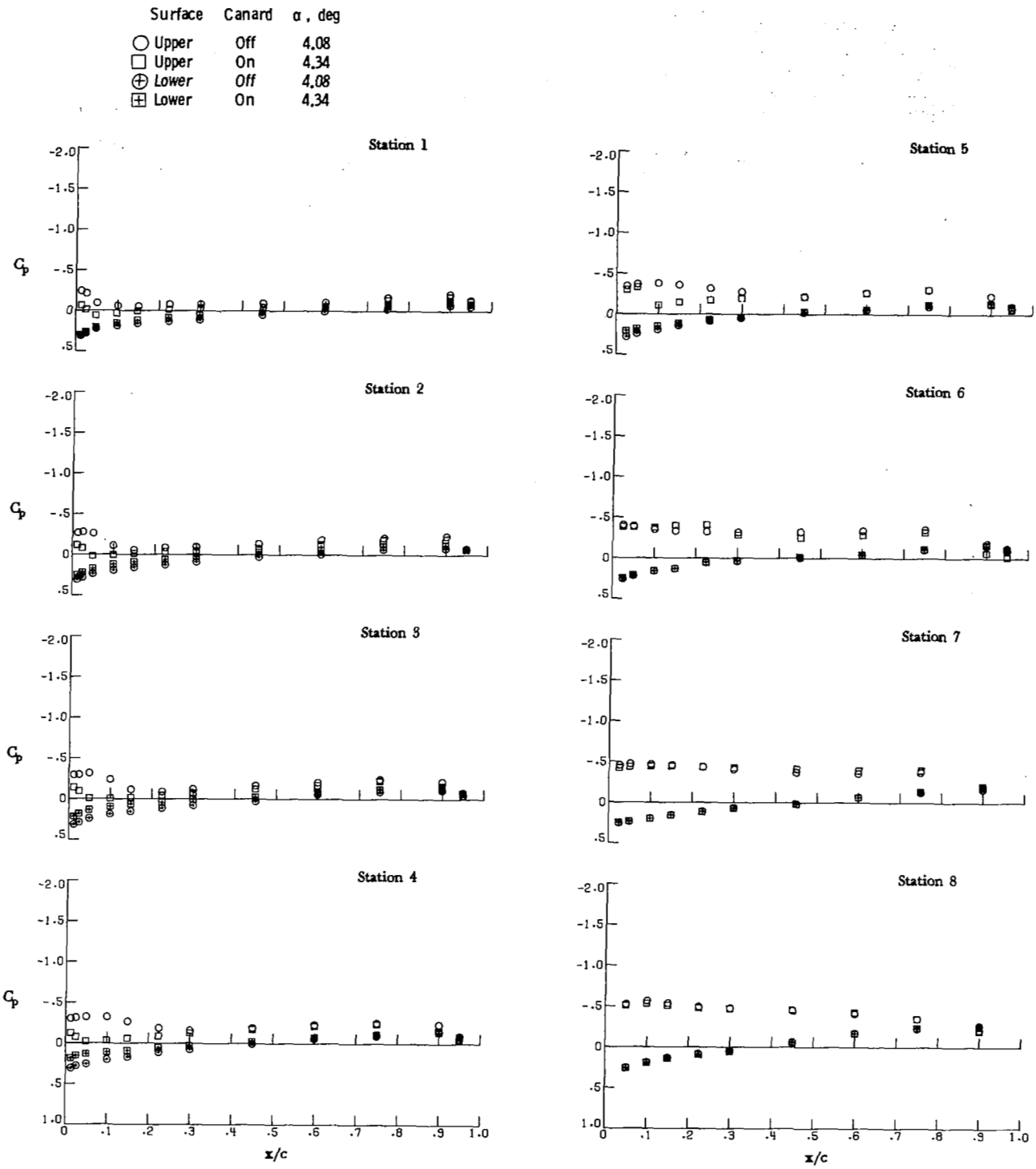

(a) $\alpha \approx 4^{\circ}$.

Figure 5.- Effect of canard flow field on wing pressures for $z/\bar{c} = 0.0$; $M_\infty = 1.20$.

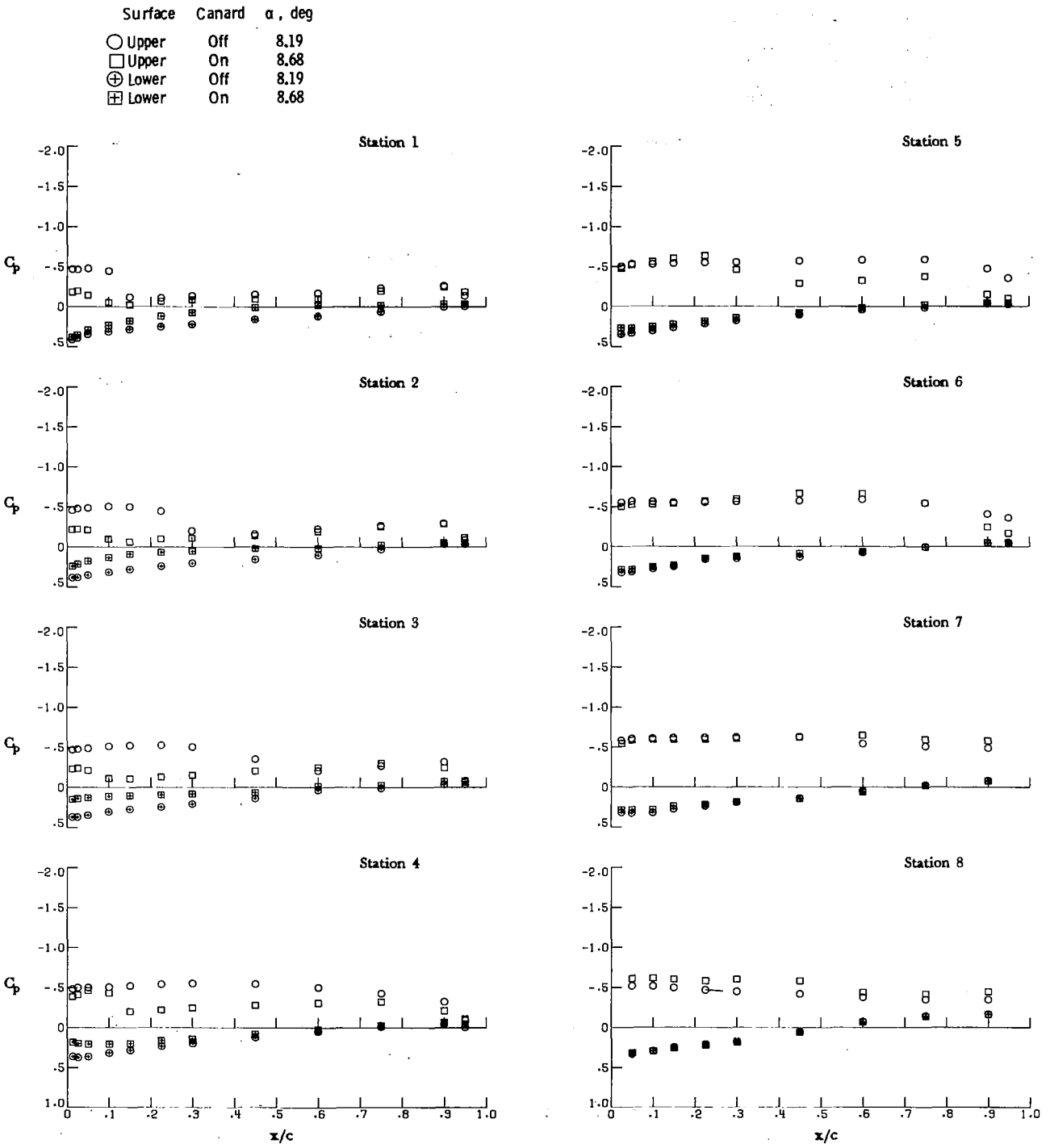

(b) $\alpha \approx 8^{\circ}$.

Figure 5.- Continued.

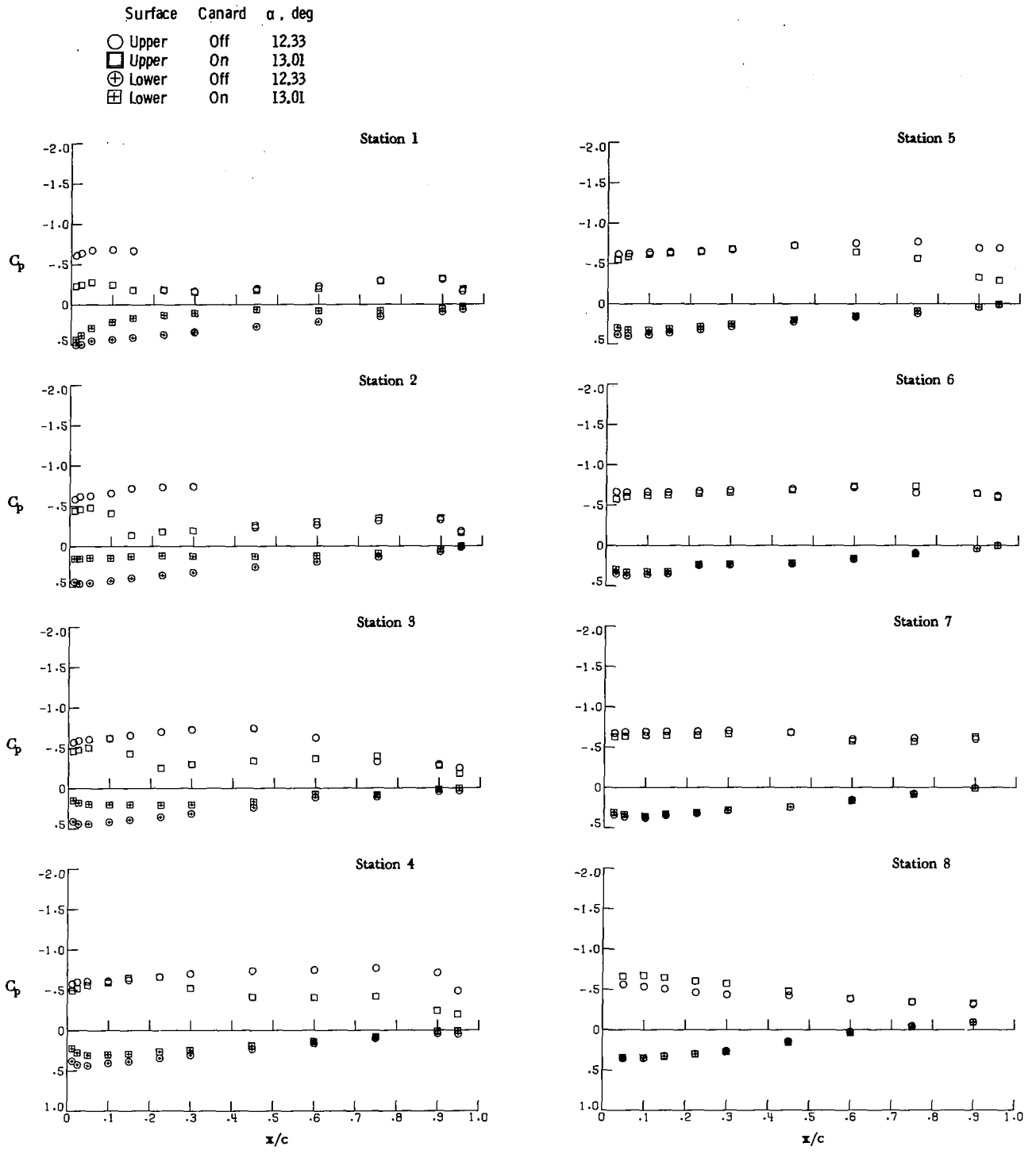

(c) $\alpha \approx 12^{\circ}$.

Figure 5.- Continued.

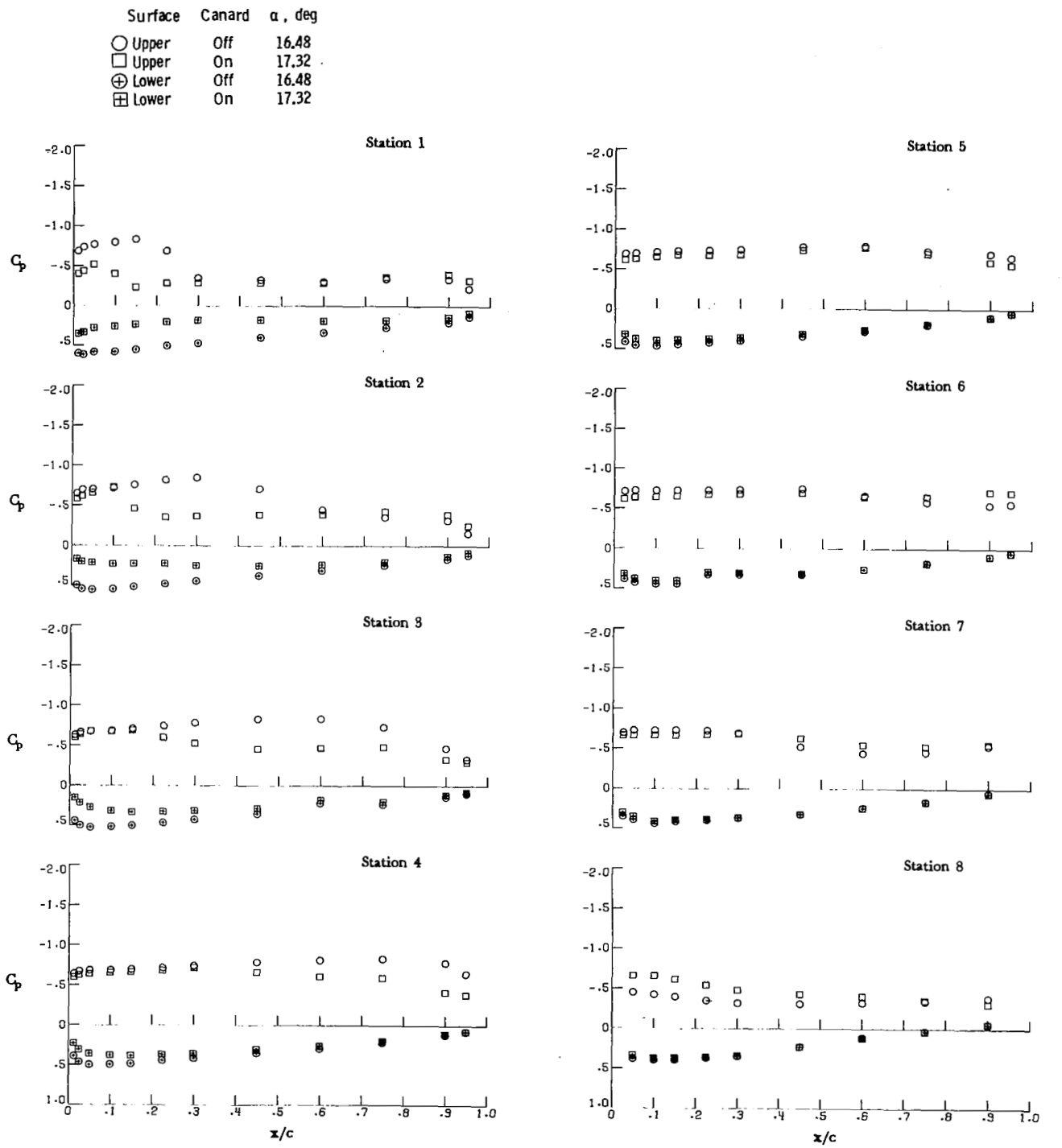

(d) $\alpha \approx 16°$.

Figure 5.- Concluded.

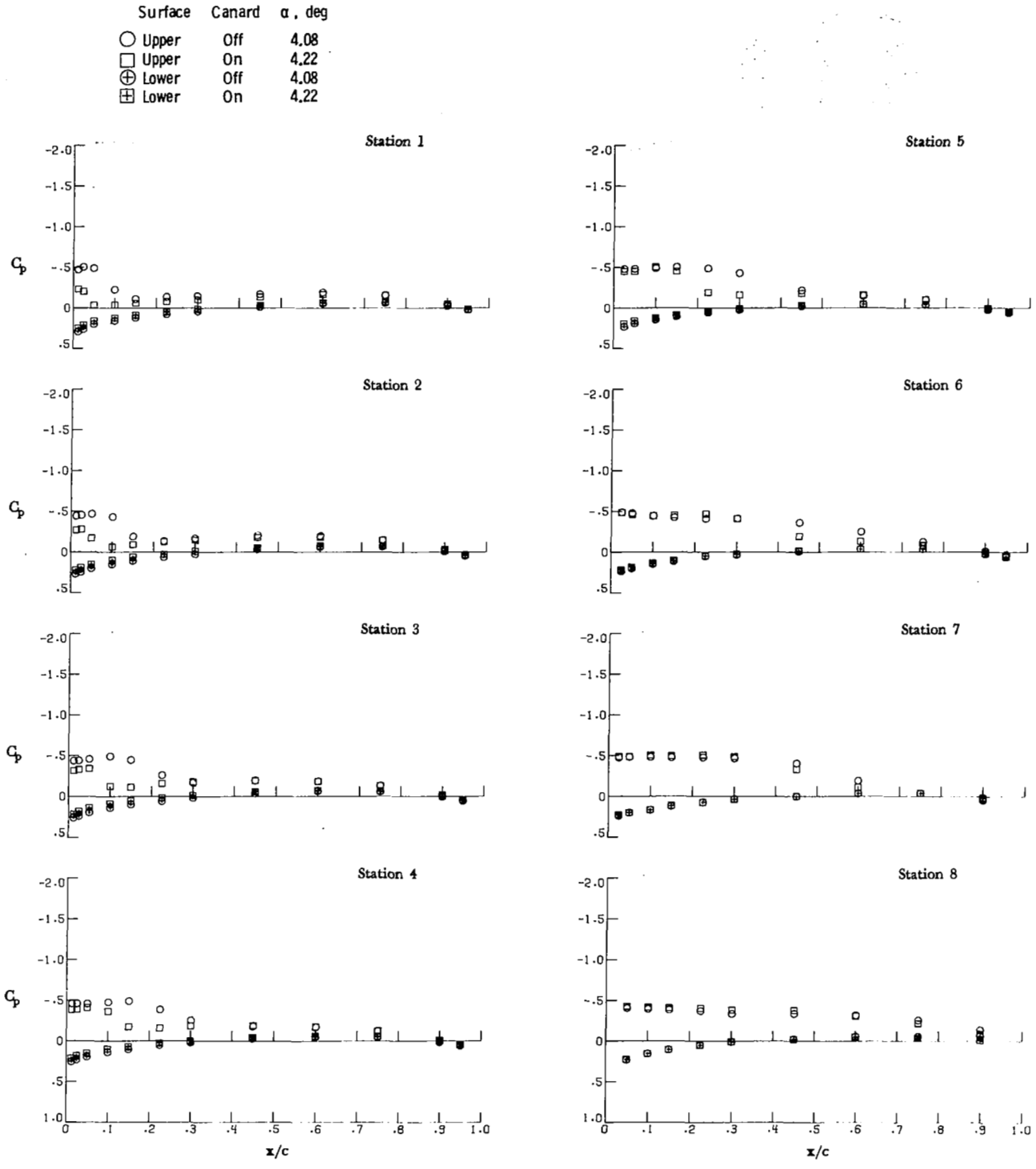

(a) $\alpha \approx 4^{\circ}$.

Figure 6.- Effect of canard flow field on wing pressures for $z/\bar{c} = 0.185$; $M_\infty = 0.70$.

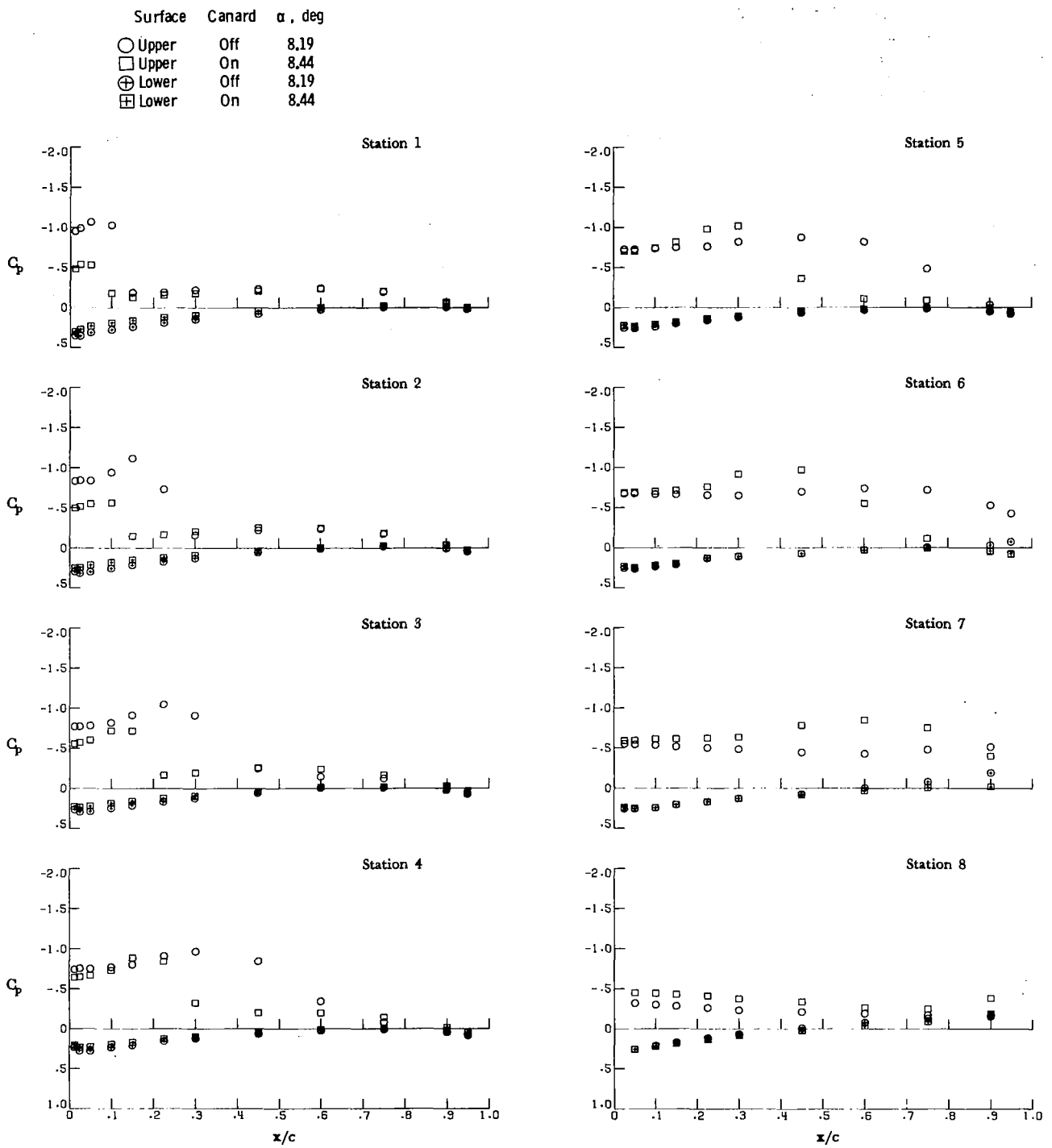

(b) $\alpha \approx 8^\circ$.

Figure 6.- Continued.

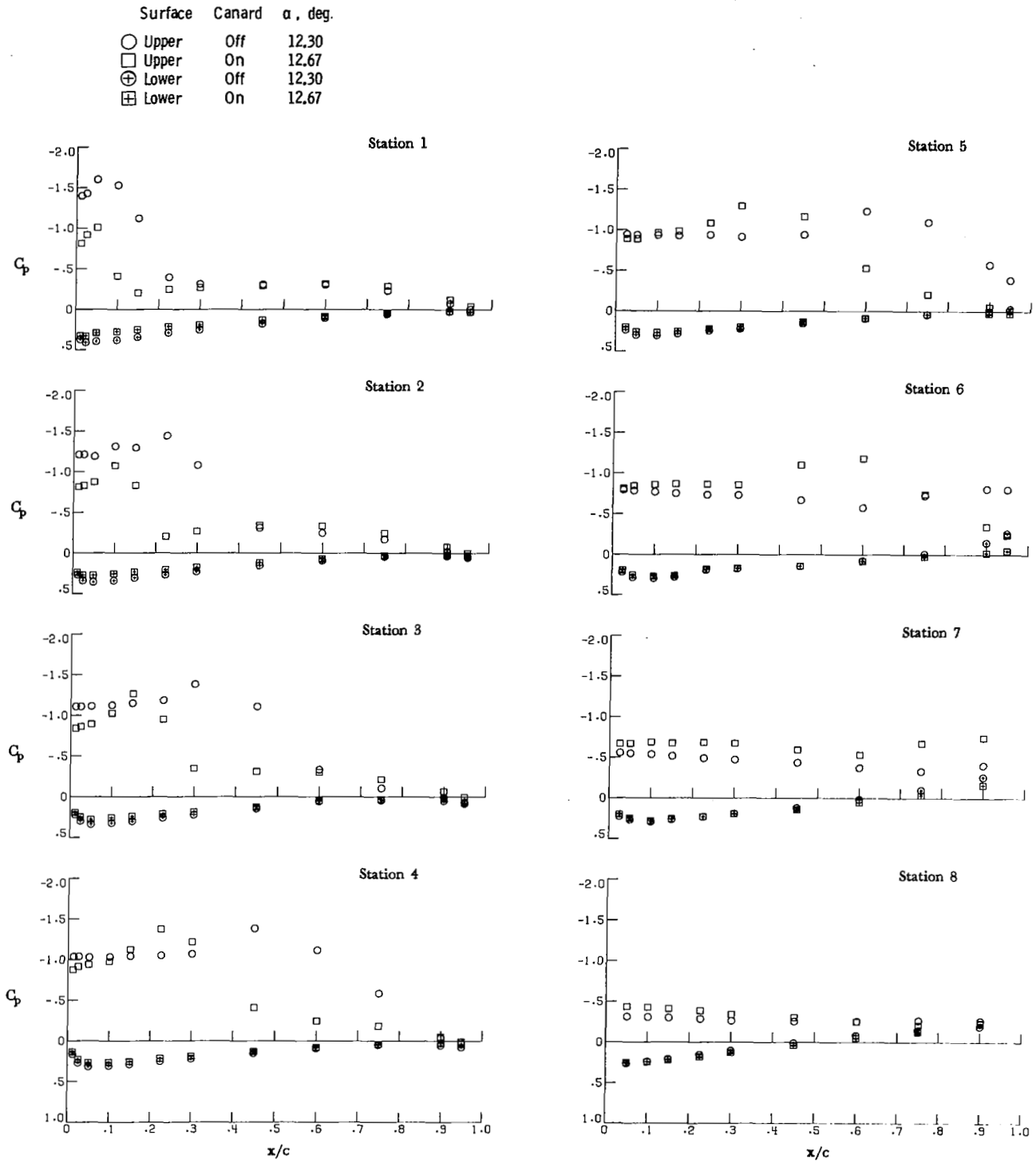

(c) $\alpha \approx 12^{\circ}$.

Figure 6.- Continued.

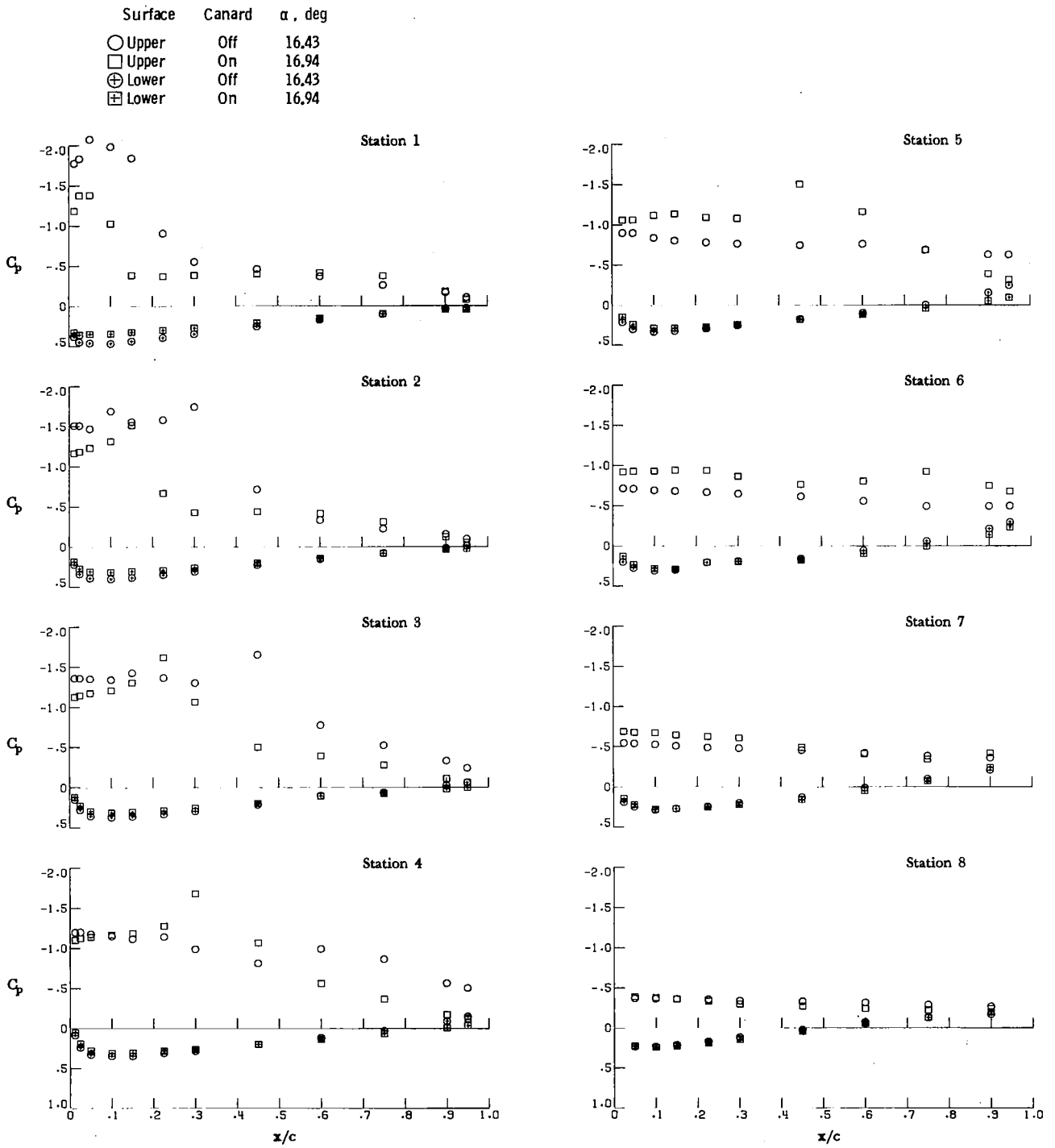

(d) $\alpha \approx 16^{\circ}$.

Figure 6.- Concluded.

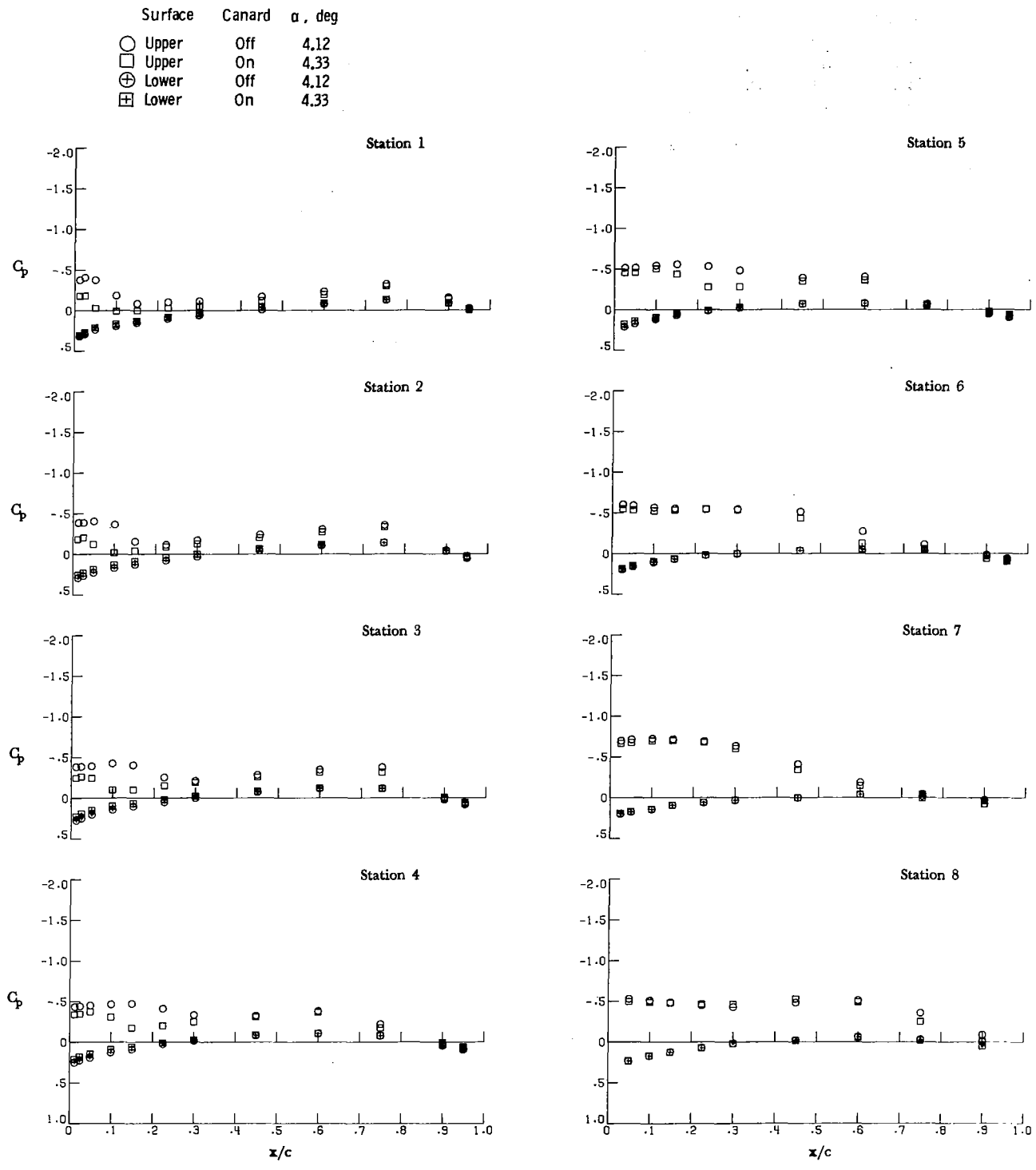

(a) $\alpha \approx 4^{\circ}$.

Figure 7.- Effect of canard flow field on wing pressures for $z/\bar{c} = 0.185$; $M_\infty = 0.95$.

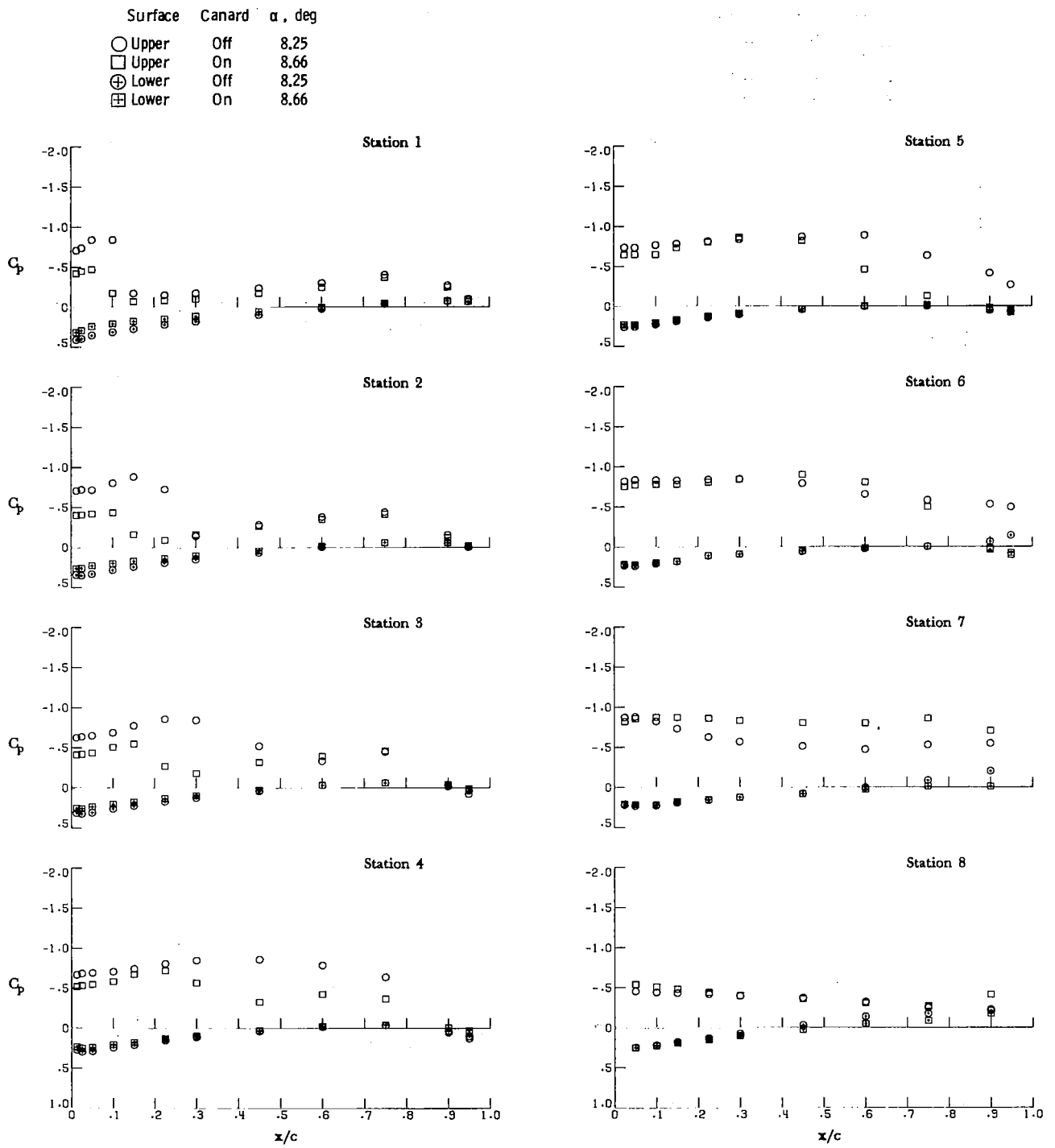

(b) $\alpha \approx 8^{\circ}$.

Figure 7.- Continued.

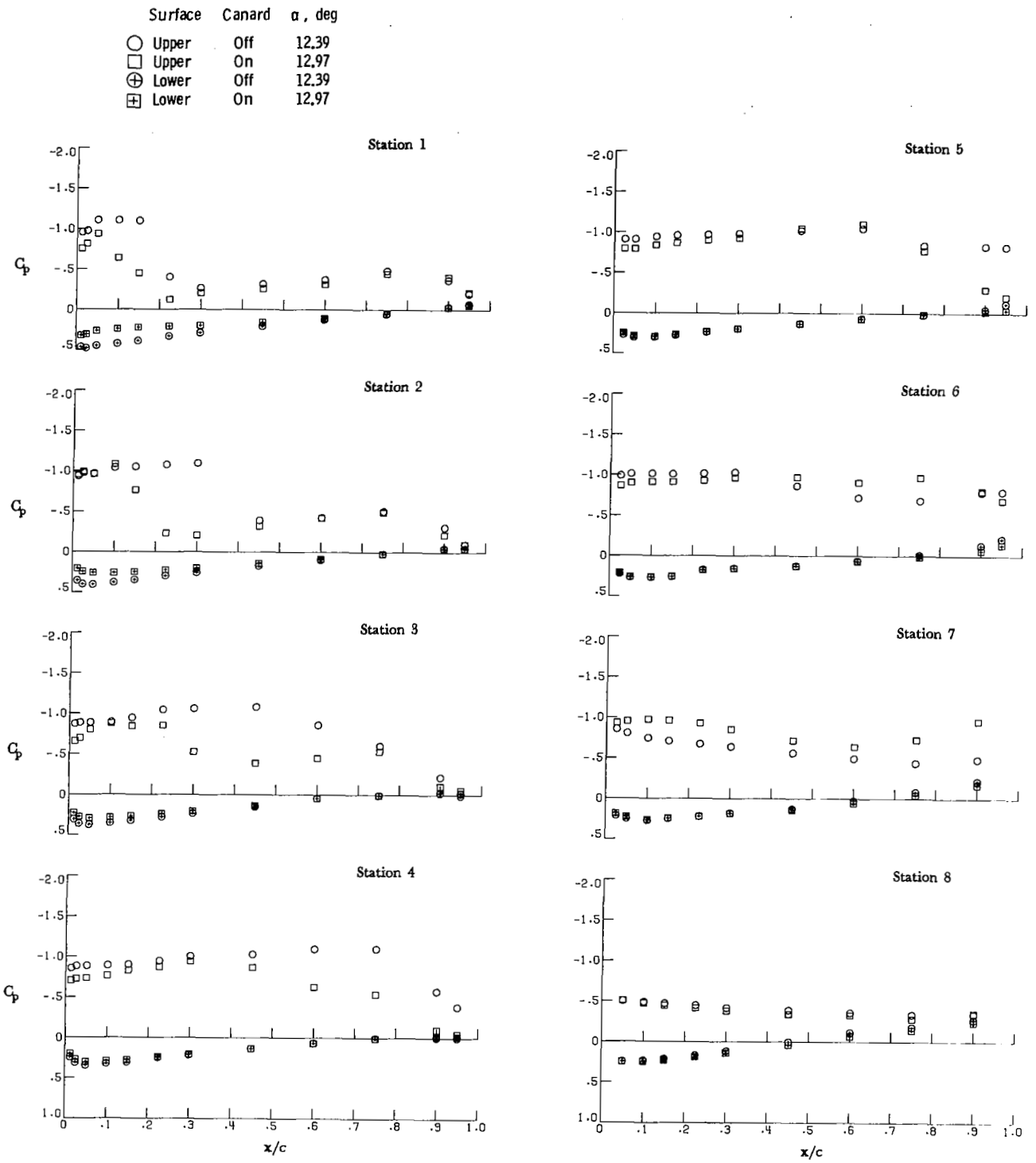

(c) $\alpha \approx 12^{\circ}$.

Figure 7.- Continued.

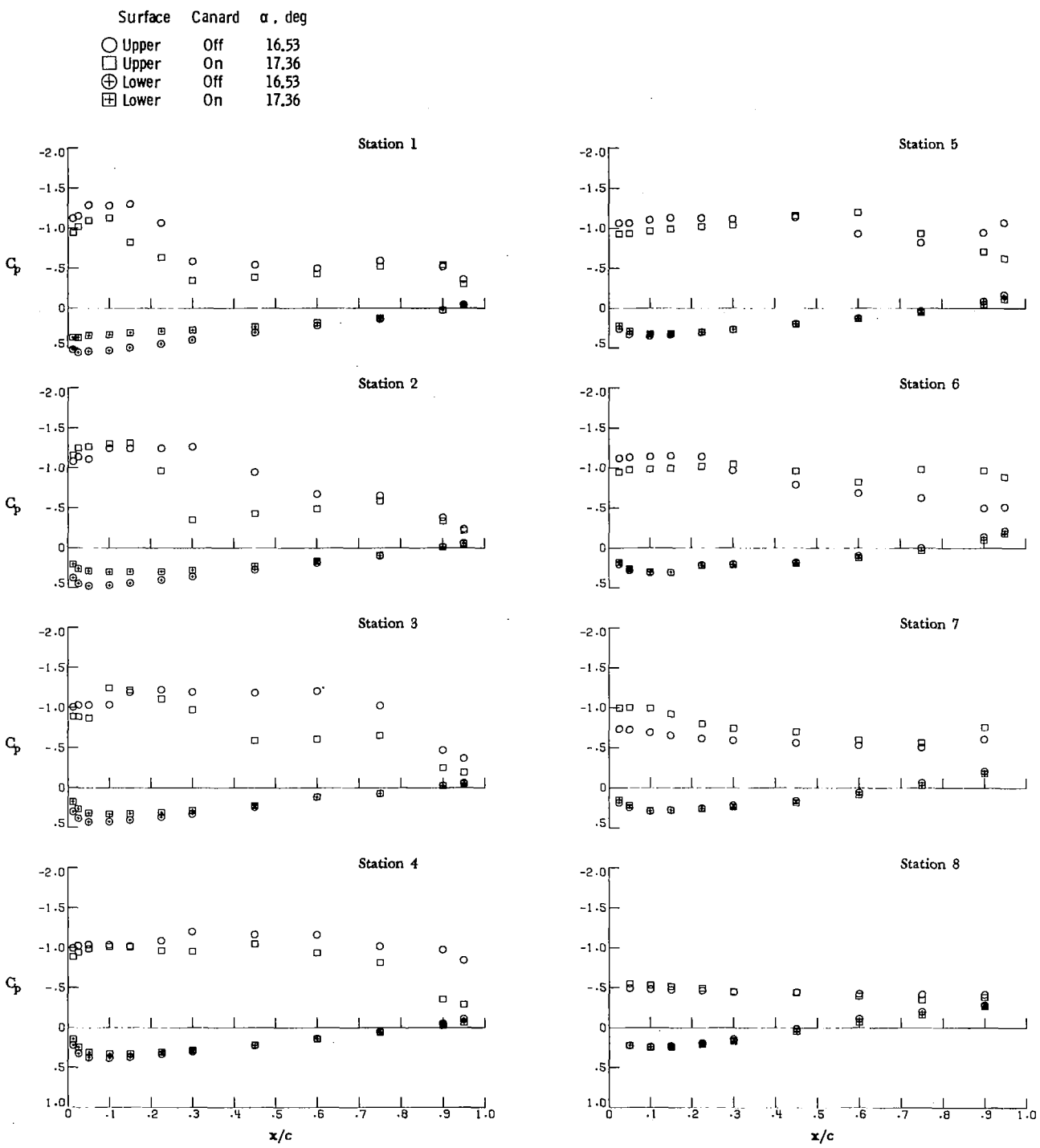

(d) $\alpha \approx 16^{\circ}$.

Figure 7.- Concluded.

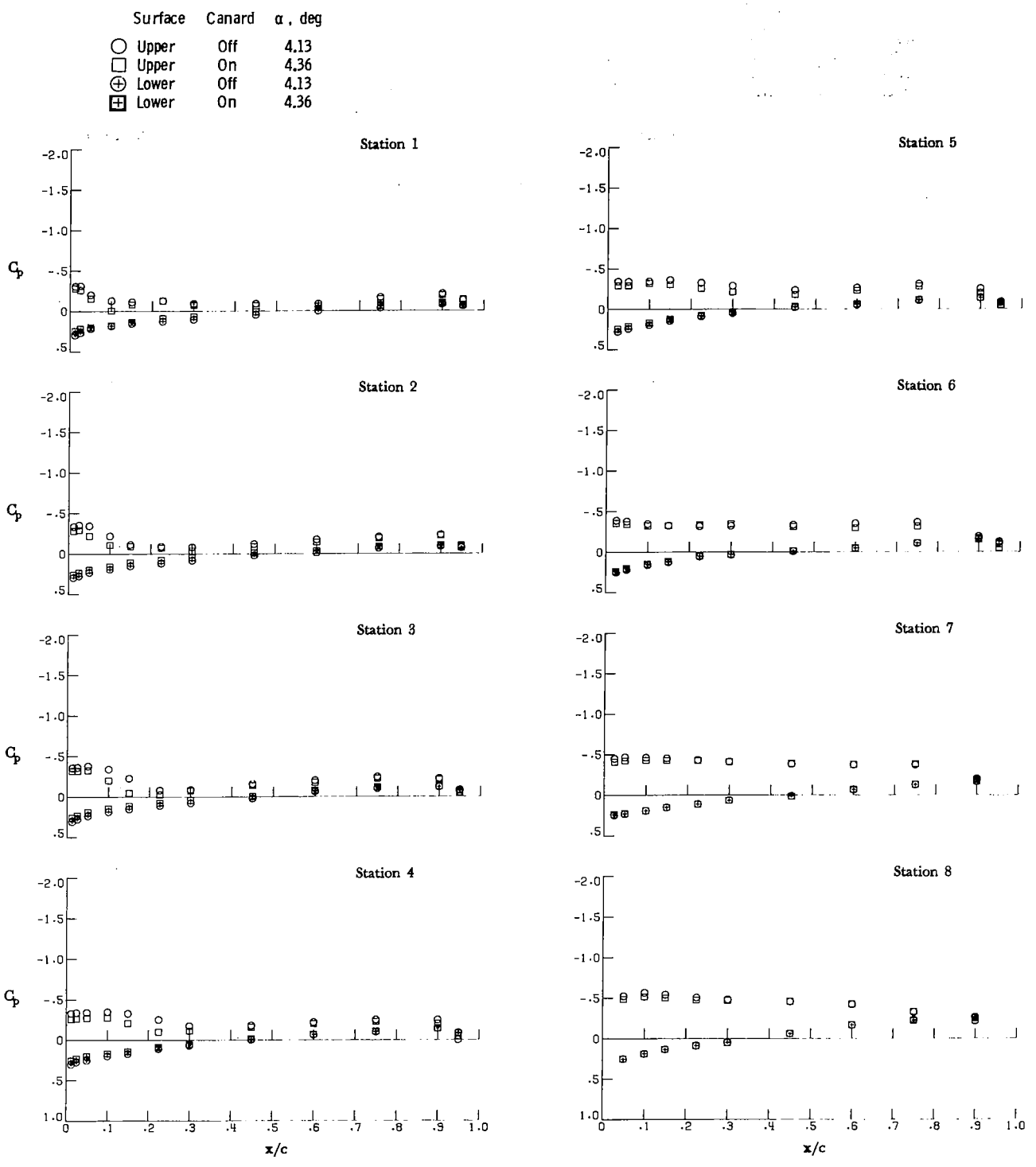

(a) $\alpha \approx 4^\circ$.

Figure 8.- Effect of canard flow field on wing pressures for $z/\bar{c} = 0.185$; $M_\infty = 1.20$.

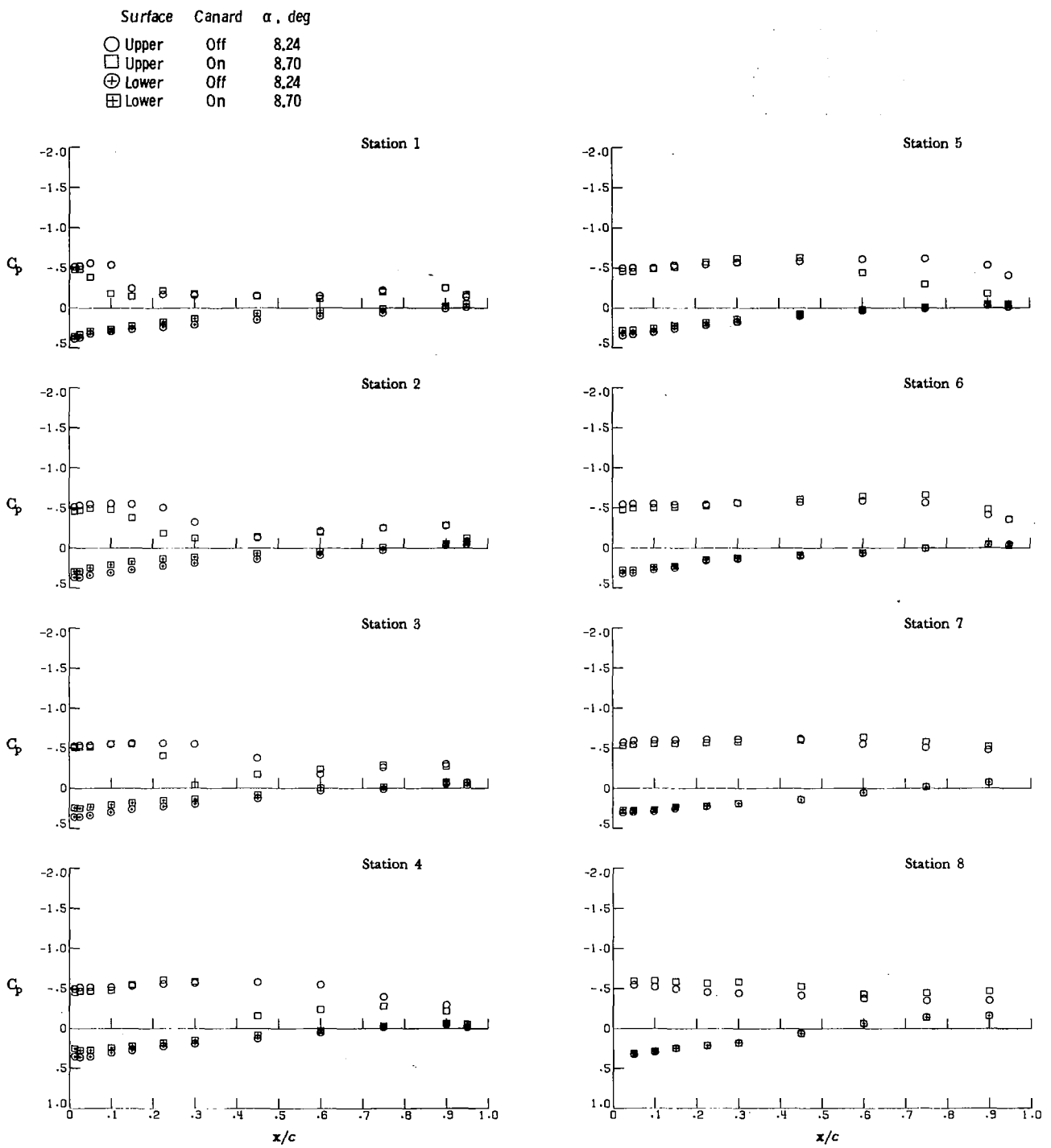

(b) $\alpha \approx 8^{\circ}$.

Figure 8.- Continued.

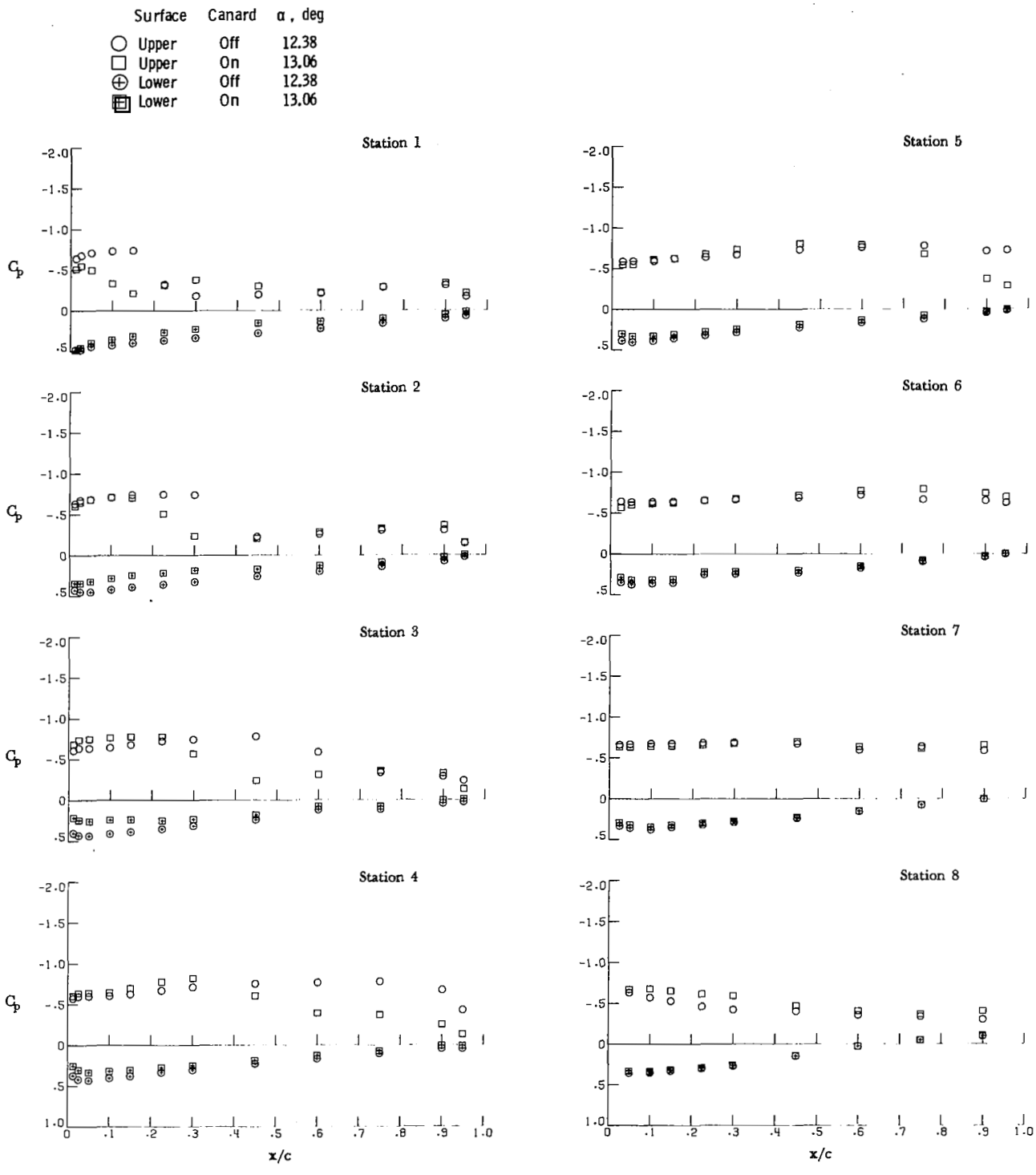

(c) $\alpha \approx 12^{\circ}$.

Figure 8.- Continued.

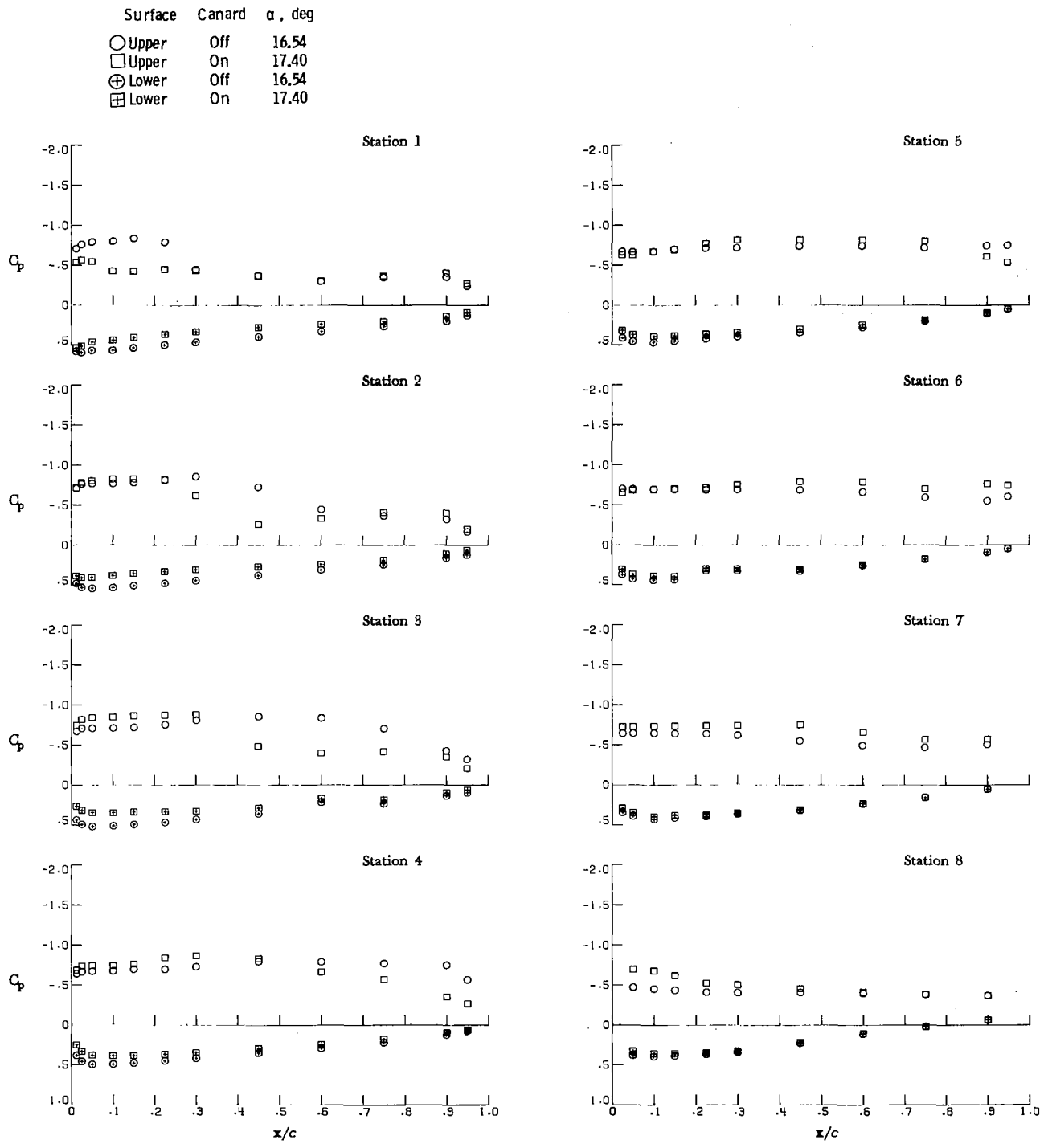

(d) $\alpha \approx 16^{\circ}$.

Figure 8.- Concluded.

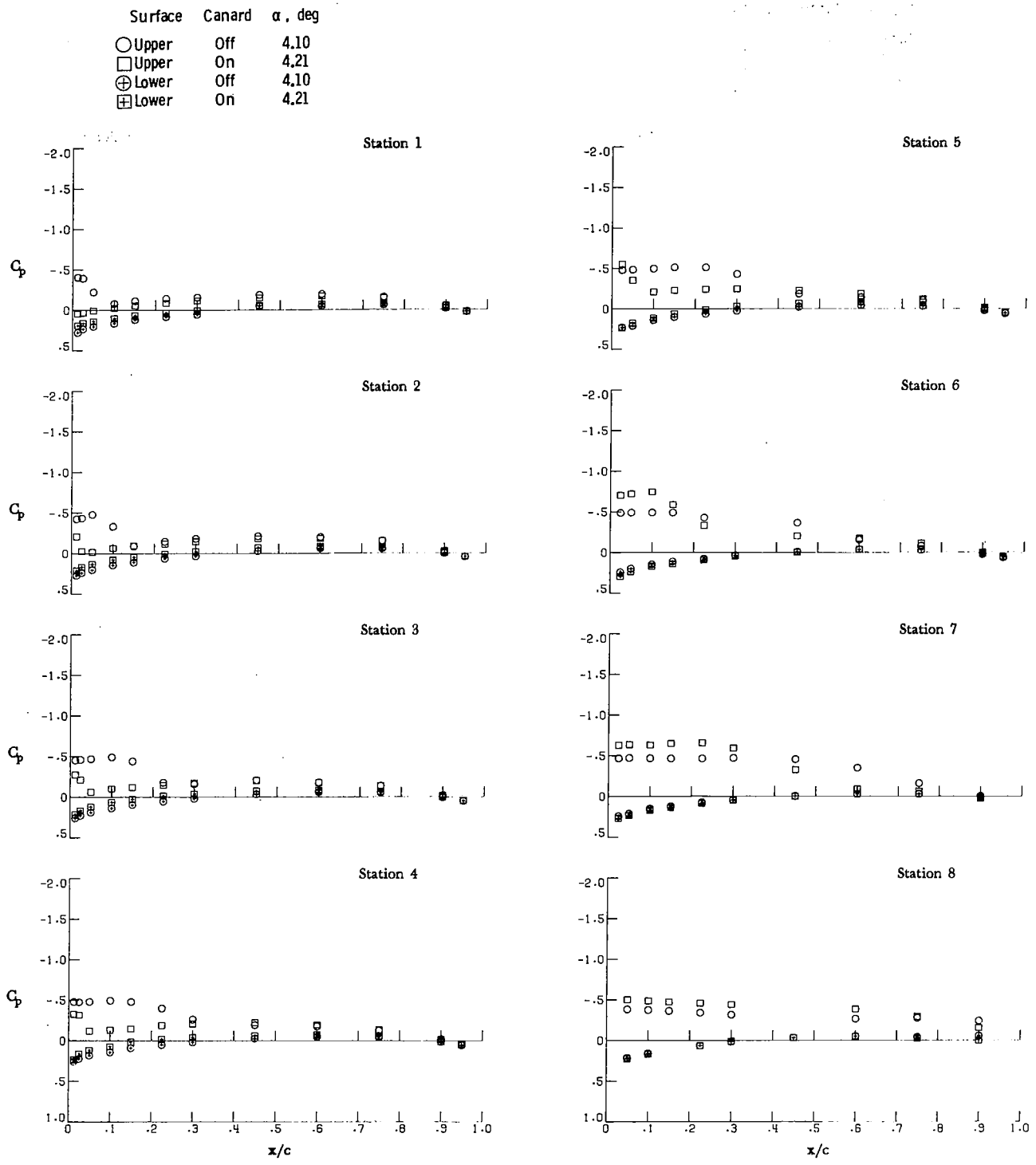

(a) $\alpha \approx 4^{\circ}$.

Figure 9.- Effect of canard flow field on wing pressures for $z/\bar{c} = -0.185$; $M_\infty = 0.70$.

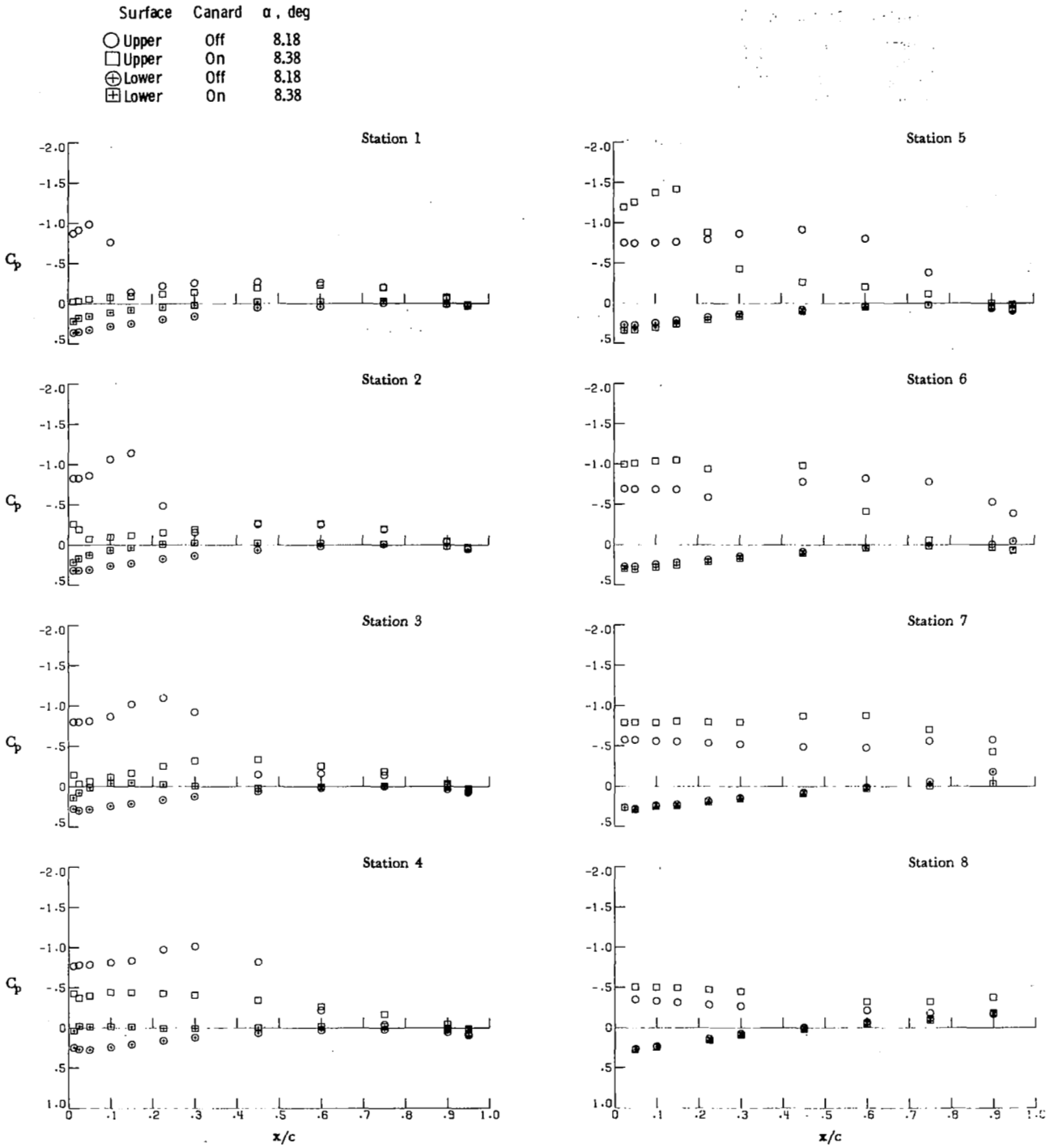

(b) $\alpha \approx 8^{\circ}$.

Figure 9.- Continued.

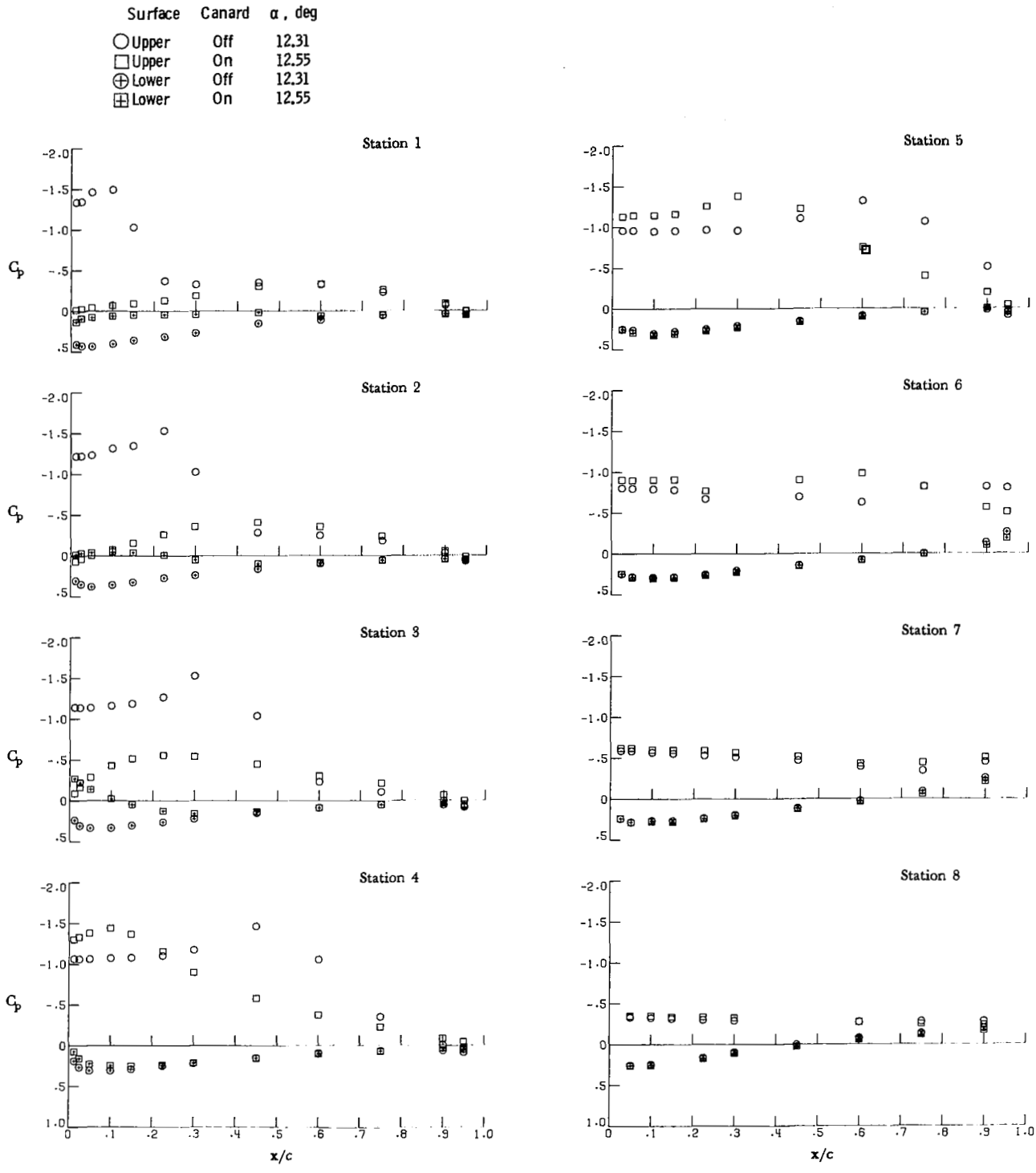

(c) $\alpha \approx 12^{\circ}$.

Figure 9.- Continued.

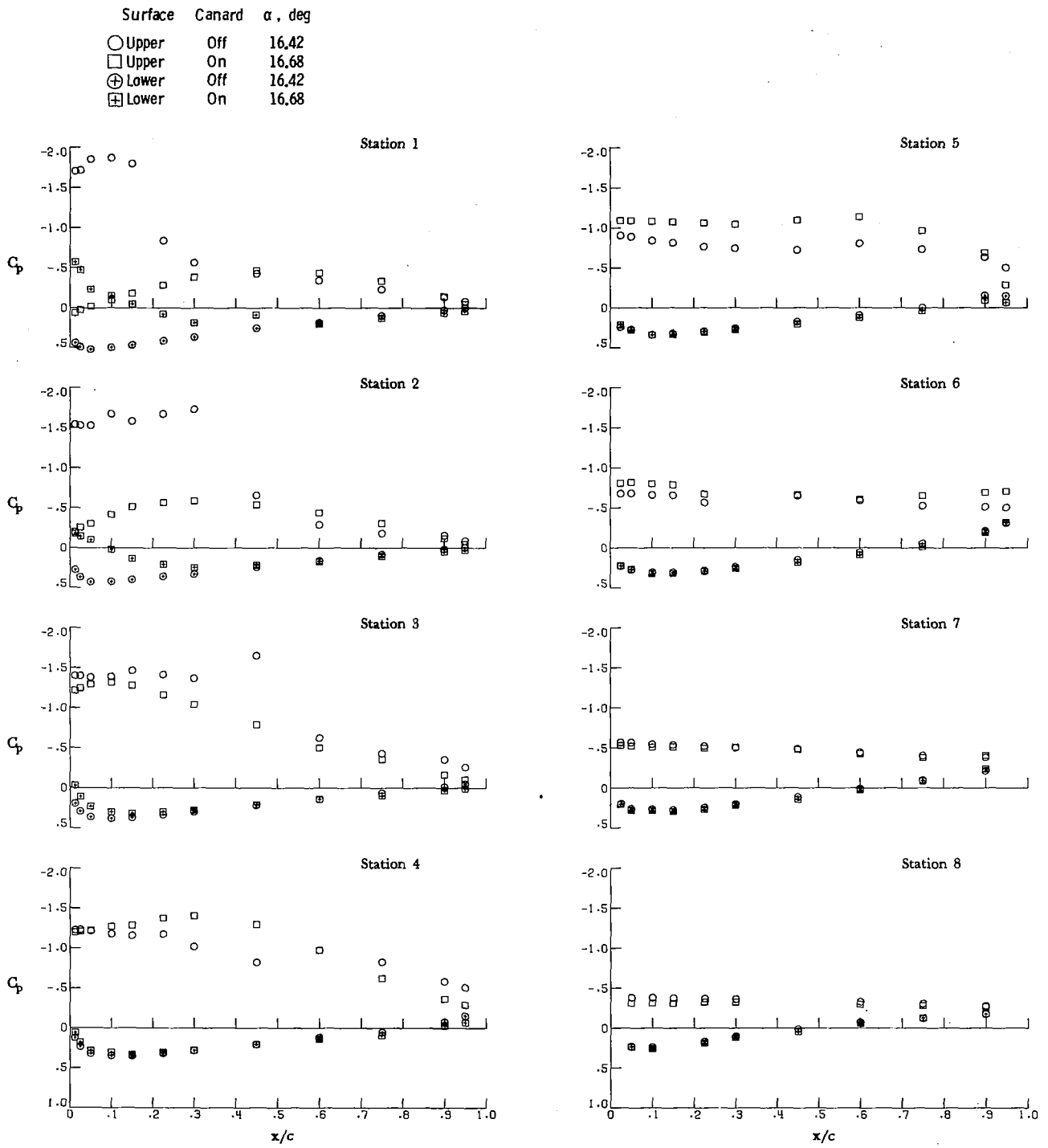

(d) $\alpha \approx 16^{\circ}$.

Figure 9.- Concluded.

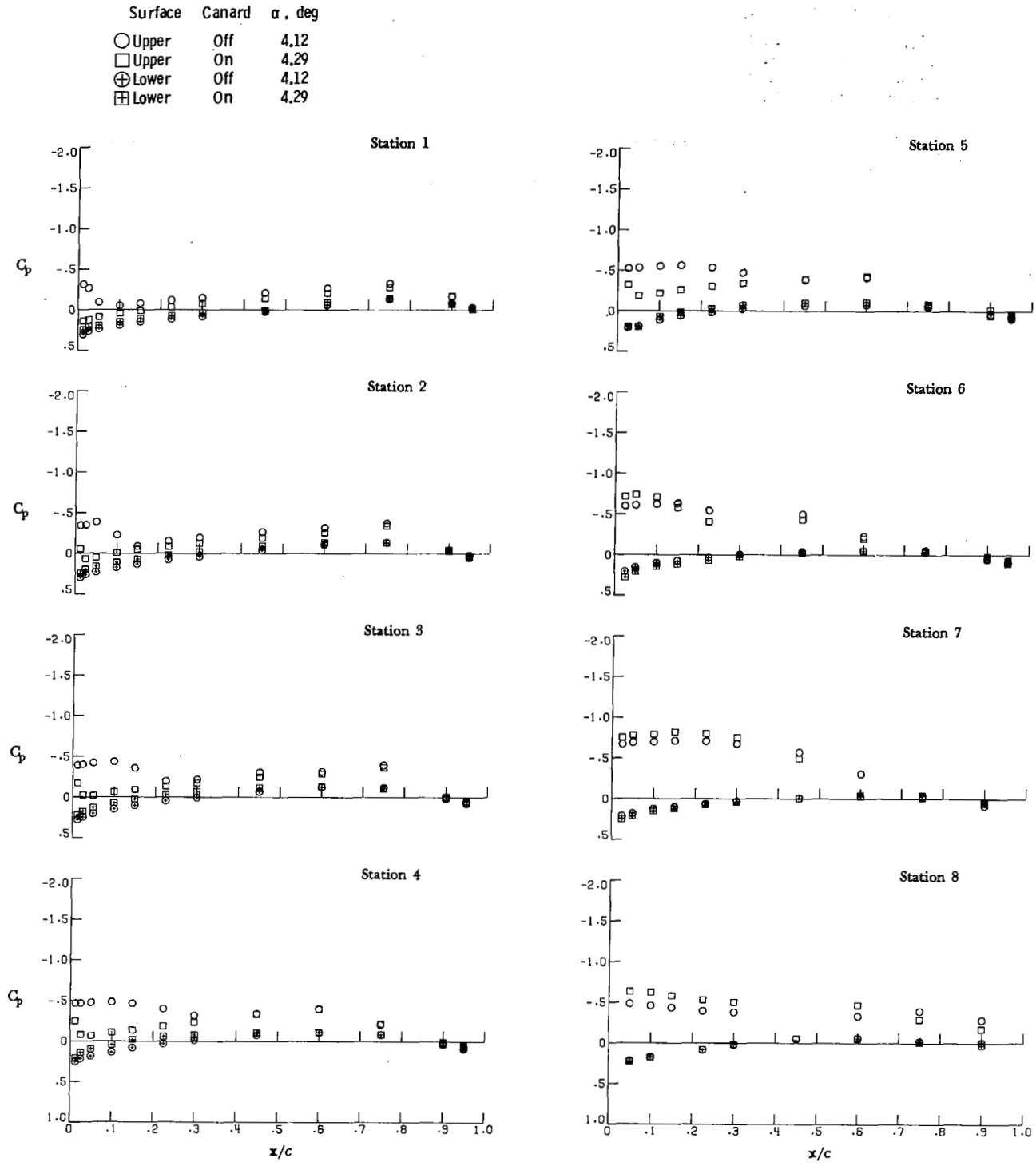

(a) $\alpha \approx 4^{\circ}$.

Figure 10.- Effect of canard flow field on wing pressures for $z/\bar{c} = -0.185$; $M_\infty = 0.95$.

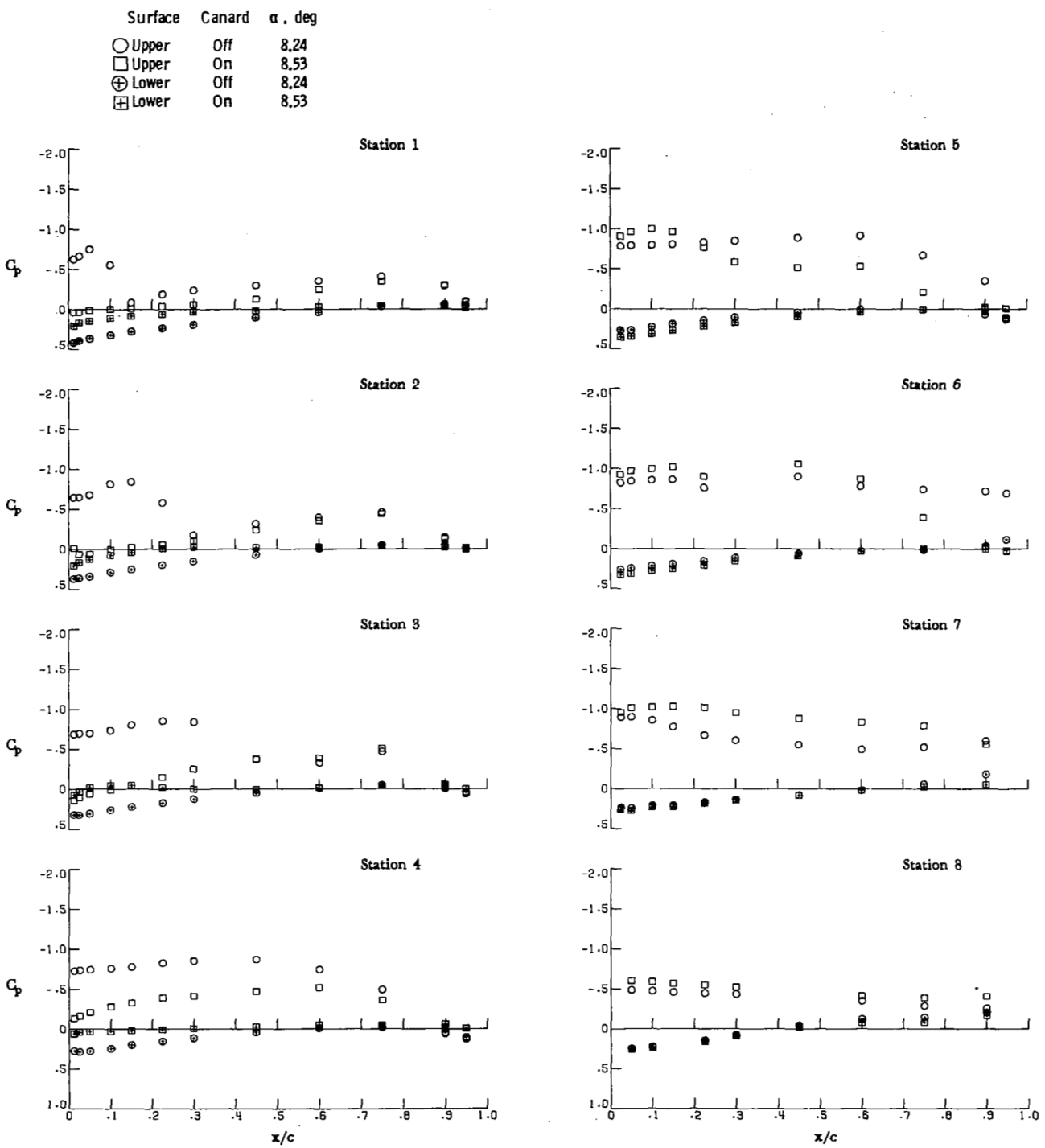

(b) $\alpha \approx 8^{\circ}$.

Figure 10.- Continued.

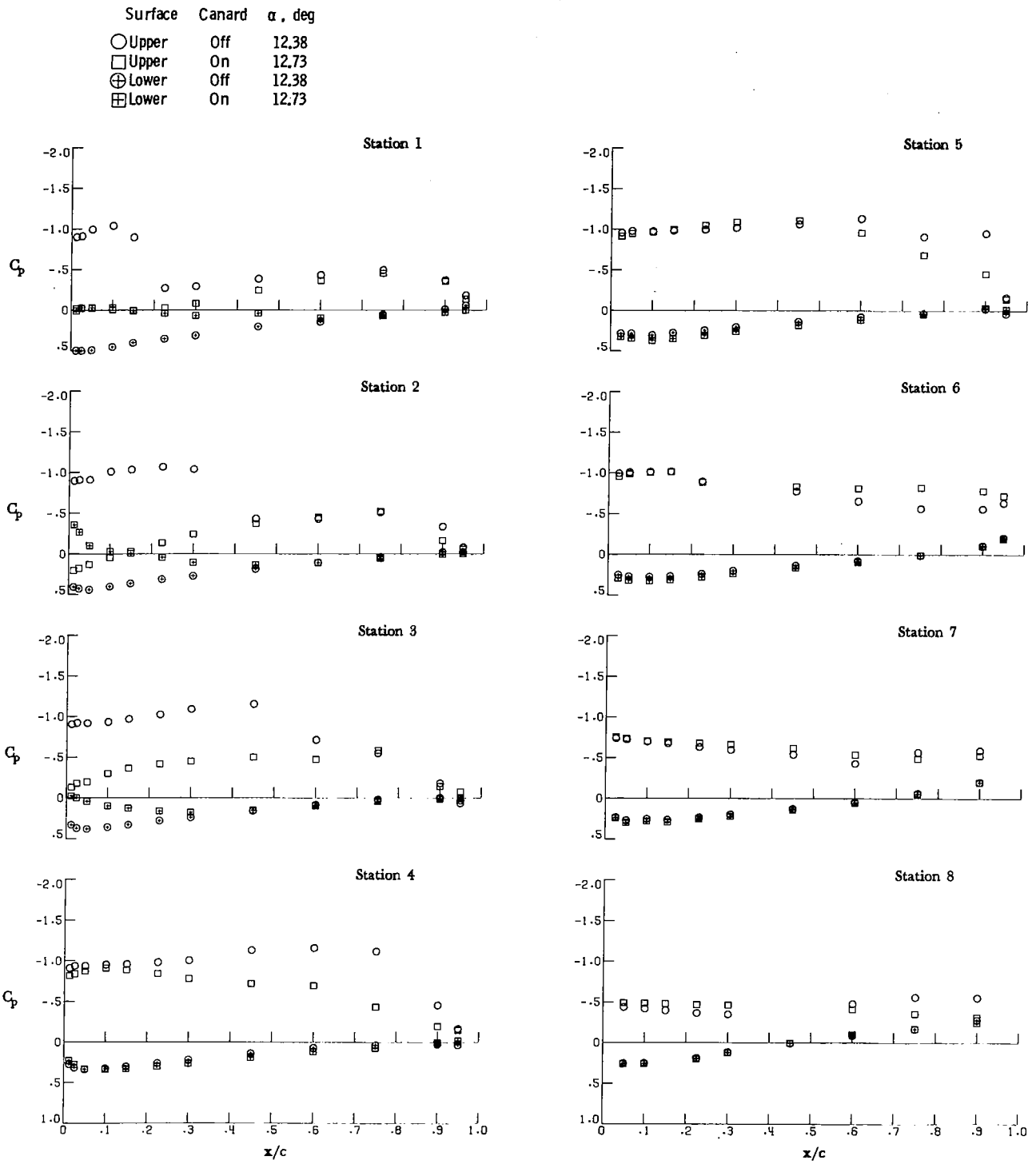

(c) $\alpha \approx 12^{\circ}$.

Figure 10.- Continued.

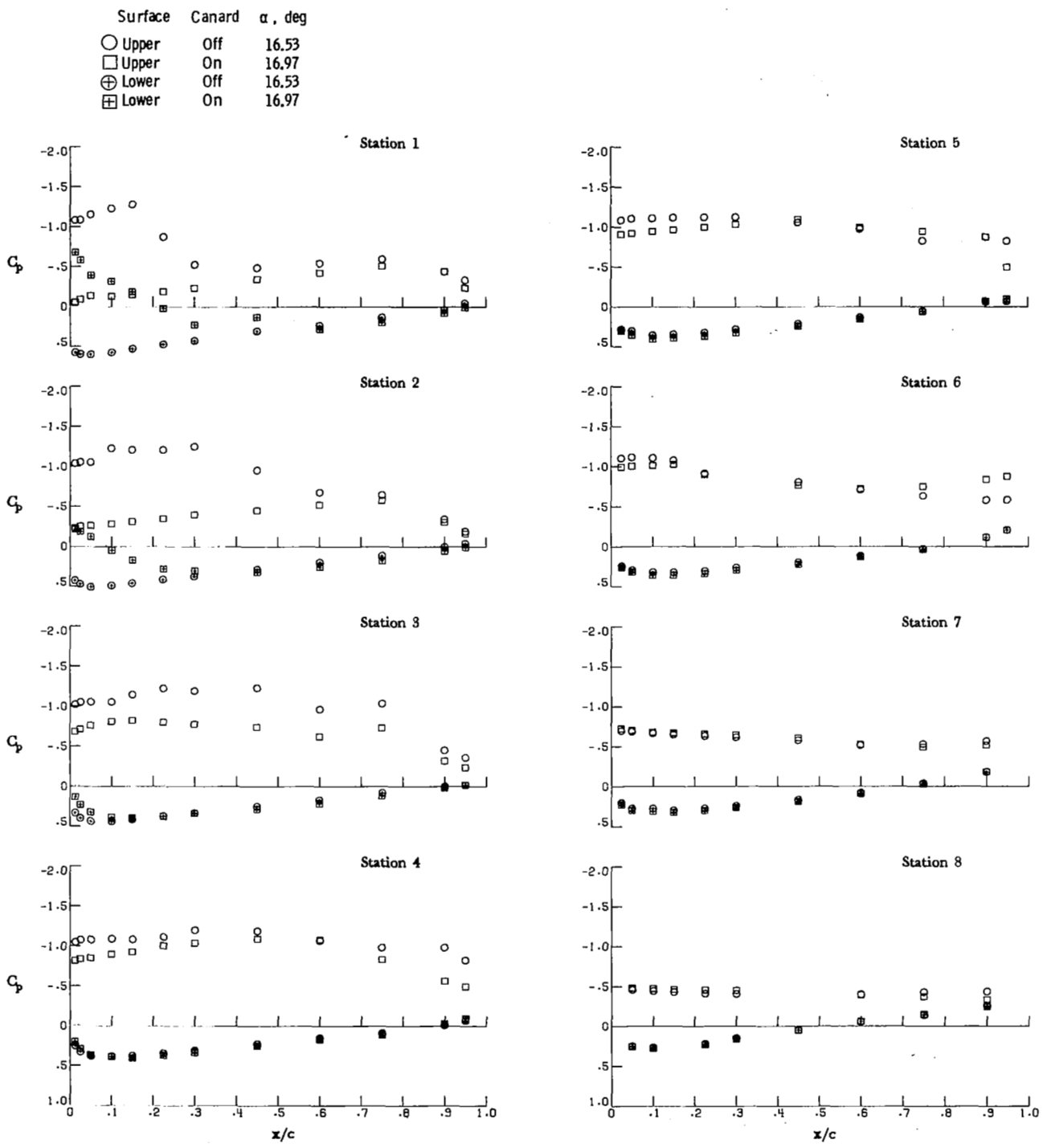

(d) $\alpha \approx 16^{\circ}$.

Figure 10.- Concluded.

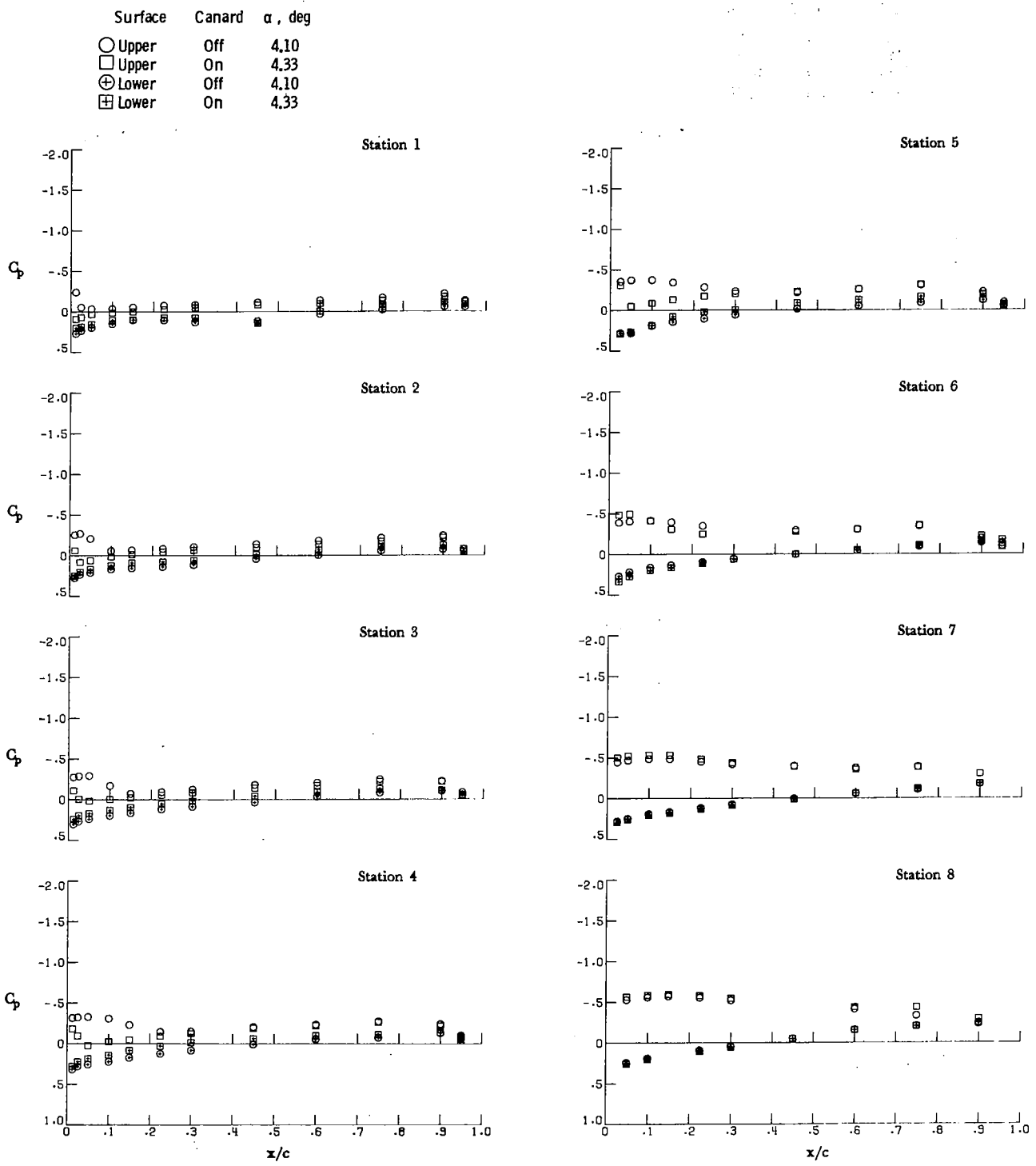

(a) $\alpha \approx 4^{\circ}$.

Figure 11.- Effect of canard flow field on wing pressures for $z/\bar{c} = -0.185$; $M_\infty = 1.20$.

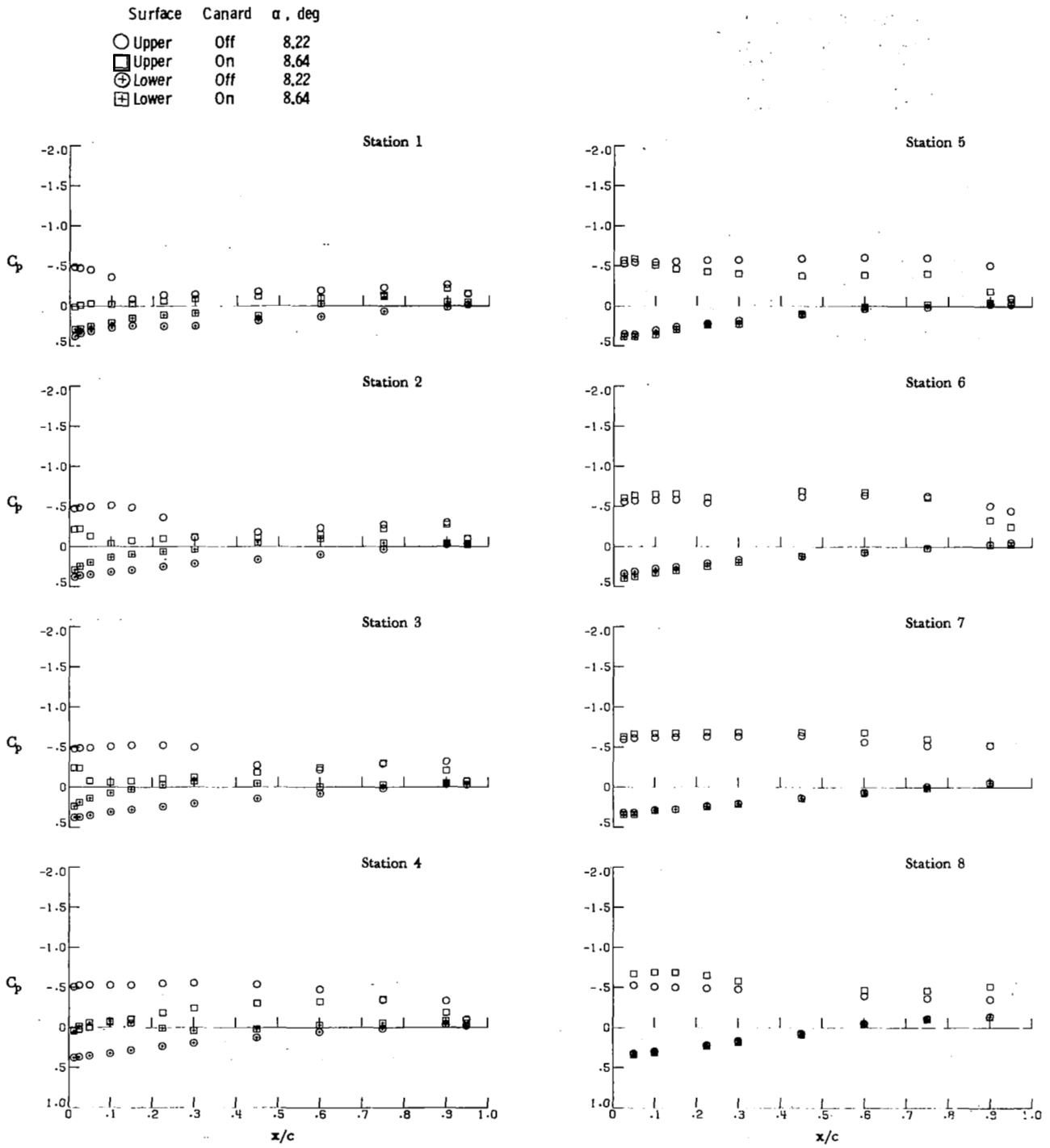

(b) $\alpha \approx 8^{\circ}$.

Figure 11.- Continued.

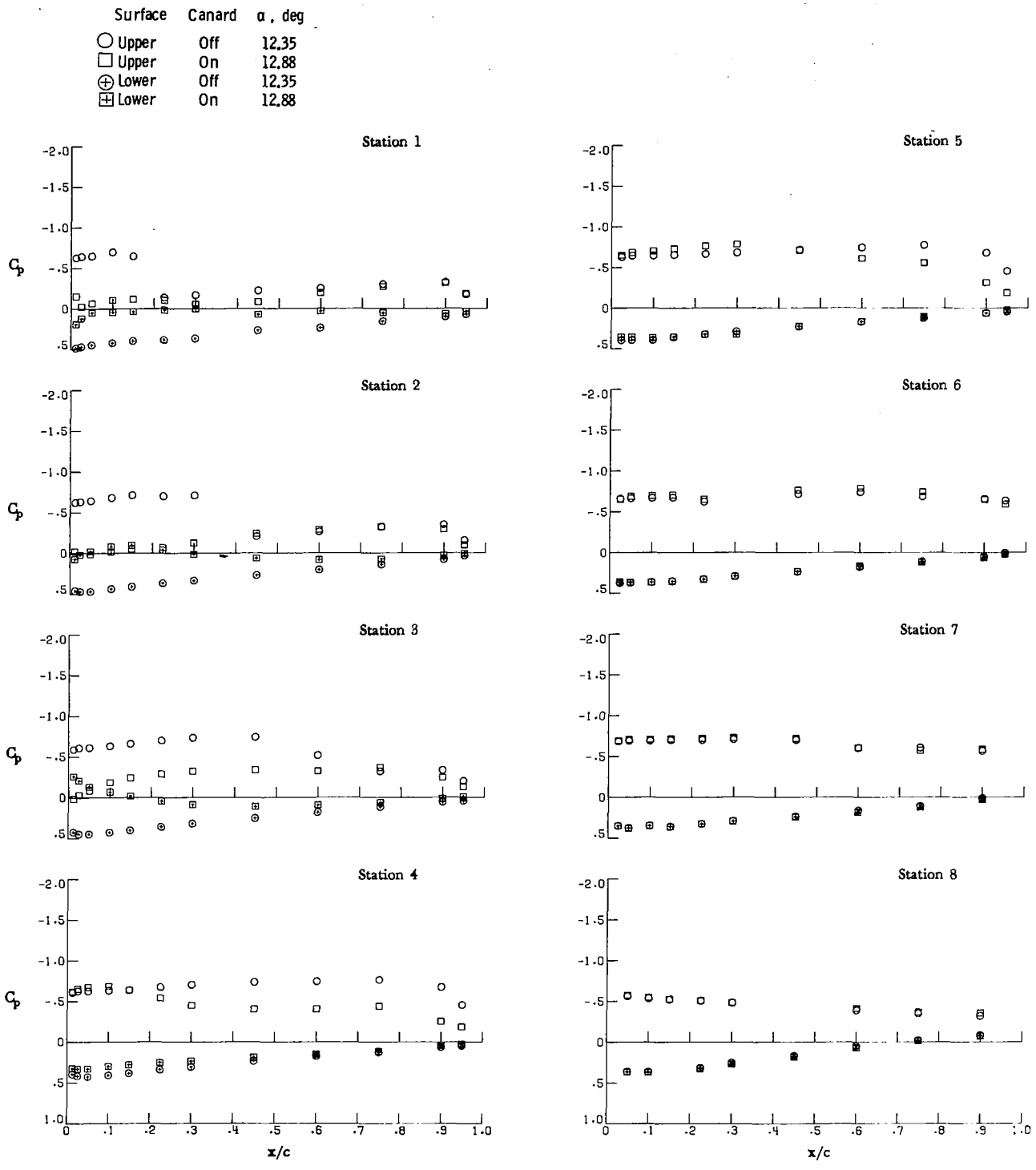

(c) $\alpha \approx 12^{\circ}$.

Figure 11.- Continued.

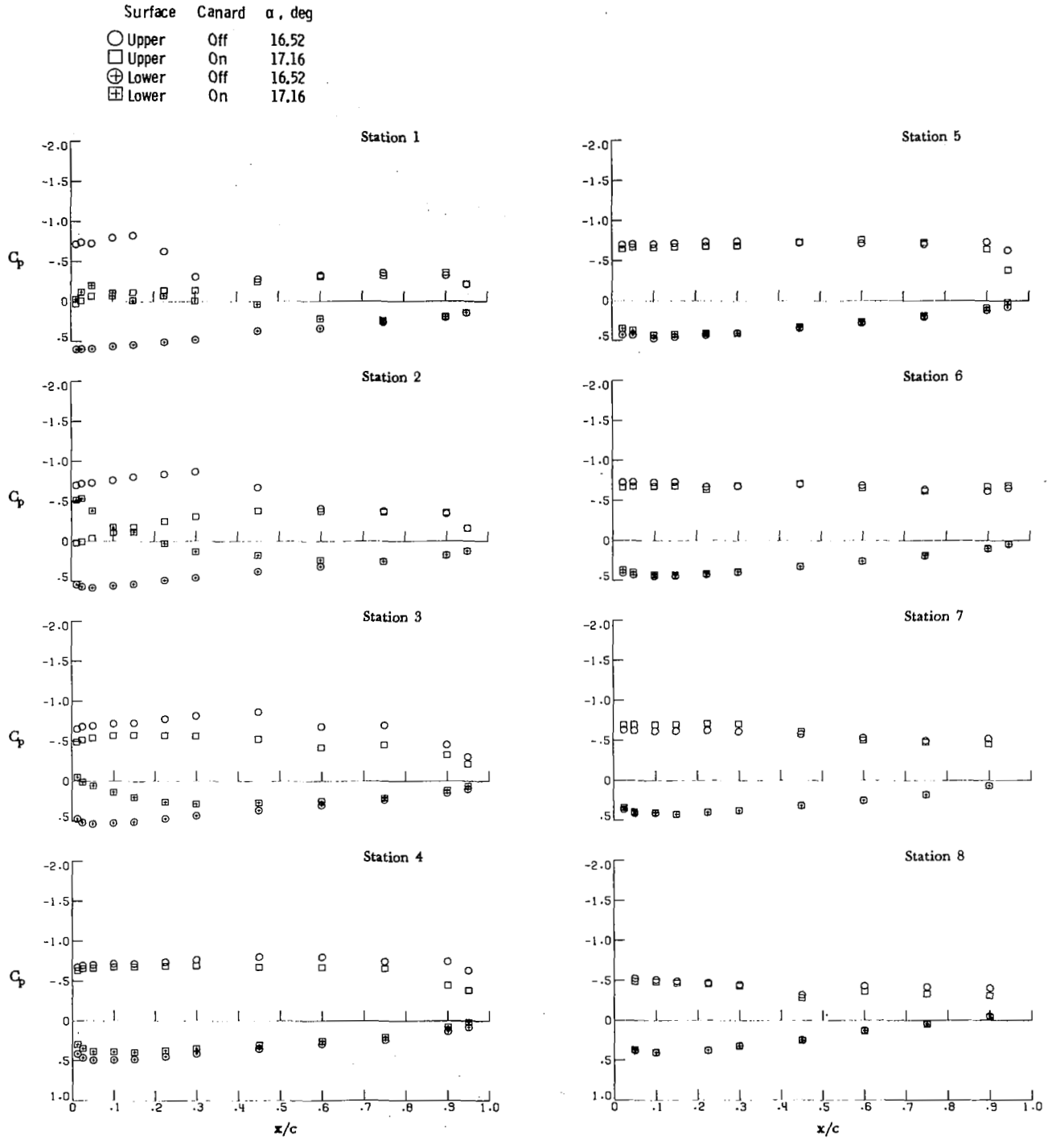

(d) $\alpha \approx 16°$.

Figure 11.- Concluded.

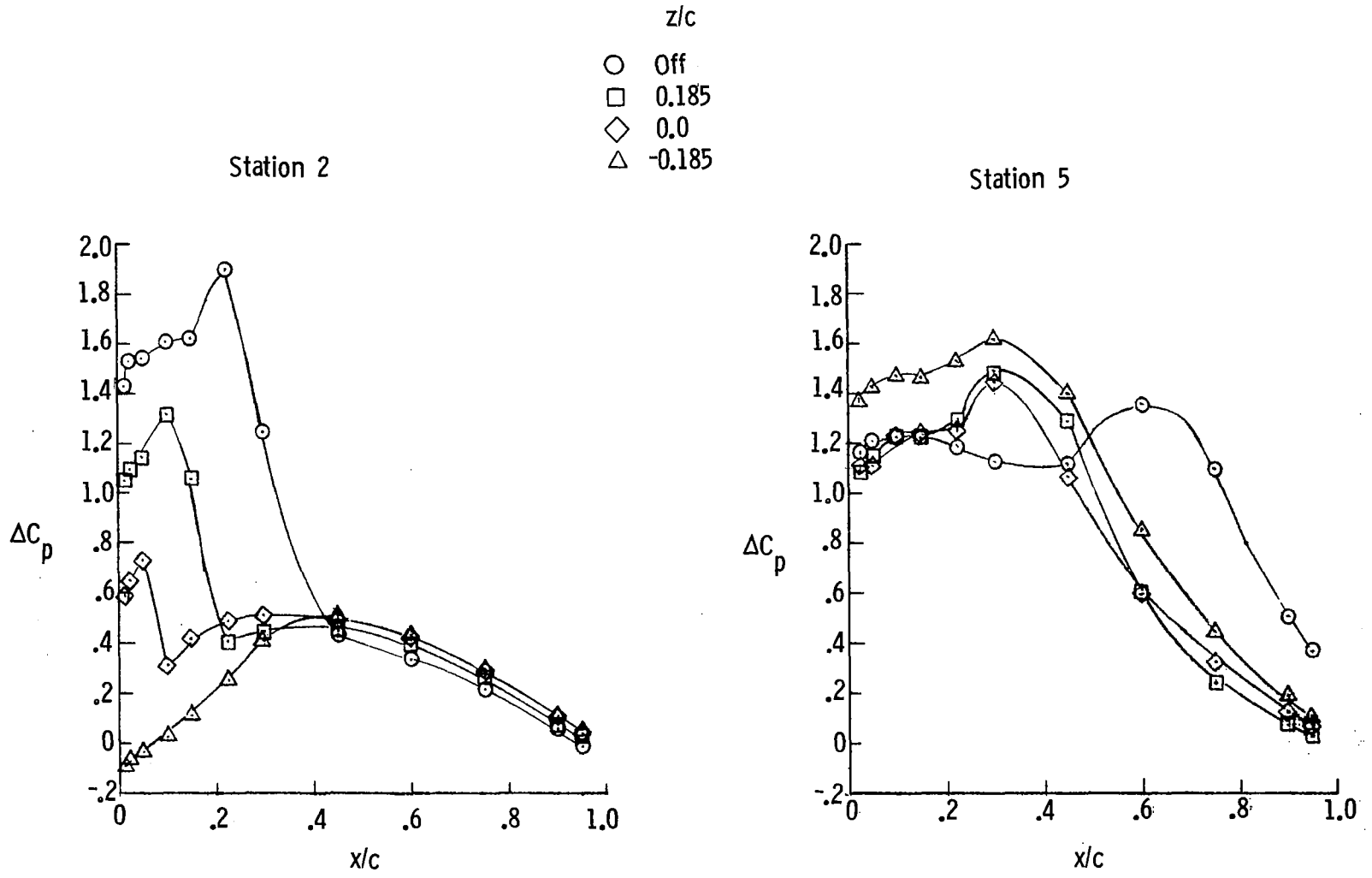

(a) $M_\infty = 0.70$.

Figure 12.- Effect of canard location on wing lifting pressures. $\alpha \approx 12^\circ$.

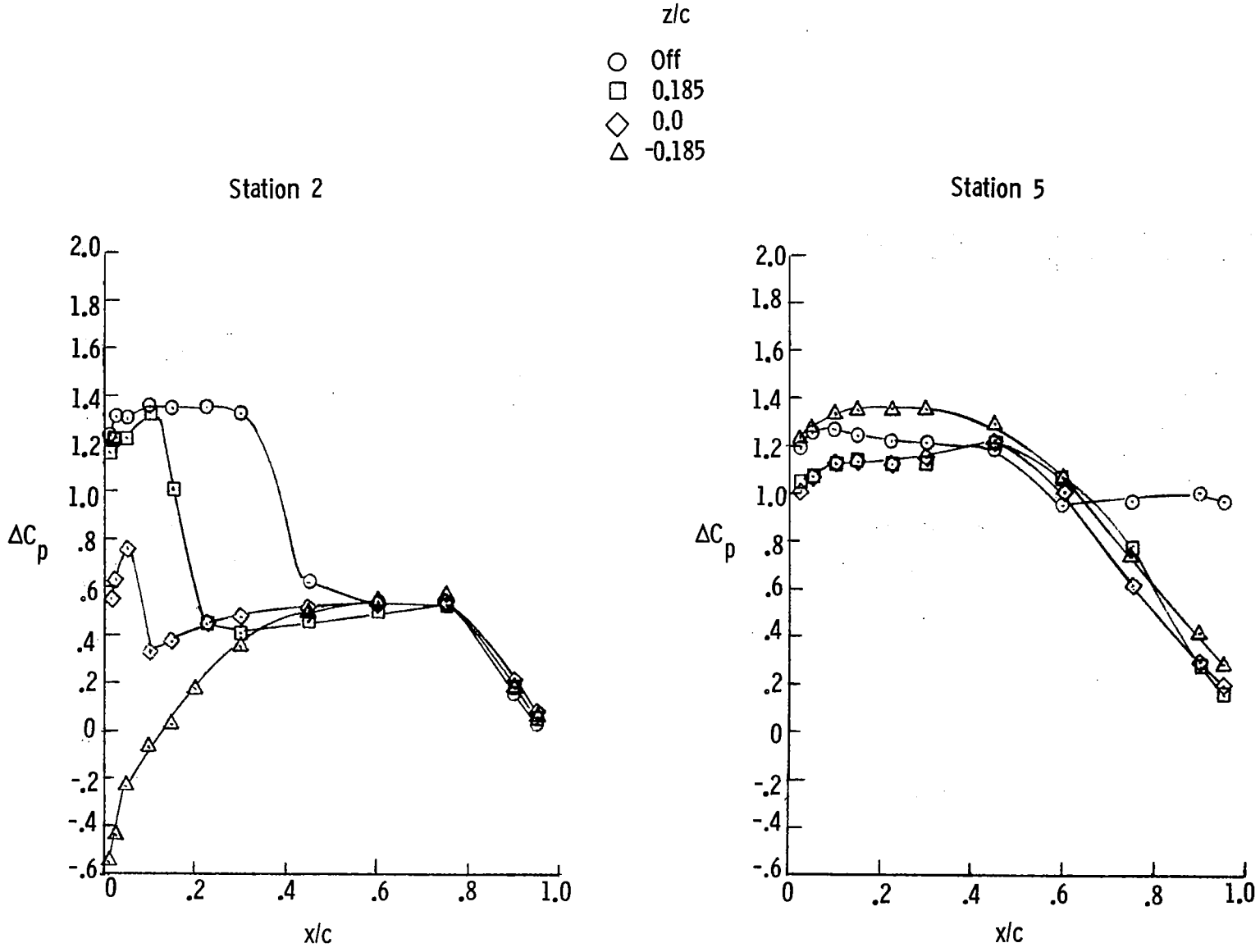

(b) $M_\infty = 0.95$.

Figure 12.- Continued.

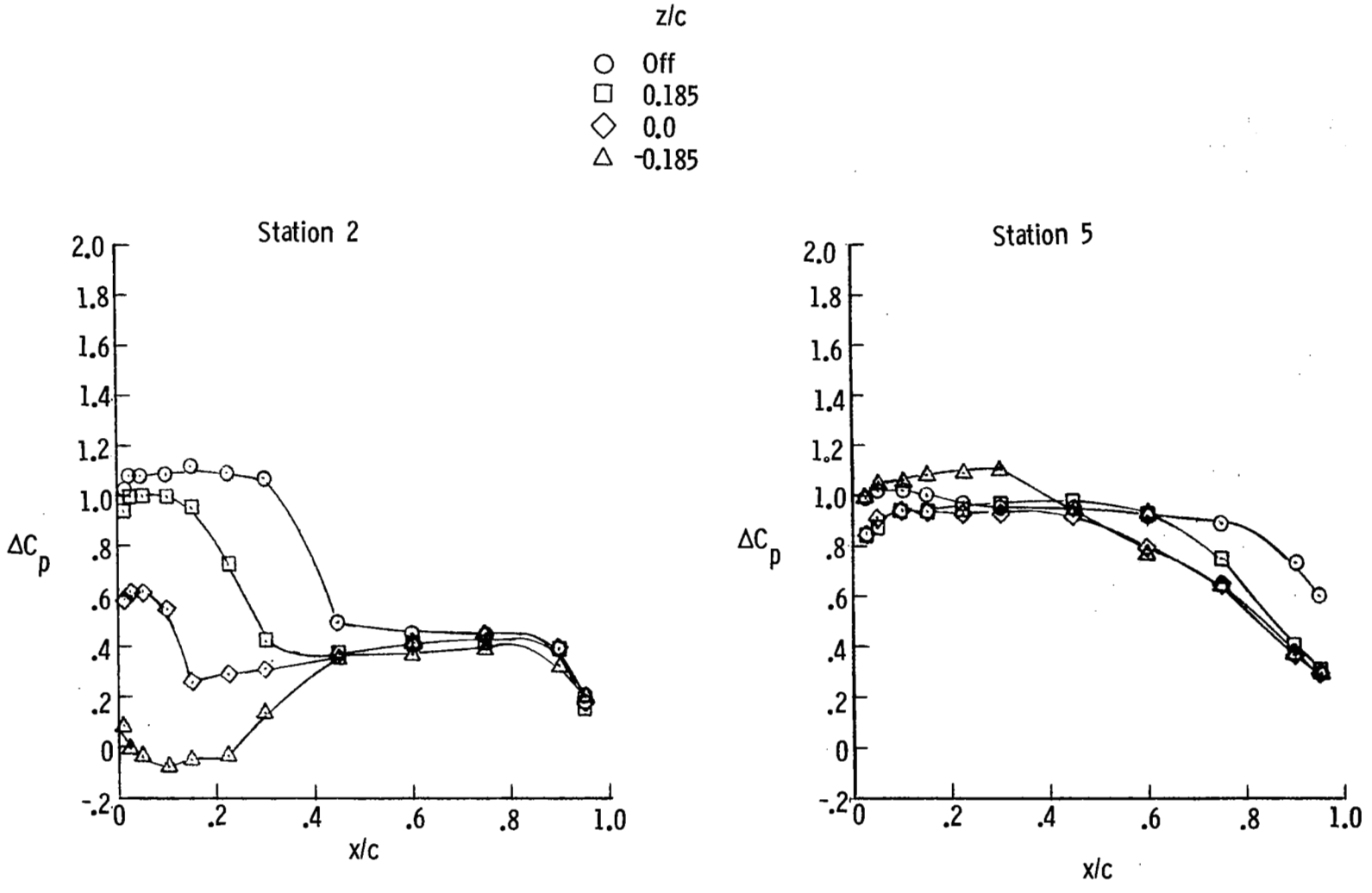

(c) $M_\infty = 1.20$.

Figure 12.- Concluded.

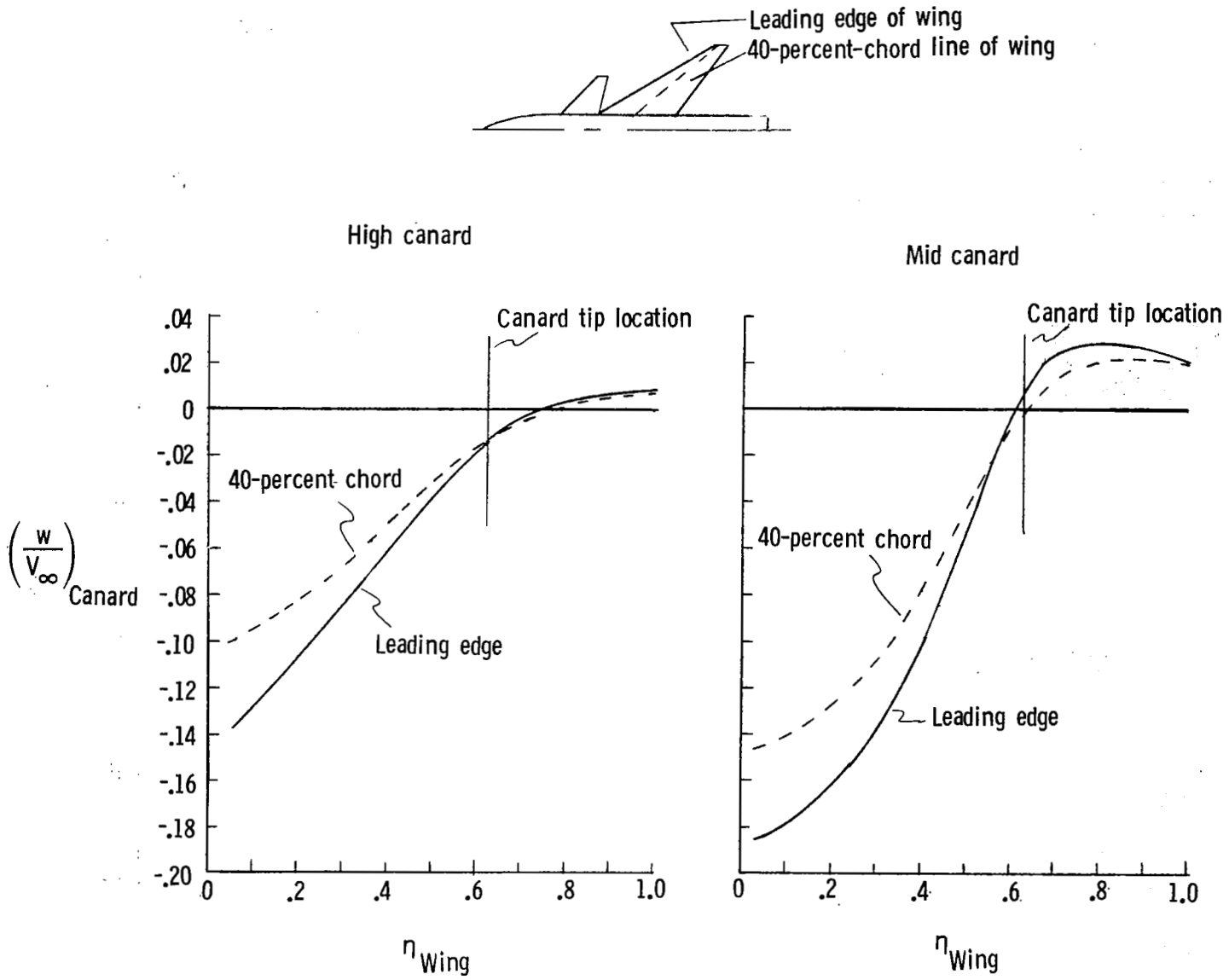

Figure 13.- Computed canard downwash at various wing locations. $M_\infty = 0.70$; $\alpha \approx 12^\circ$.

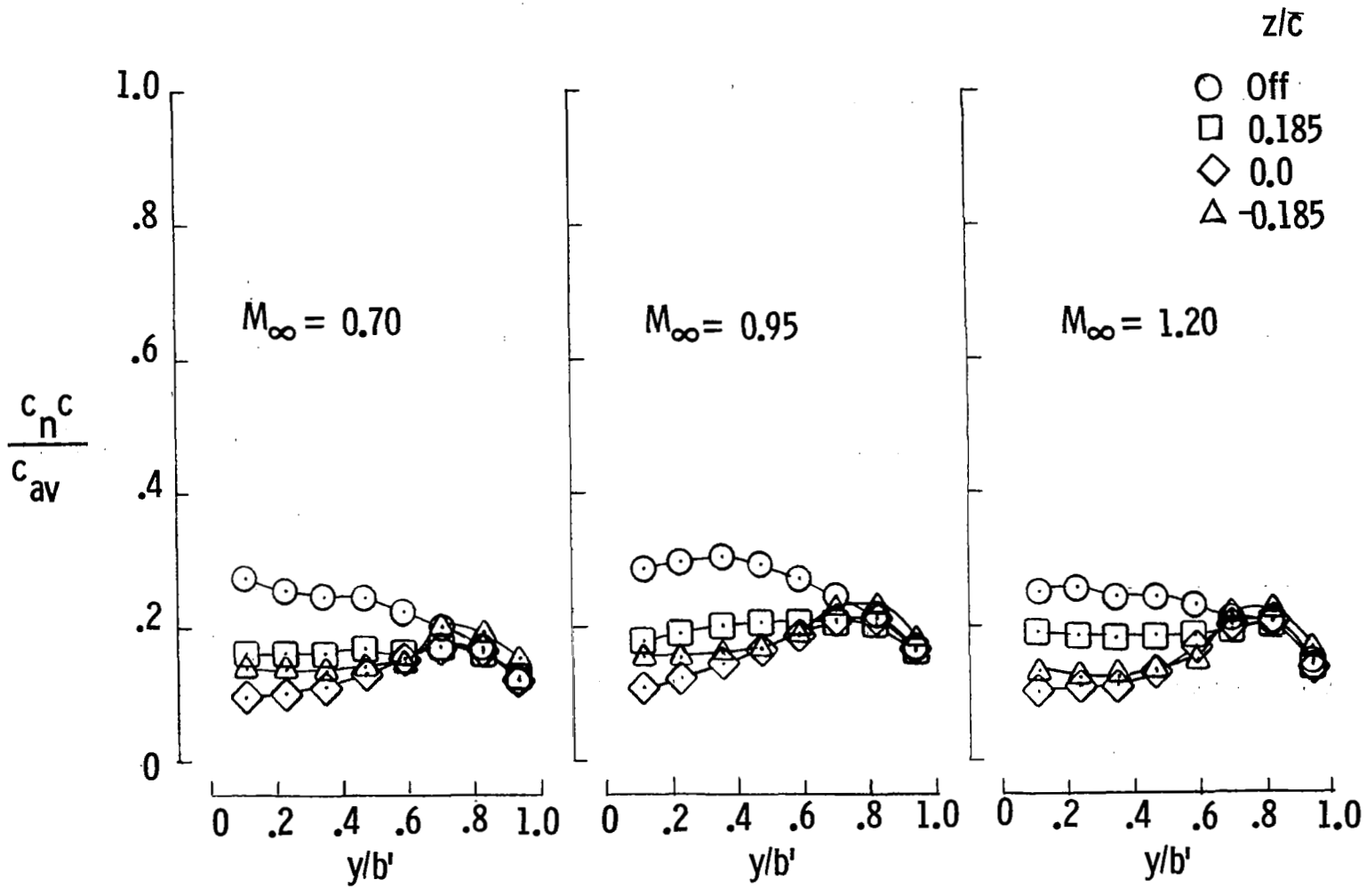

(a) $\alpha \approx 4^\circ$.

Figure 14.- Effect of canard location on spanload distribution.

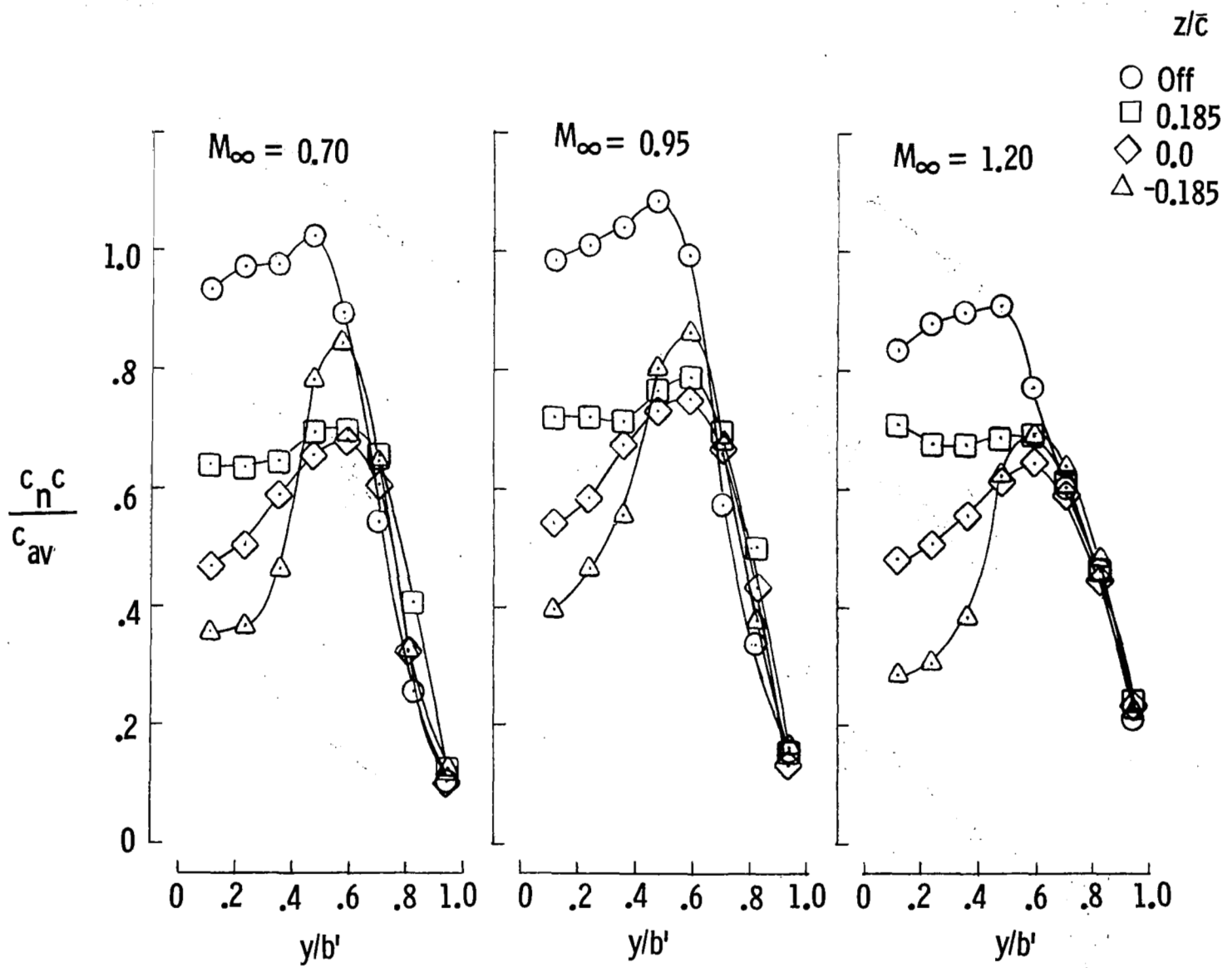

(b) $\alpha \approx 12^{\circ}$.

Figure 14.- Concluded.

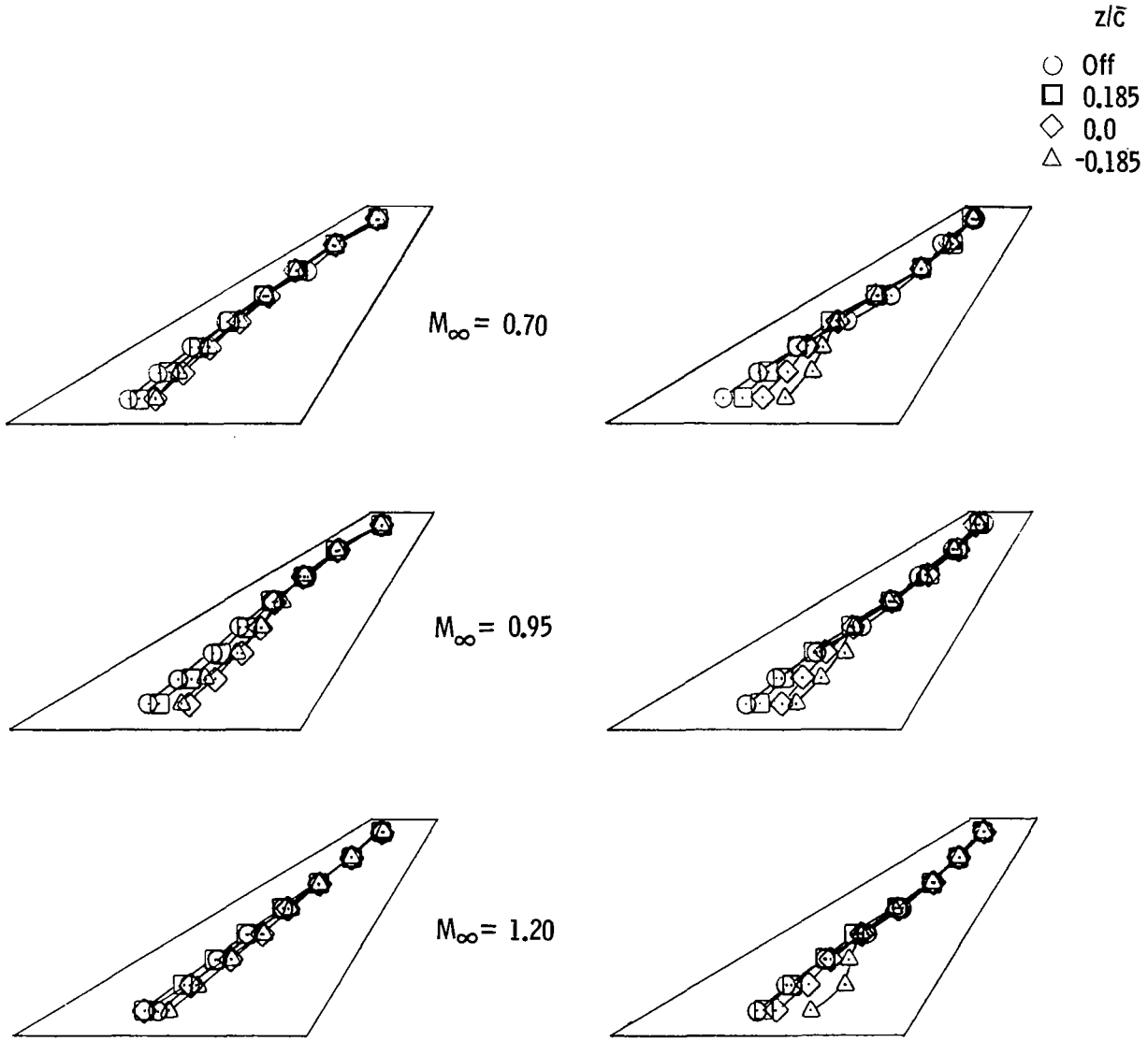

Figure 15.- Effect of canard location on wing sectional center-of-pressure locations.

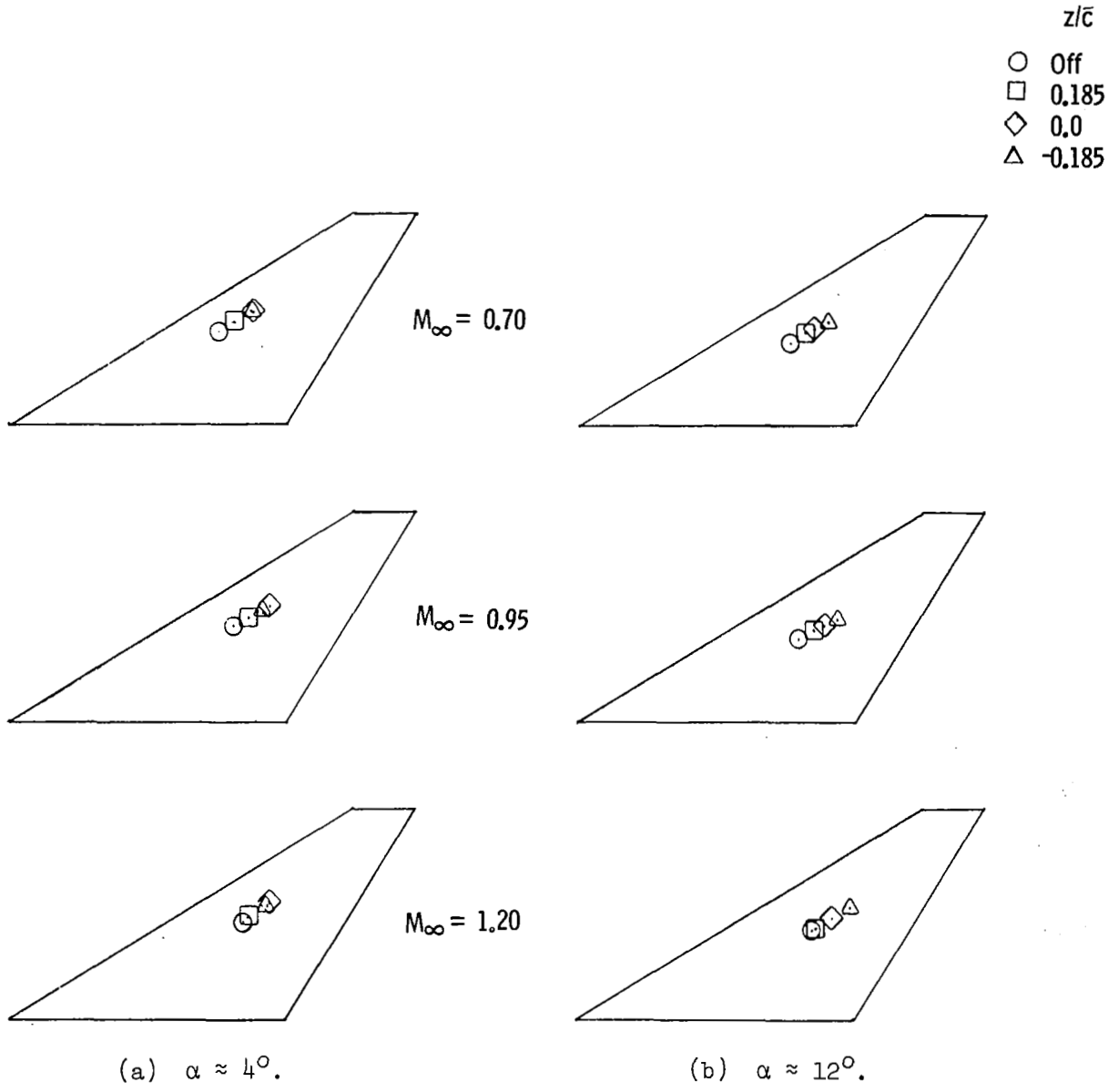

(a) $\alpha \approx 4^{\circ}$.

(b) $\alpha \approx 12^{\circ}$.

Figure 16.- Effect of canard location on wing center-of-pressure location.

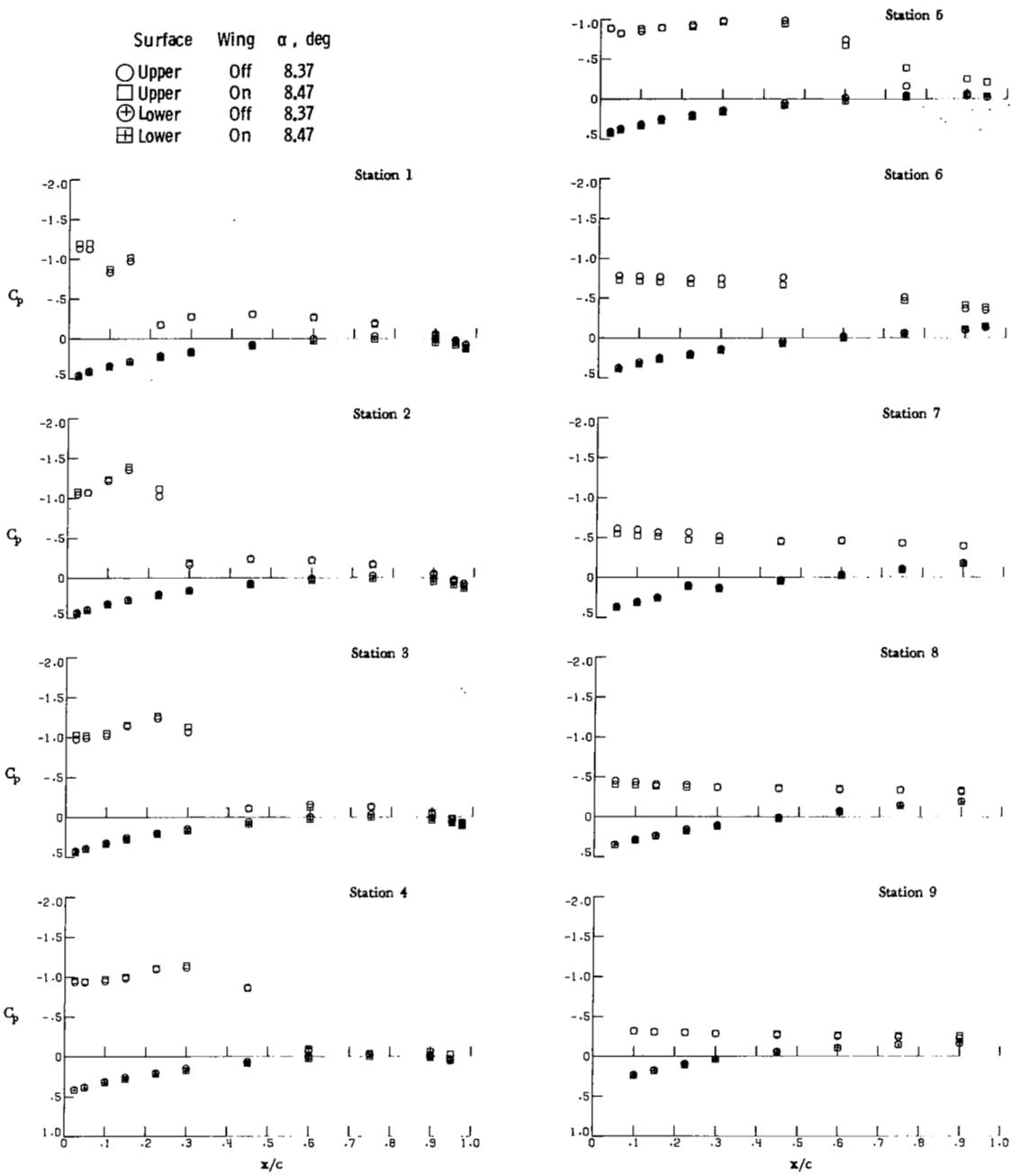

(a) $\alpha \approx 8^{\circ}$.

Figure 17.- Effect of wing on canard pressures. $z/\bar{c} = 0.0$; $M_{\infty} = 0.70$.

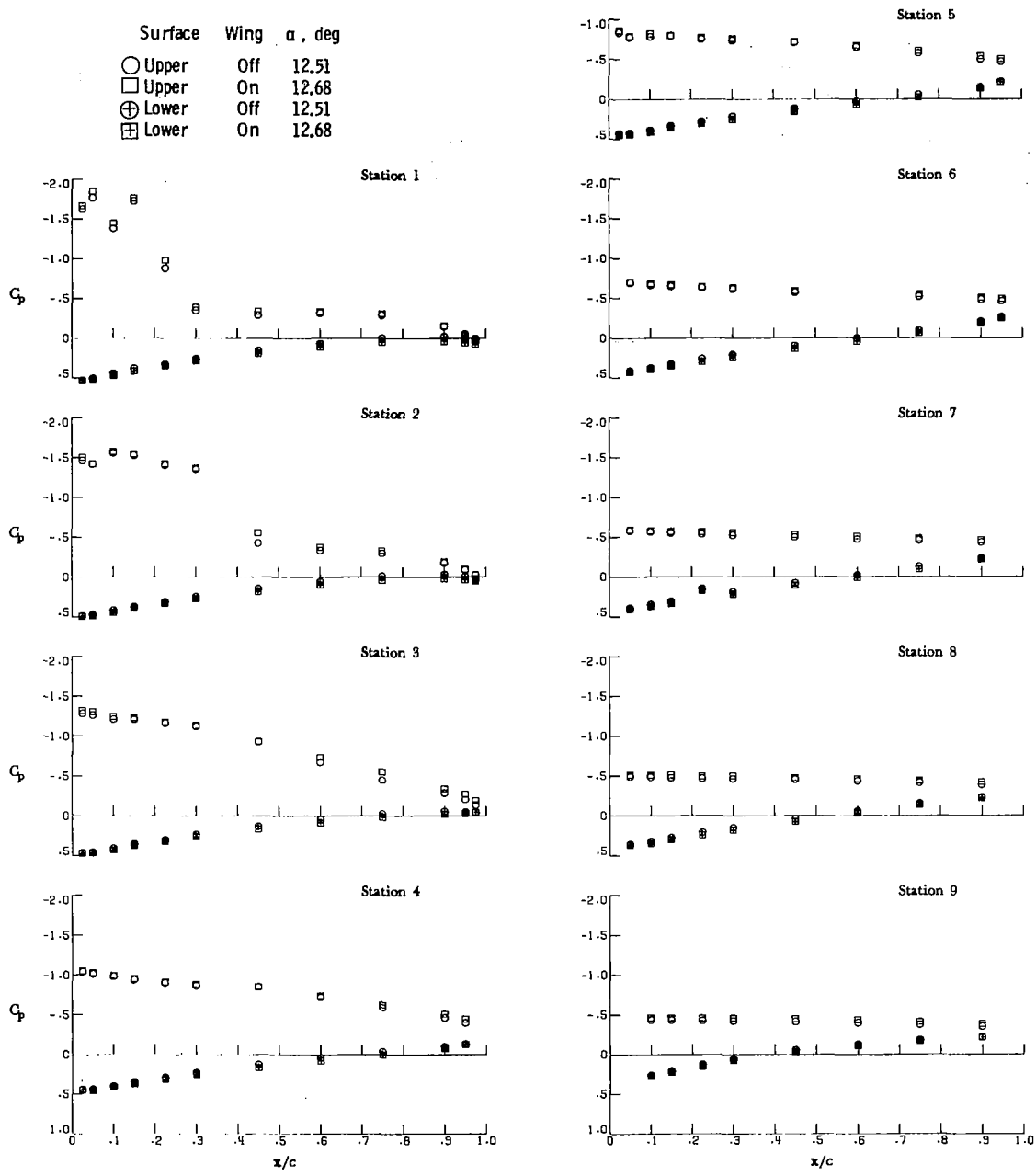

(b) $\alpha \approx 12^{\circ}$.

Figure 17.- Continued.

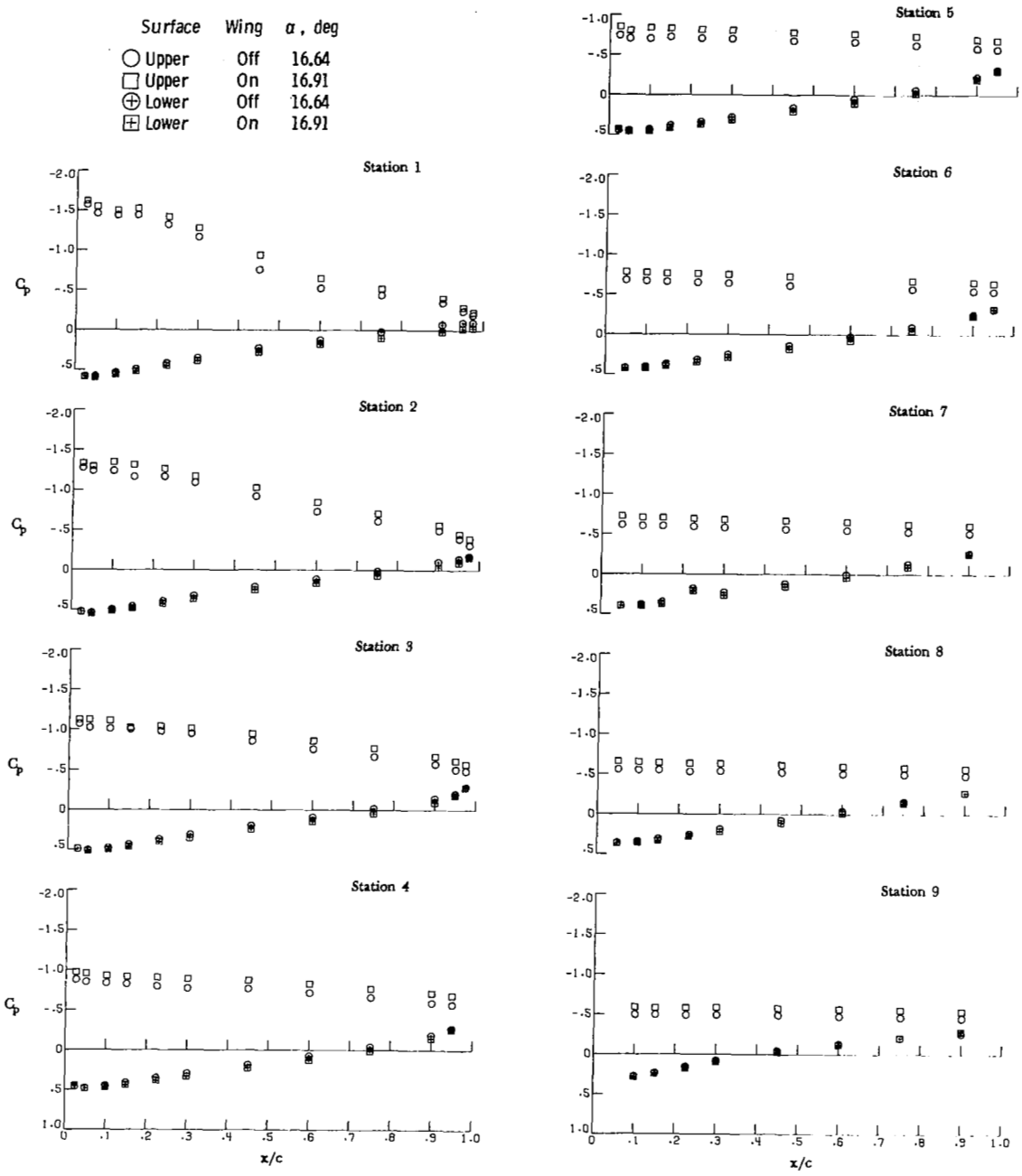

(c) $\alpha \approx 17^{\circ}$.

Figure 17.- Concluded.

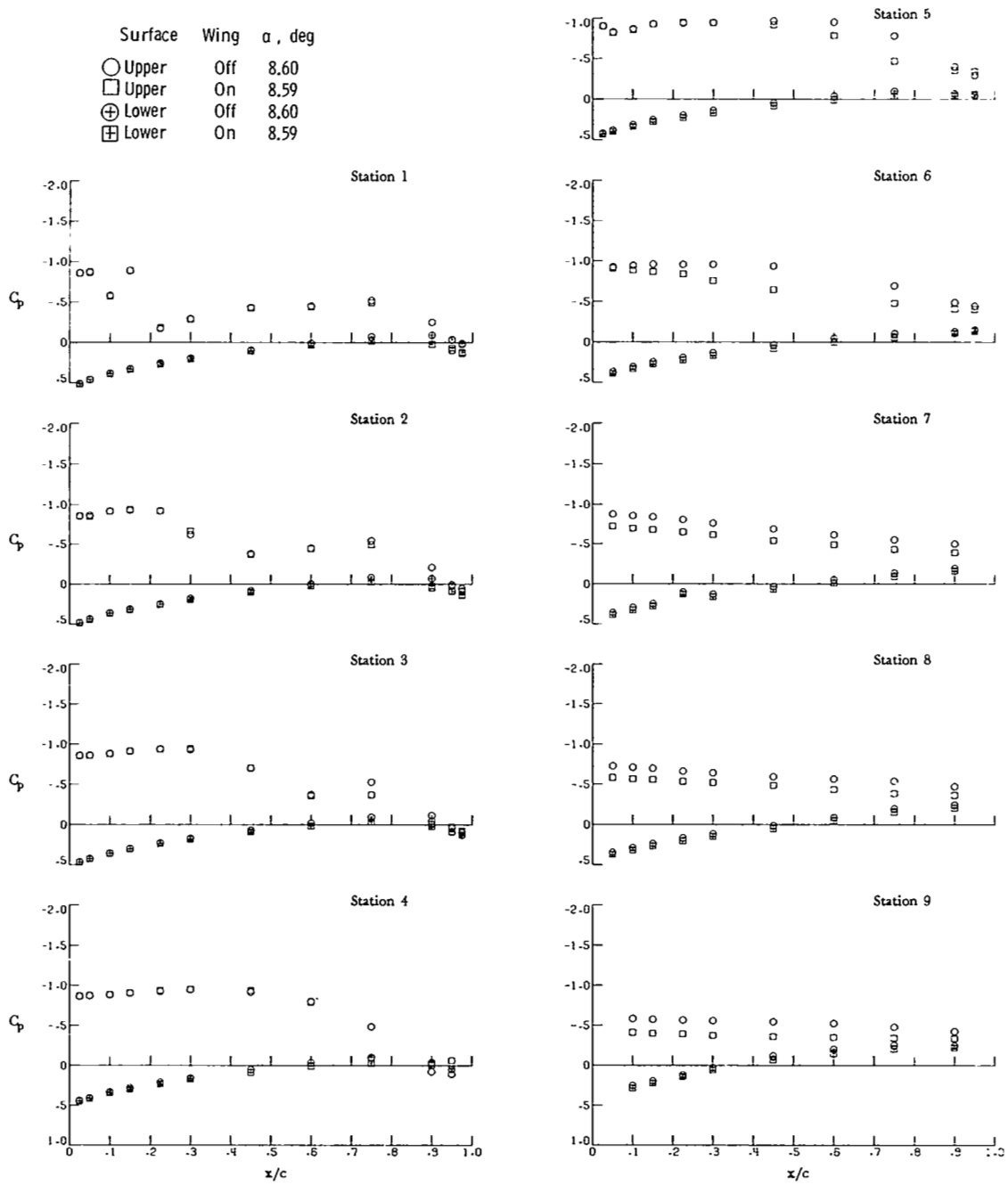

(a) $\alpha \approx 8^{\circ}$.

Figure 18.- Effect of wing on canard pressures. $z/\bar{c} = 0.0$; $M_\infty = 0.95$.

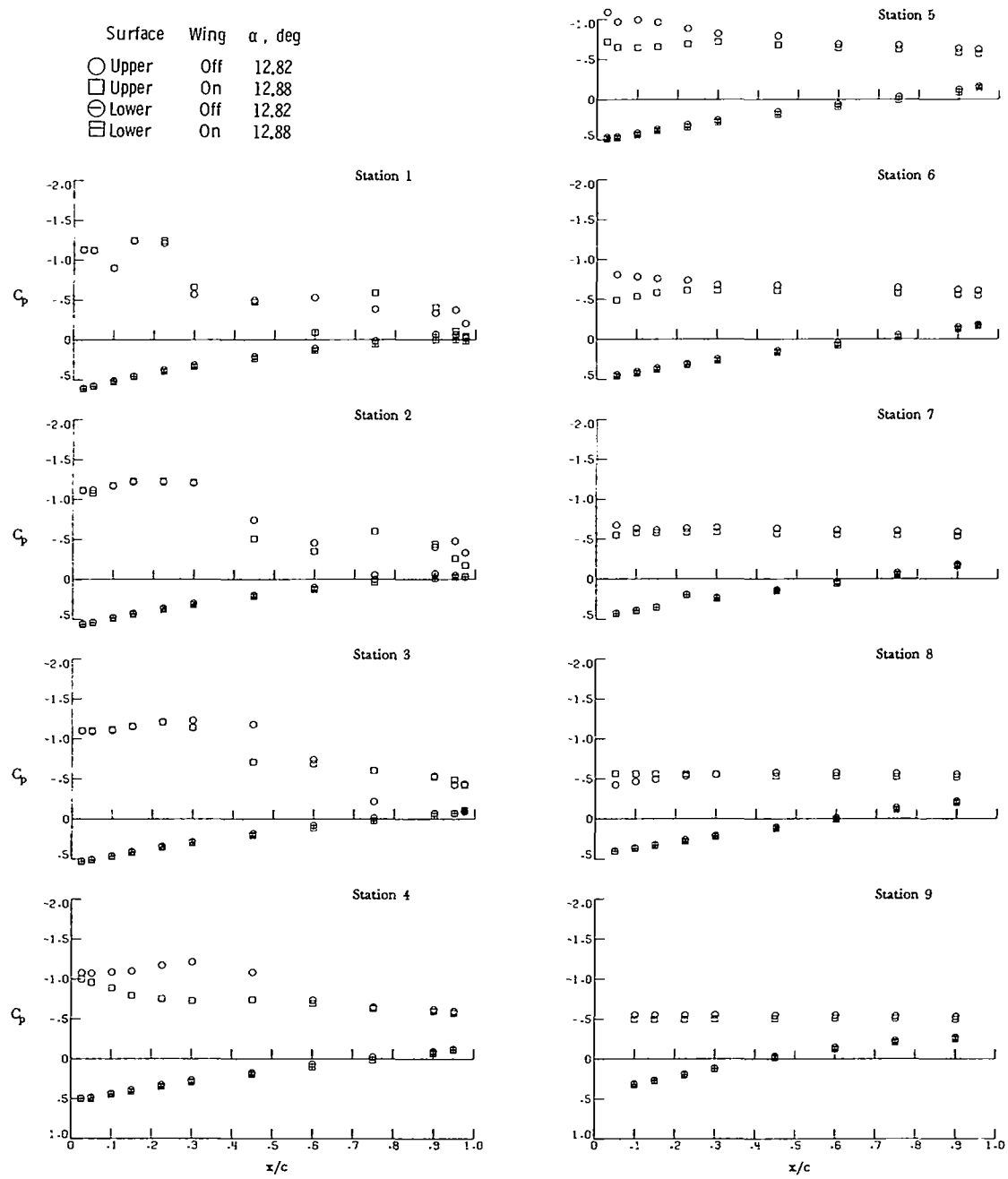

(b) $\alpha \approx 12^{\circ}$.

Figure 18.- Continued.

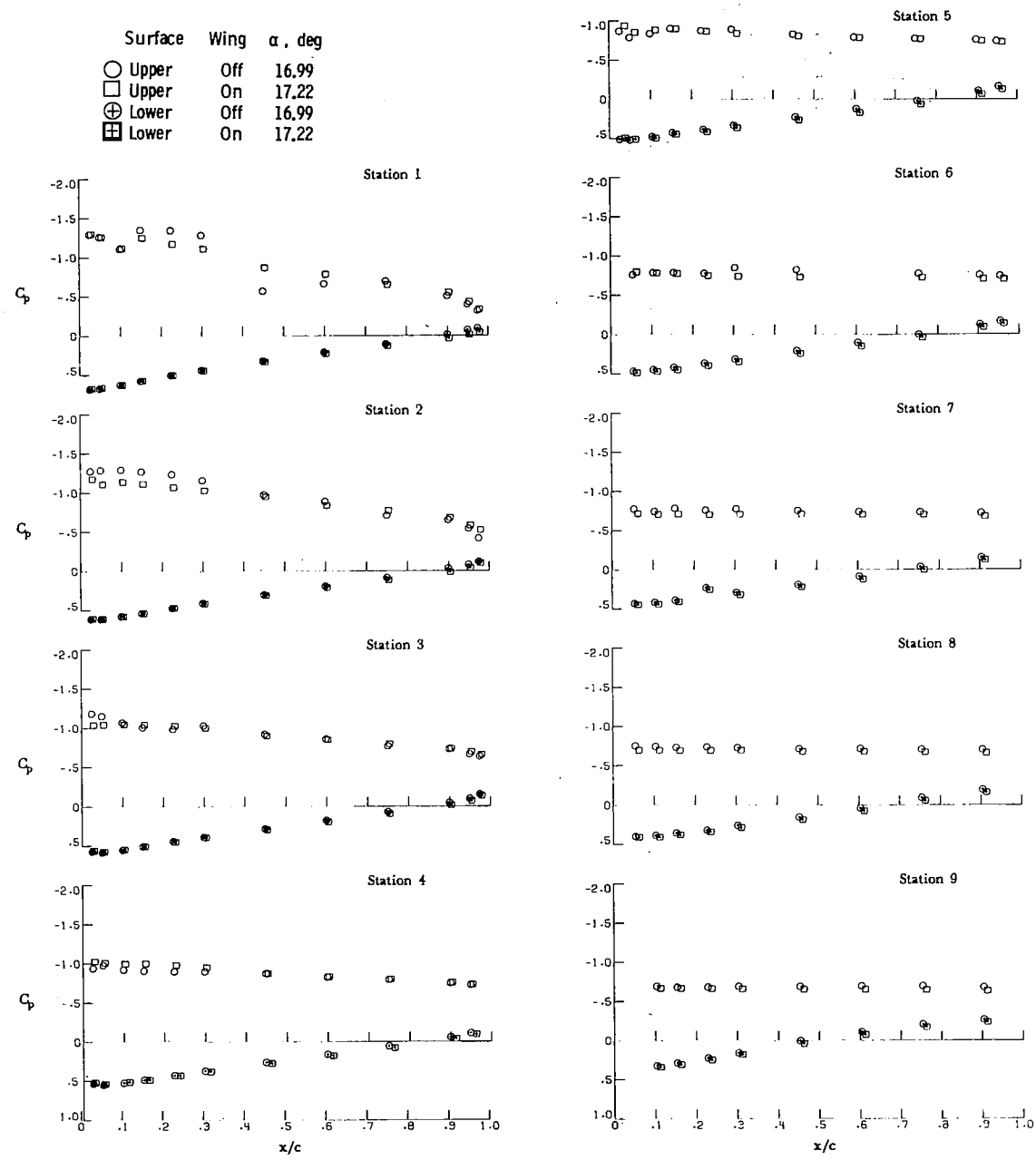

(c) $\alpha \approx 17^{\circ}$.

Figure 18.- Concluded.

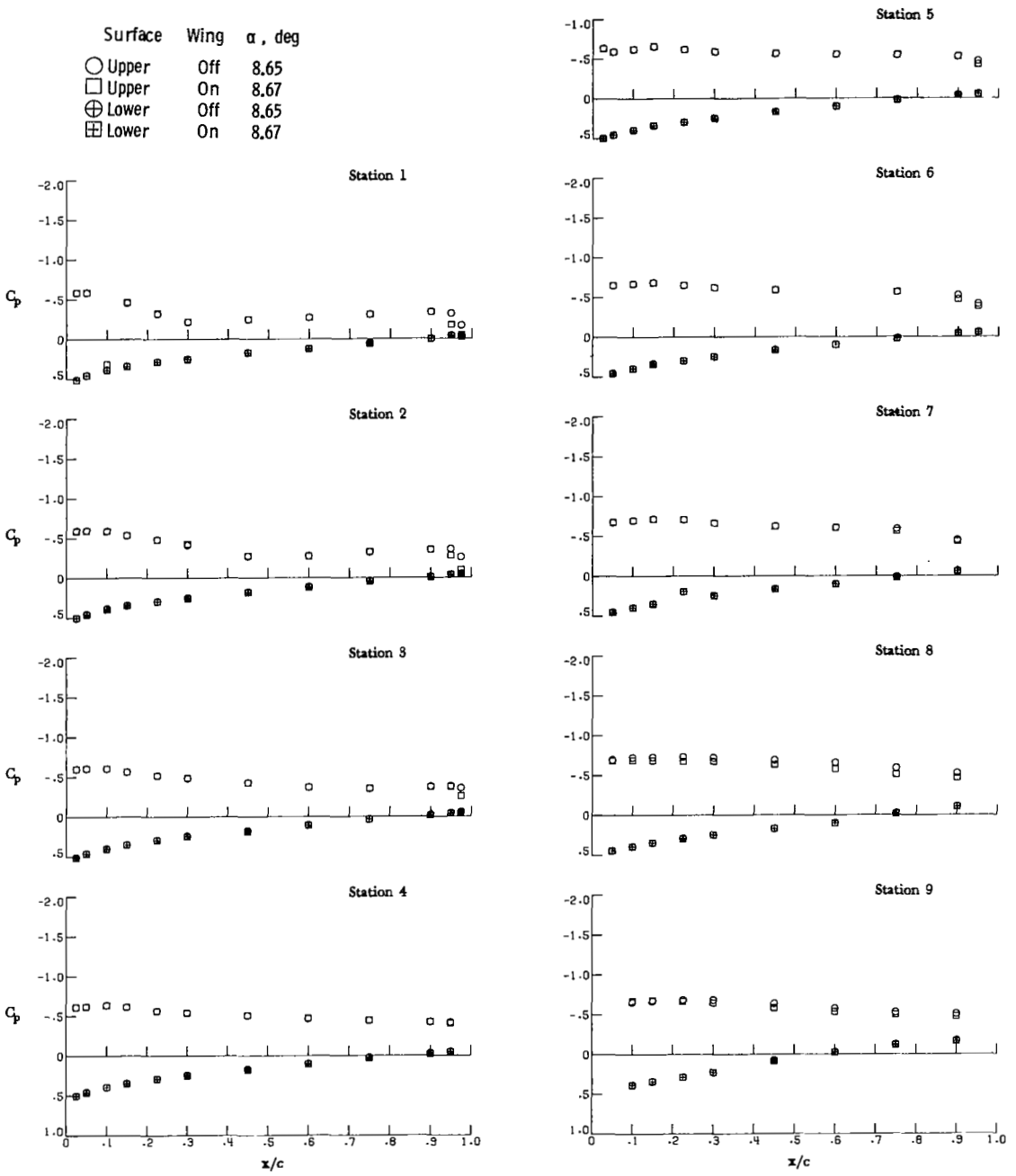

(a) $\alpha \approx 8^{\circ}$.

Figure 19.- Effect of wing flow field on canard surface pressures. $z/\bar{c} = 0.0$; $M_{\infty} = 1.20$.

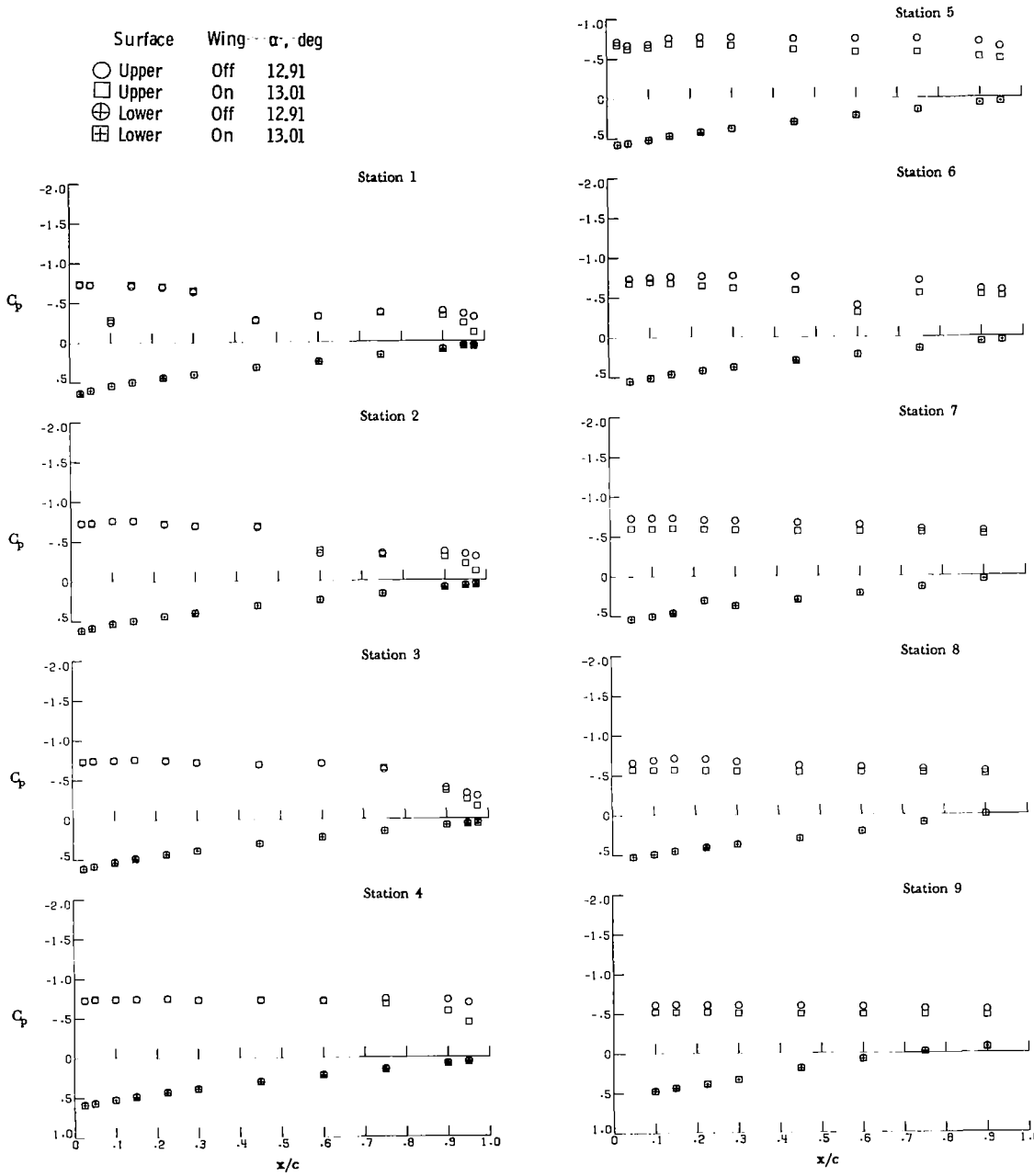

(b) $\alpha \approx 12^{\circ}$.

Figure 19.- Continued.

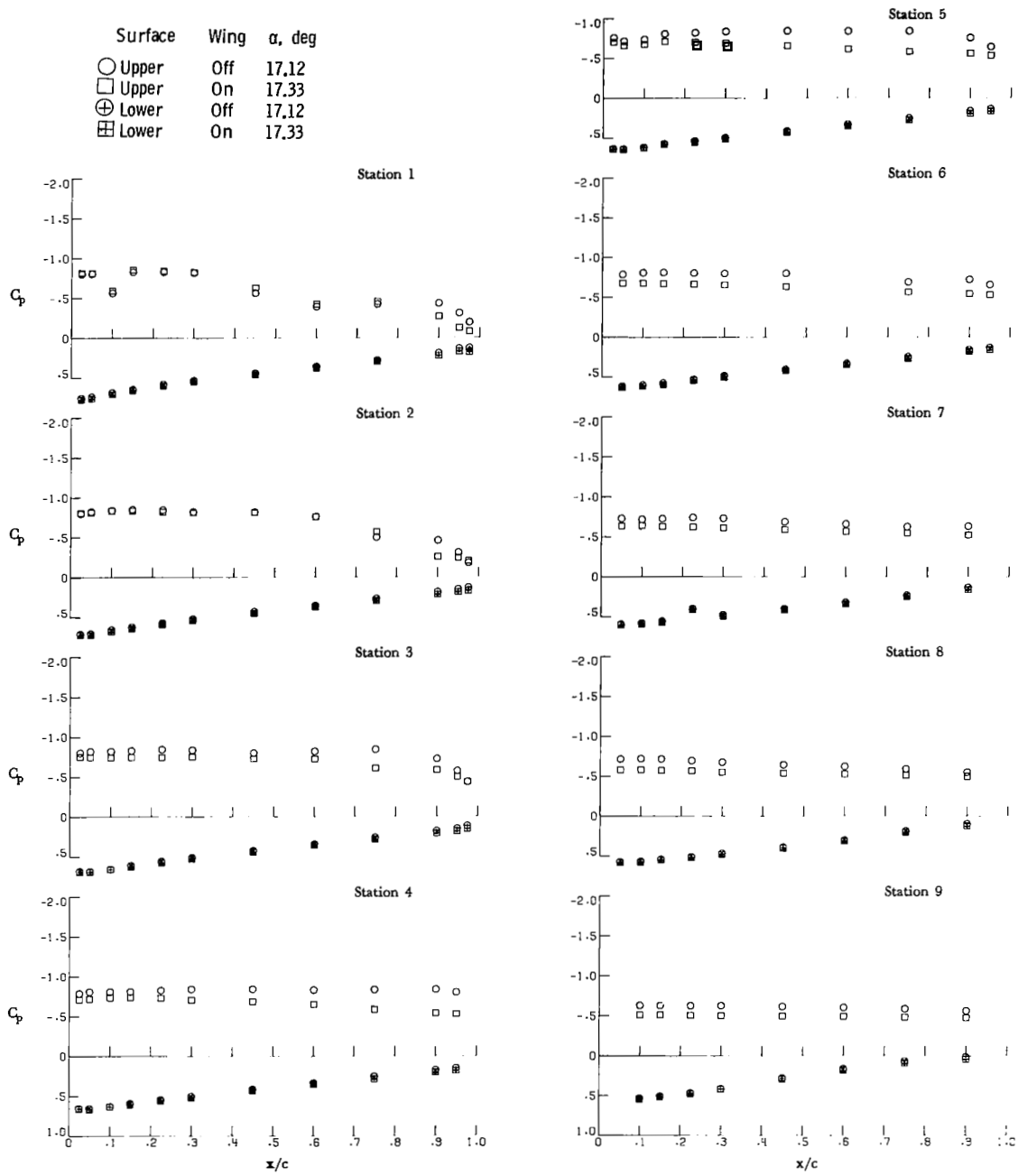

(c) $\alpha \approx 17^{\circ}$.

Figure 19.- Concluded.

1. Report No.	2. Government Accession No.	3. Recipient's Catalog No.
NASA TP-1355		

4. Title and Subtitle	5. Report Date
A STUDY OF CANARD-WING INTERFERENCE USING EXPERIMENTAL PRESSURE DATA AT TRANSONIC SPEEDS	January 1979
	6. Performing Organization Code
7. Author(s)	8. Performing Organization Report No.
Blair B. Gloss and Karen E. Washburn	L-12491
	10. Work Unit No.
9. Performing Organization Name and Address	505-11-23-13
NASA Langley Research Center Hampton, VA 23665	11. Contract or Grant No.
	13. Type of Report and Period Covered
12. Sponsoring Agency Name and Address	Technical Paper
National Aeronautics and Space Administration Washington, DC 20546	14. Sponsoring Agency Code

15. Supplementary Notes

16. Abstract

A close-coupled canard-wing model was tested in the Langley 8-foot transonic pressure tunnel at Mach numbers from 0.70 to 1.20 to determine the canard-wing interference effects on canard and wing loadings. The results indicated that the direct canard downwash effects on the wing loading are limited to the forward half of the wing directly behind the canard. The wing leading-edge vortex is located farther forward for the wing in the presence of the canard than for the wing-alone configuration. The wake, from the canard located below the wing chord plane, physically interacts with the wing inboard surface and produces a substantial loss of wing lift. For the Mach number 0.70 case, the presence of the wing increased the loading on the canard for the higher angles of attack. However, at Mach numbers of 0.95 and 1.20, the presence of the wing had the unexpected result of unloading the canard.

17. Key Words (Suggested by Author(s))	18. Distribution Statement
Canard wing Transonic loads Canard interference	Unclassified - Unlimited Subject Category 02

19. Security Classif. (of this report)	20. Security Classif. (of this page)	21. No. of Pages	22. Price*
Unclassified	Unclassified	68	$5.25

* For sale by the National Technical Information Service, Springfield, Virginia 22161

NASA-Langley, 1979

3 1 1U,A, 010879 S00903DS
DEPT OF THE AIR FORCE
AF WEAPONS LABORATORY
ATTN: TECHNICAL LIBRARY (SUL)
KIRTLAND AFB NM 87117